2001

Optical Studies of Layered Inorganic Solids: A Novel Phase Transition and Energy Transfer Studies.

Christie L. Larochelle

OPTICAL STUDIES OF LAYERED INORGANIC SOLIDS: A NOVEL PHASE TRANSITION AND ENERGY TRANSFER STUDIES

By

Christie L. Larochelle

B.S. Johns Hopkins University, 1995

A THESIS

Submitted in Partial Fulfillment of the

Requirements for the Degree of

Doctor of Philosophy

(in Physics)

The Graduate School

The University of Maine

August, 2001

Advisory Committee:

Howard H. Patterson, Professor of Chemistry, Advisor
James P. McClymer, Associate Professor of Physics
Susan R. McKay, Professor of Physics
Richard A. Morrow, Professor of Physics
Charles W. Smith, Professor of Physics

External Reader:

Jeffrey Zink, Professor of Chemistry, Department of Chemistry and Biochemistry, University of California, Los Angeles

OPTICAL STUDIES OF LAYERED INORGANIC SOLIDS: A NOVEL PHASE TRANSITION AND ENERGY TRANSFER STUDIES

By Christie L. Larochelle

Advisor: Dr. Howard H. Patterson

An Abstract of the Thesis Presented
in Partial Fulfillment of the Requirements for the
Degree of Doctor of Philosophy
(in Physics)
August, 2001

The optical properties of a group of dicyanoargentates(I) and dicyanoaurates(I) have been studied. The samples include $K_2Na[Ag(CN)_2]_3$, $Tb[Ag(CN)_2]_3$, $Tb[Au(CN)_2]_3$ and a series of compounds of the form $Tb_xLa_{1-x}[Ag(CN)_2]_3$ with x=0.001, 0.01 and 0.1. Additionally, a novel type of silver-gold mixed- metal sample ($La[Ag_xAu_{1-x}(CN)_2]_3$ with x=0.9 and 0.5) was synthesized and characterized.

The compound $K_2Na[Ag(CN)_2]_3$ has earlier been shown to exhibit a phenomenon known as luminescence thermochromism, whereby only one emission band is present at very low temperatures and very high temperatures, but a second, lower energy band is also present at intermediate temperatures. This prompted further investigation to explain this behavior. This investigation revealed the existence of an interesting structural change which is postulated to be an example of a novel type of phase transition, but did not explain the luminescence thermochromism. Further study, including luminescence lifetime results, was necessary to form a model involving energy transfer at lower temperatures and back-energy transfer at higher temperatures.

These dicyanoaurates(I) and dicyanoargentates(I) were also studied in the context of energy transfer from the $M(CN)_2^-$ donor ion to Tb^{3+} acceptor ions. The energy transfer is found to follow the Dexter exchange mechanism by a process of elimination of other possible mechanisms. The energy transfer is found to be more efficient in the case of the dicyanoargentate(I) donor than in the case of the dicyanoaurate(I) donor as the spectral overlap between donor and acceptor is greater.

The mixed-metal samples display an anomalously strong luminescence at ambient temperatures that cannot be explained by the optical results alone. This luminescence is also strongly *tunable* in that changing physical parameters such as temperature, excitation wavelength or Ag/Au ratio results in changes in the emission energy of the sample. Results are presented which support the use of mixed-metal systems as tunable donors for energy transfer studies.

ACKNOWLEDGEMENTS

First and foremost, I am deeply indebted to my family for being there for me during my "perpetual student" years. My parents in particular have supported me in so many ways. I must thank them with all my heart for their faith and belief in me and in my abilities.

My advisor, Professor Howard Patterson deserves much credit for inspiring me and helping me realize this goal. Also, my committee members have helped out with numerous questions and suggestions, keeping me focused and giving support: Professor Susan McKay, for never being too busy to give advice and encouragement; Professor James McClymer and Professor Charles Smith for helping with so many experimental questions; and Professor Richard Morrow for his help not only as a committee member, but also for keeping me on track through his role as Graduate Coordinator. I must also give great thanks to my external reader, Professor Jeffrey Zink of UCLA.

Partial financial support for my graduate work was provided by a grant from the American Chemical Society's Petroleum Research Fund and is gratefully acknowledged.

A number of collaborators contributed to this work: Professor George Shankle of Angelo State University helped by growing a number of crystals for us; X-ray and neutron diffraction for the work in Chapter 3 was provided by Dr. Peter Fischer of ETH Zurich and Paul Scherrer Institute and Dr. Brian Lucas of University of Queens-

land, Australia; X-ray diffraction for Chapter 5 was provided by Dr. Richard Staples at Harvard University; Professor Antonio Laguna and Jose Lopez de Luzuriaga Fernandez of Universidad de Zaragoza for their help with density functional theory calculations. Many thanks to all of them for their helpful (e-mail) conversations and experimental work.

So many fellow graduate students (too many to list individually) have helped out not only as practice audiences and sounding boards for ideas, but also with friendship and support through the traumas of graduate life.

Most of the work in this thesis would not have been possible without the assistance of David LaBrecque, Instrumentation Specialist in the Department of Chemistry at the University of Maine, the most versatile and adaptable jack-of- all trades I have ever met.

Last, but most certainly not least, I must thank Scott for being there for me through the most difficult part of this process and, most of all, for agreeing to pick up his life and "follow" me where my career leads. I feel so fortunate to have him in my life.

TABLE OF CONTENTS

List of Tables

List of Figures

1 INTRODUCTION: BACKGROUND AND MOTIVATION

This thesis seek to explores the structural and electronic properties of a small subset of compounds of the type $R[M(CN)_2]_3$ (R=K_2Na, Tb, La; M=Au, Ag). Dicyano complexes of Ag(I) and Au(I) have been investigated for over half a century, yet their photoluminescence properties are so rich that researchers have only begun to explore them to their full potential. Many applications have been suggested for a variety of Au(I) and Ag(I) compounds. For example, Ag(I)-doped zeolites show great potential as photocatalysts for nitric oxide decomposition.[4] A recent study reported the discovery of an Ag(I) thiolate polymer that is a semiconductor, a fact that is in contrast with all other known examples of this type of compound.[5] It was also recently reported that there exist both Ag(I) and Au(I) polymeric materials that have antimicrobial properties.[6,7] Additionally, certain Au(I) compounds exhibit completely reversible changes in the presence of volatile organic compounds, making them ideal candidates for environmental sensors.[8]

The goal in continuing research on dicyanoargentates and dicyanoaurates is to better understand their luminescence properties so that they might be considered for use in similar applications. This thesis describes three projects, all aimed at the pursuit of this goal. The first delves into the unusual luminescence behavior of $K_2Na[Ag(CN)_2]_3$. The second looks at energy transfer in dicyanoargentates and

dicyanoaurates and the third explores a novel group of mixed-metal materials that exhibit characteristics considered desirable for donors in energy transfer studies.

1.1 Luminescence Thermochromism and $K_2Na[Ag(CN)_2]_3$

Luminescence thermochromism refers to an optical phenomenon in which changes in temperature result in the presence of different emission bands. This completely reversible phenomenon has been observed in tetranuclear Cu(I) clusters[9-11] as well as in certain dicyanoargentates.[12,13]

In certain Cu(I) compounds, such as $Cu_4I_4py_4$, two emission bands are present, which are poorly coupled, as evidenced by their widely different lifetimes and different excitation spectra. At room temperature, the higher energy band is very weak and almost undetectable. However, as the temperature is lowered, this band becomes much more prominent and the lifetimes of the two bands become very similar. At the same time, the lower energy band first red-shifts, then blue-shifts. It is proposed that the higher energy state be attributed to an iodide to ligand charge transfer character while the lower energy state is a state of mixed character delocalized over the Cu_4I_4 core, which the authors refer to as "cluster centered." The luminescence thermochromism exhibited by this compound is then attributed to the different temperature responses of the two excited states.[11]

In $K_2Na[Ag(CN)_2]_3$, there are two emission bands: a lower energy emission at 410 nm and a higher energy emission at 315 nm. The higher energy band (315 nm) dominates at very low temperature values (e.g., 10 K) and room temperature, while

the lower energy band increases in intensity to dominate at about 80 K before decreasing in intensity upon further increasing the temperature.[13] In this thesis, $K_2Na[Ag(CN)_2]_3$ is investigated in an attempt to explain this behavior through a study of its structure, vibrational spectra and luminescence decay characteristics.

1.2 Energy Transfer

Under the right circumstances, excitation of one species within a sample can lead to emission from a different species. This phenomenon, sometimes referred to as sensitized luminescence, is due to the radiationless transfer of electronic energy from the first species (the donor) to the second species (the acceptor). In order for this process to take place, there must exist a spectral overlap between the emission of the donor and the absorption of the acceptor. In this thesis, the goal is to explore how the emission bands of the donor species change with changes in physical parameters, such as temperature and excitation wavelength. These changes can lead to changes in the spectral overlap between the donor and acceptor, allowing the energy transfer to be switched on and off.

1.2.1 Structure of Dicyanoargentate(I) and Dicyanoaurate(I) Compounds

The structures of $M(CN)_2^-$ (M=Ag, Au) ions in solution as well as in solid crystals of $KAg(CN)_2$ and $KAu(CN)_2$ were revealed through detailed Raman scattering and X-ray diffraction studies during the 1950's and 1960's.[14-20] In all cases, the ion is

found to be linear, in the form N≡C-M-C≡N. Single crystals of $R[M(CN)_2]_x$ (R=Tl, K, Tb, Eu, Gd, La, for example; x is determined by the valence of R) grow as layered structures, with layers of $M(CN)_2^-$ ions alternating with layers of R^{x+} ions and waters of hydration.[21–23] As an example, Figure 1.1 shows the structure of $K_2Na[Ag(CN)_2]_3$, a crystal that will be discussed in great detail in Chapter 3. The layering is clearly present in this crystal, with layers of K^+ and Na^+ ions alternating with layers of $Ag(CN)_2^-$ ions.

1.2.2 Excimers and Exciplexes in Dicyanoargentates

Oligomers that form through excited state interactions are referred to as excimers and exciplexes. The terms were originally used to refer to dimeric excited state complexes between either two identical species (excimers) or two different species (exciplexes). Exciplexes have been recognized in organic compounds for many years.[24] The first known example of the formation of excimers was reported by Förster after discovering that increasing concentrations of pyrene in n-heptane solution caused a quenching of the monomer emission (highly- structured emission at about 25,000 cm^{-1}) along with an increase in the intensity of the excimer emission (unstructured emission at about 20,000 cm^{-1}). More recently, investigators have discovered inorganic excimers and exciplexes.[25] Excimers and exciplexes have been reported to form as a result of metal-metal bonding between Pt and Tl in tetrakis(μ-diphosphito)diplatinate(II) and -thallium(I) in aqueous solution,[26] Pt and Au in solution between $Au(CN)_2^-$ ions

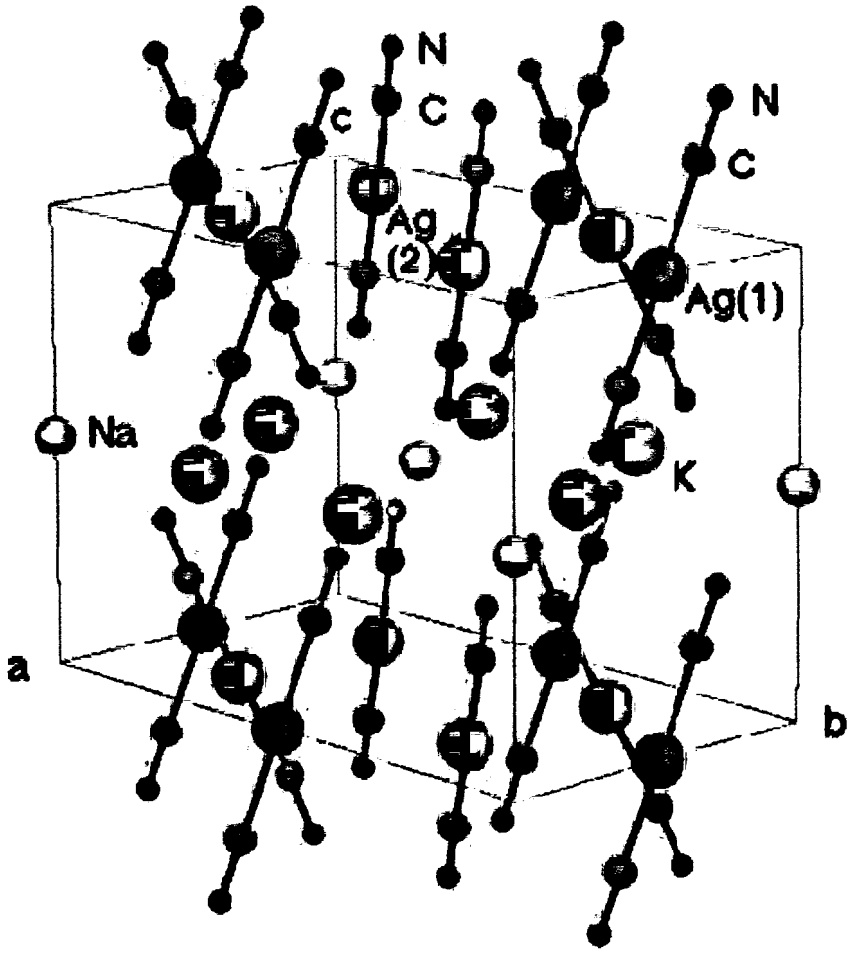

Figure 1.1: Structural model of $K_2Na[Ag(CN)_2]_3$ at 30 K.

λ_{max}^{em}, nm	Assignment	
285-300	$*[Ag(CN)_2^-]_2$	excimers
320-360	cis-$*[Ag(CN)_2^-]_3$	localized exciplexes
390-430	trans-$*[Ag(CN)_2^-]_3$	localized exciplexes
490-530	$*[Ag(CN)_2^-]_n$	delocalized exciplexes

Table 1.1: Band assignments for dicyanoargentate emissions arising from exciplex formation within the crystal.

and $Pt_2(P_2O_5H_2)_4^{4-}$ ions,[27] as well as Cu and Ag in Cu^+/Ag^+ doped β"-alumina[28] and Cu with itself in copper(I)-doped Na^+-β"- alumina.[29]

In crystals of the type $R[Ag(CN)_2]_x$, the M-M distances within the layers are quite short. In $TlAg(CN)_2$, for example, the shortest Ag-Ag distance is found to be 3.11 Å, shorter than any previously determined in a silver dicyanide salt. This short Ag-Ag separation leads to ligand-unsupported excited state interactions, and consequently the formation of luminescent exciplexes, or $*[Ag(CN)_2^-]_n$ oligomers.[30] Additionally, electronic structure calculations reveal a deeper potential well between silver ions in the first excited state than in the ground state.[22] Typical results from such calculations are shown in Figure 1.2. Ground state metal-metal interactions for silver are not expected since Ag(I) has a closed shell in the ground state (i.e., all the 4d orbitals are filled). However, the presence of these excited state bonding interactions can be understood since in the excited state an electron has been promoted and the Ag(I) ion now has an open shell configuration.

Based on theoretical calculations coupled with experimental results, four emission bands have been attributed to $[Ag(CN)_2^-]_n$ ($n \geq 2$). These are listed in Table 1.1.[31] Calculations such as the ones mentioned earlier have been used to show that

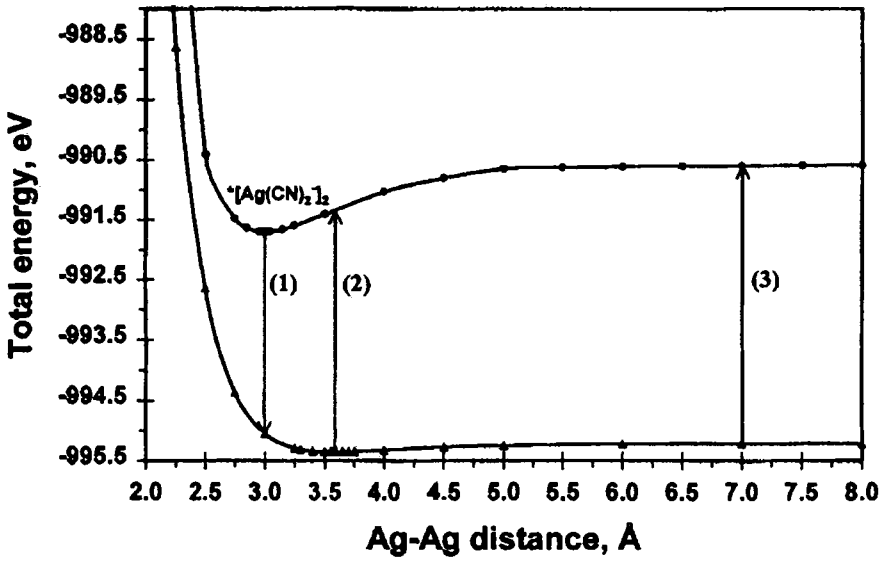

Figure 1.2: Potential energy diagram for the ground (bottom curve) and the lowest excited state (top curve) of $[AgC(N)_2^-]_2$ plotted from extended Hückel calculations. Optical transitions shown are: (1) excimer emission; (2) solid-state excitation; (3) solution absorption.[1]

the emission energies of $*[Ag(CN)_2^-]_n$ decrease significantly as n increases.[31] Extensive experimental studies and theoretical calculations have gone into the assignments listed.[31,32]

Since the presence of these emission bands is highly dependent on excitation wavelength (i.e., *tunable*), compounds of $R[Ag(CN)_2]_x$ are investigated in this thesis as donors for tunable energy transfer.

1.2.3 Experiments on Energy Transfer

The sharply defined energy levels of the lanthanide ions (see Figure 1.3) make them excellent acceptors for the study of energy transfer processes. For this reason, most energy transfer studies implement lanthanides as acceptors[33,34] or as both donors and

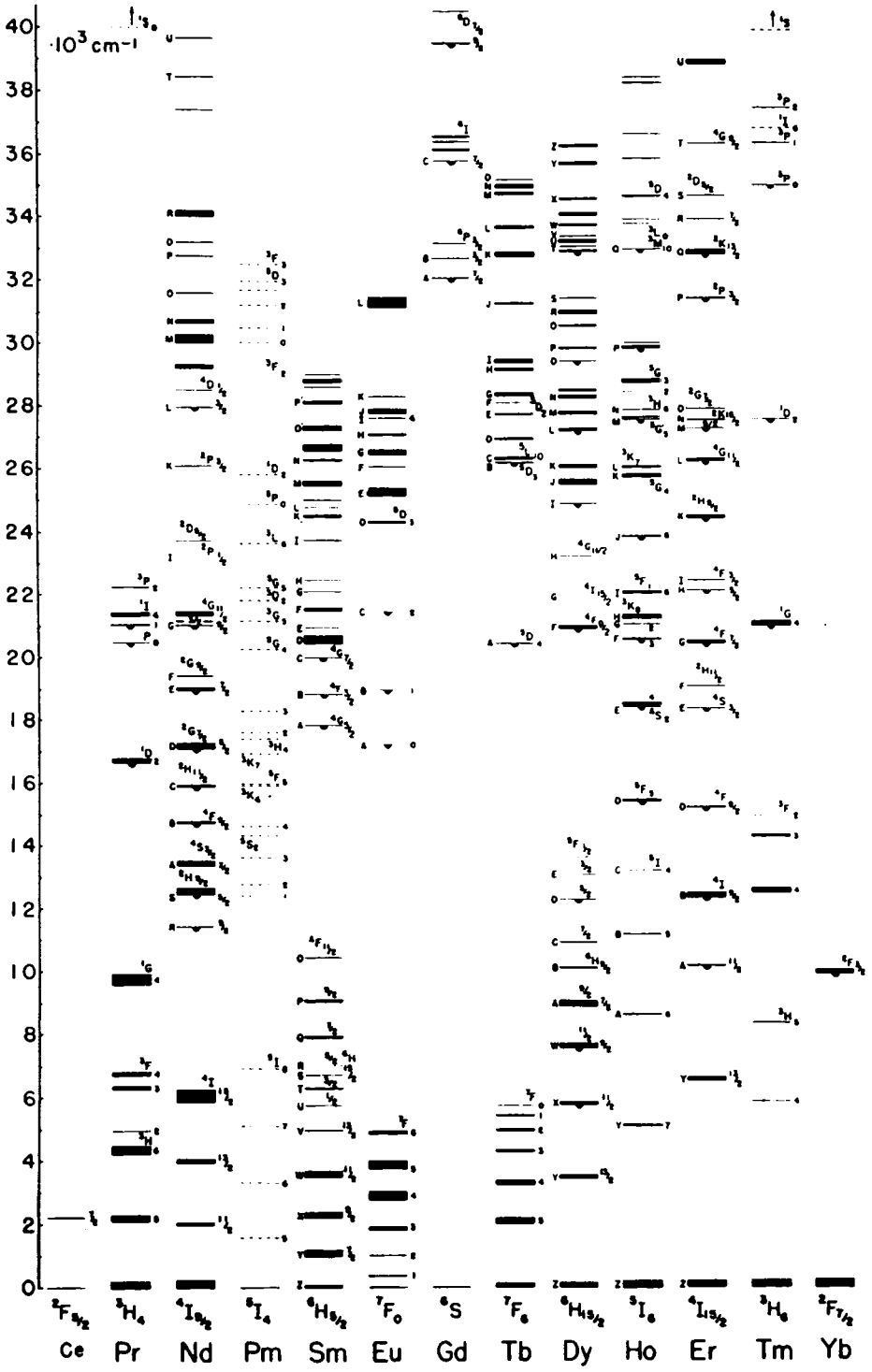

Figure 1.3: Electronic energy levels for the lanthanide ions.[2]

acceptors.[35–37] Lanthanides are also commonly employed in studies of upconversion processes where excitation at a certain energy produces emission at a higher energy.[38] For example, in Dy^{3+}-doped $CsCdBr_3$, a yellow-green luminescence can be seen upon excitation in the near infrared.[39]

1.2.4 Energy Transfer in Dicyanoargentate(I) and Dicyanoaurate(I) Compounds

The work on dicyanoargentates and dicyanoaurates is promising because these donor ions provide a method of *tuning* the energy transfer by simply changing certain physical parameters. For example, a study of $Eu[Au(CN)_2]_3$ showed that the $Au(CN)_2^-$ donor emission energy red shifts with increasing pressure[40] as well as with decreasing temperature.[41] These shifts have an effect on the spectral overlap between the donor and acceptor, which can result in a change in the efficiency of energy transfer. This is shown in an energy level diagram in Figure 1.4. The emission of $Ag(CN)_2^-$ donor ions can be tuned by simply changing the excitation wavelength due to the presence of the aforementioned exciplexes.

1.2.5 Development of Theoretical Models of Energy Transfer

By far the most widely encountered and studied mechanism of energy transfer is energy transfer via multipolar interactions. This non- radiative type of energy transfer may occur between atoms or molecules separated by over 70 Å.[24] It depends on the presence of a "spectral overlap" between the emission of the donor and the absorption

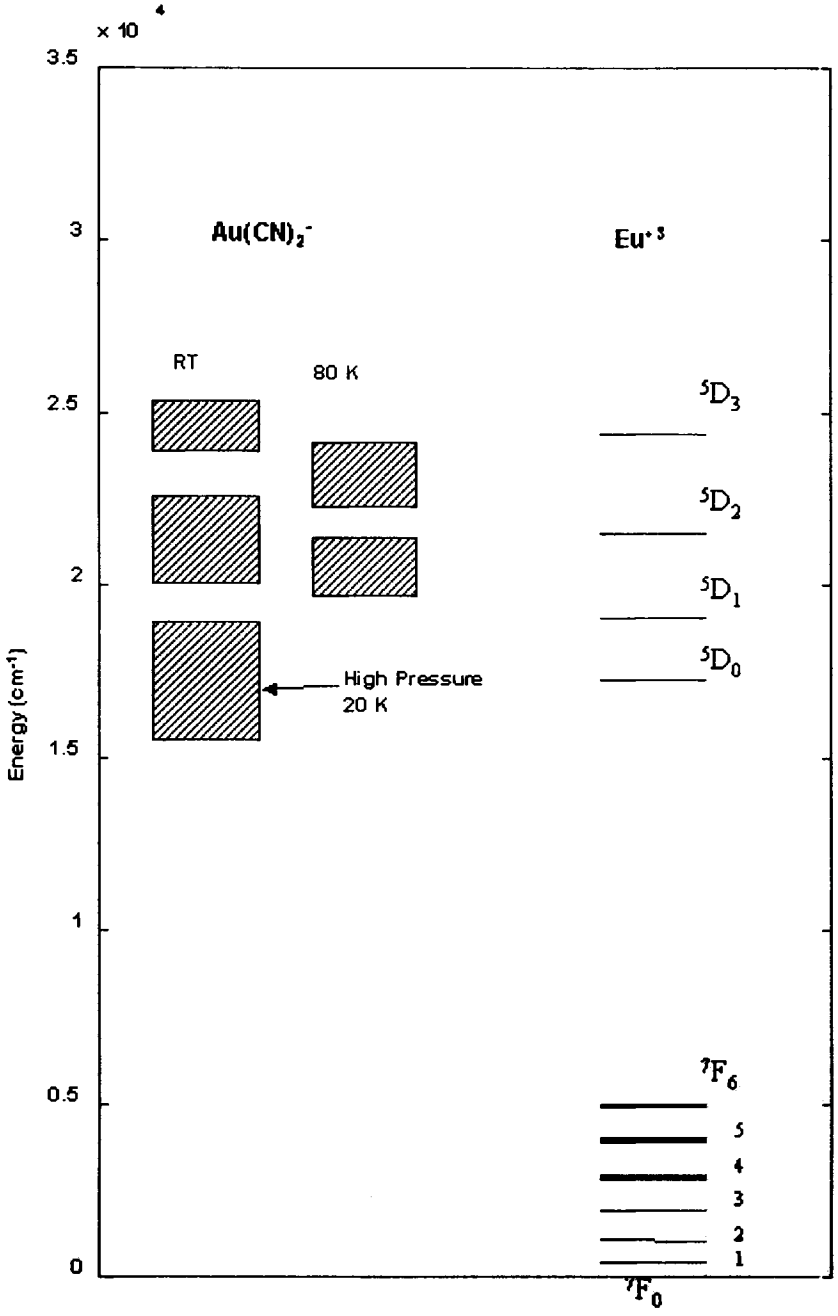

Figure 1.4: Energy level diagram for Eu^{3+} acceptor ions and $Au(CN)_2^-$ donor ions showing how the spectral overlap between the donor and acceptor changes as a function of temperature and applied pressure.

of the acceptor. One example of a multipolar interaction is an electric dipole-dipole interaction, in which the optical transitions of both donor and acceptor are allowed for electric dipole radiation. Current modeling of the multipolar interaction mechanism is based primarily on the theories of Förster[24] and Dexter,[42] which have been expanded and generalized many times over the last 45 years.[43–46] This type of transition is common in organic and biological systems, as in the case of energy transfer between $[Ru(bpy)_3]^{2+}$ and $[Os(bpy)_3]^{2+}$ in doped metal tris-oxalate network structures.[47]

While electric dipole allowed transitions are common in organic systems, energy transfer involving forbidden transitions in the acceptor have long been recognized in inorganic solids.[42] When a forbidden transition is present, accompanied by a short donor-acceptor distance, one can consider the possibility of energy transfer via the exchange mechanism. This mechanism was first proposed by Dexter[42] and further developed by Inokuti and Hiryama.[43] The exchange mechanism is also non-radiative and depends on the overlap between the atomic orbitals of the donor and acceptor.

The development of mathematical modeling of the multipolar interaction mechanism has significantly outpaced that of the exchange mechanism. Most modeling of the exchange mechanism has been purely theoretical in nature.[43,48–50] The pioneering Inokuti-Hirayama equation for energy transfer via exchange is given by:

$$I(t) = exp[-\frac{t}{\tau_0} - \gamma^{-3}\frac{c}{c_0}g(e^{\gamma}\frac{t}{\tau_0})]; g(z) = 6z\sum_{m=0}^{\infty}\frac{(-z)^m}{m!(m+1)^4} \qquad (1.2.1)$$

where c is the acceptor concentration and c_0 is a parameter called the critical transfer concentration. The first term in the exponential describes the intrinsic decay of the donor (τ_0 is the intrinsic lifetime of the donor), while the second term attempts to describe the effect of energy transfer on the luminescence decay. This model has been modified by a number of investigators.[48–51] The modifications even sparked a debate in the literature about the accuracy of one version of the model over another.[49,50] Despite these numerous attempts to modify the theory, a conclusive match between theory and experiment has yet to be reported.[50]

The structures of layered dicyanoargentates and dicyanoaurates have been well studied[21–23,52] and studies indicate a direct and close coordination between the cyanide ligand and the lanthanide ion in single crystals. For example, in $Eu[Au(CN)_2]_3$ the Eu-N separation is 2.54 Å and in $Tb[Au(CN)_2]_3$ the Tb-N separation is 2.44 Å.[21] It is not surprising, then, that the Dexter exchange mechanism is the proposed mechanism for transfer in systems such as $Eu[Au(CN)_2]_3$[40] and $Tb[M(CN)_2]_3$ (M=Au, Ag).[3]

The goal in this thesis is to determine the mechanism of energy transfer between $[M(CN)_2^-]$ ions and rare earth ions.

1.3 Mixed-Metal Compounds

The idea of studying mixed-metal compounds is not a new one. In the 1980's, Viswanath *et al.* studied mixed Pt-Pd and Pt-Ni tetracyanide quasi-one-dimensional chain structures and compared their results to those obtained from the pure systems.[53,54] They found that there existed excited states that were *delocalized* over the

Pt-Pd and Pt-Ni centers. This emission has been accurately described by a three-level model in which two of the levels arise from spin-orbit coupling for the lowest electronic state. These are proposed to be self-trapped exciton states.

Preliminary results on compounds of the type $La[Ag_xAu_{1-x}(CN)_2]_3$ are similar to the results of the Pt-Pd and Pt-Ni studies. Rather than seeing emission bands that could be attributed to either the dicyanoaurate or the dicyanoargentate, one sees emission bands whose energies lie between those of the pure systems.

2 EXPERIMENTAL METHODS

2.1 Synthesis

Many of the samples used in these studies were synthesized by Professor George Shankle at Angelo State University in San Angelo, Texas. All others were synthesized at the University of Maine. Two methods were employed for crystal growing. The $K_2Na[Ag(CN)_2]_3$ single crystals were grown in Texas by the evaporation method. Stoichiometric amounts of NaCN, KCN and AgCN were mixed in solution and allowed to evaporate. These crystals form according to the following equation, which determines the stoichiometry of the reaction:

$$2KCN + NaCN + 3AgCN \longrightarrow K_2Na[Ag(CN)_2]_3. \qquad (2.1.1)$$

The second method was used to synthesize all of the samples used in the energy transfer studies, as well as the mixed-metal samples. These crystals were grown in either commercial u-tubes or homemade glass L-shaped tubes connected by a small piece of Tygon tubing. A 1% agar gel solution was prepared by dissolving 1 g of agar powder in 100 ml of boiling water. This solution filled the bottom of the tubes. Stoichiometric solutions of the appropriate $KM(CN)_2$ (M=Ag, Au) and $Ln(NO_3)_3$ (Ln=La, Tb, Eu, Gd) were then placed above the gel on opposite sides of the tubes, as depicted in Figure 2.1. These crystals form according to the following equation,

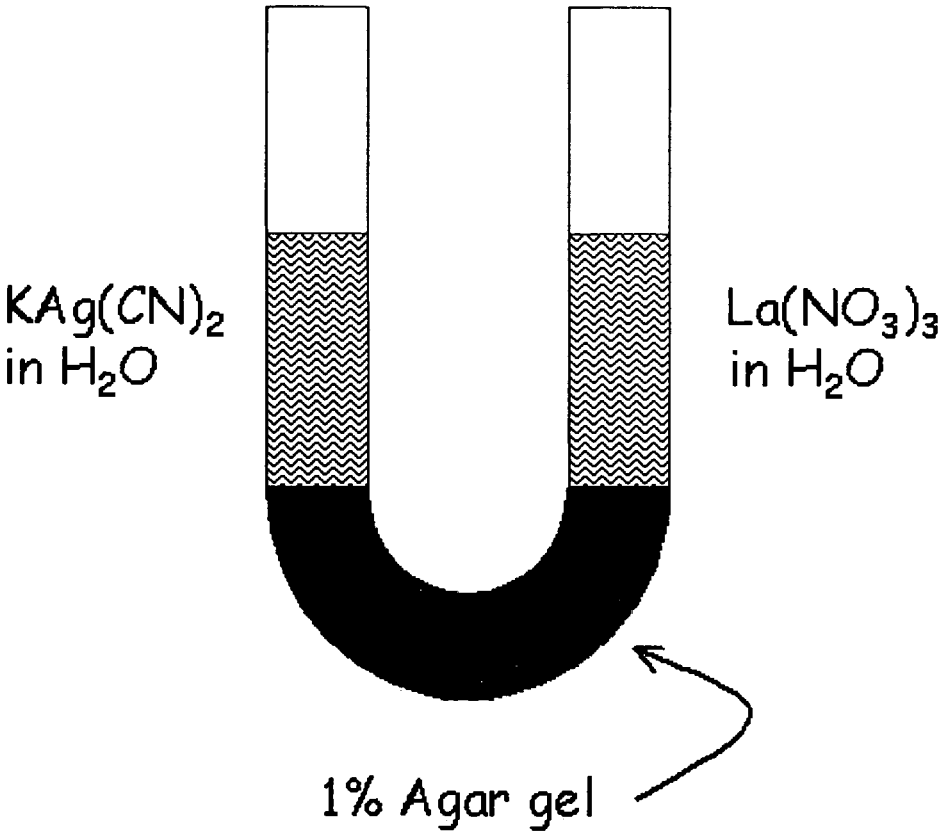

Figure 2.1: Depiction of the apparatus used to grow crystals.

which determines the stoichiometry of the reaction:

$$3KM(CN)_2 + Ln(NO_3)_3 \longrightarrow Ln[M(CN)_2]_3 + 3KNO_3 \qquad (2.1.2)$$

The solutions were placed in a hood with stoppers in both sides of the u-tubes and allowed to diffuse together. Usable crystals could be harvested within a month.

2.2 Low-Temperature Methods

Two continuous flow cryostats were employed in the studies reported herein. The first is a Model Lt–3–110 Heli-Tran cryogenic liquid transfer system modified to include a T-type thermocouple and Omega model CN132 temperature process controller. This cryostat is capable of achieving temperature values between 80 K and room temperature, with a precision of $\pm$ 1 K. The other cryostat is a Janis model ST-100 for which temperature control was achieved with a silicon diode thermocouple, digital voltmeter with a serial bus interface, a 25 Ω heater coil and a personal computer programmed to convert voltage from the silicon diode into temperature in Kelvin. The lowest temperature achieved with this cryostat is 4.4 K and the precision is greater than 0.5 K. In both systems, the sample was mounted on a copper holder using a mixture of high vacuum grease and copper dust. The copper-grease mixture has been tested and does not detectably luminesce in any of the regions of interest. Liquid nitrogen was used as the coolant for most of the low-temperature experiments. Liquid helium was used for measurements made below 80 K, using the Janis ST-100.

2.3 Vibrational Spectroscopy

Two instruments were used in collecting Raman spectra. Some of the room temperature measurements were obtained using a Renishaw Raman Imaging Microscope System 1000. Signal detection is achieved through the use of a sensitive charge coupled device (CCD) array detector. The excitation source is an SDL-XC30 diode laser, SDL Inc. It operates at a wavelength of 785 nm with a maximum power output of between 170 and 300 mW at the head. The aquisition software is WiRE/GRAMS/32C.

At low temperatures and for the remaining room temperature measurements, the experiments were carried out using the 514.5 nm line of an Innova 90–2A Argon-ion laser as the excitation source. An interference filter was used to eliminate laser plasma lines. The scattered light was collected using a Ramanor 2000M holographic double monochromator and detected with a Princeton Applied Research Model 1140 water-cooled quantum photometer. The monochromator is computer controlled and all data were recorded using a simple QBasic program that both drives the monochromator and records intensity from the photometer as a function of wavenumber.

2.4 Structural Analysis

Structural analysis was accomplished by two methods: X-ray and neutron diffraction. X-ray diffraction for $La[Ag(CN)_2]_3$ was completed through a collaboration with Dr. Richard Staples in the Department of Chemistry and Chemical Biology at Harvard University. Data were collected using a Bruker SMART CCD (charge coupled

device) based diffractometer equipped with an LT-2 low-temperature apparatus operating at 213 K. Crystals were mounted on a glass fiber using grease. Data were measured using omega scans of 0.3^o per frame for 10 seconds, such that a hemisphere was collected. A total of 2850 frames were collected with a maximum resolution of 0.75 Å. The first 50 frames were recollected at the end of data collection to monitor for decay. Cell parameters were retrieved using SMART[55] software and refined using SAINT[56] on all observed reflections. Data reduction was performed using the SAINT software which corrects for LP (laser plasma) and decay. Absorption corrections were applied using SADABS[57] supplied by George Sheldrick. The structures are solved by the direct method using the SHELXS-97[58] program and refined by a least squares method on F^2 (the corrected experimental data) by SHELXL-97,[59] incorporated in SHELXTL-PC V 5.10.[60]

Complementary high-resolution synchrotron X-ray and high-resolution neutron diffraction investigations of well crystalline powder samples of $K_2Na[Ag(CN)_2]_3$ were performed at the Swiss-Norwegian Beam Lines at the European Synchrotron Radiation Facility (SNBL/ESRF) and on diffractometer D1A at the high flux reactor of ILL, Grenoble, respectively in the temperature range from 1.5 K to 300 K. For the diffraction experiments crystallites of $K_2Na[Ag(CN)_2]_3$ were powdered and enclosed under a He gas atmosphere into thin quartz capillaries or into a container of 15 mm diameter and approximately 5 cm height in case of X-rays and neutrons, respectively.

2.5 Steady-State Luminescence

Steady state photoluminescence spectra were collected using a Photon Technology International Model QuantaMaster-1046 spectrophotometer equipped with a 75 W Xenon lamp. Wavelengths were selected with two excitation monochromators and a single emission monochromator. The instrument is interfaced with a computer and software supplied by the manufacturer was used to collect and record data. All excitation spectra were corrected for spectral variations in the lamp using the quantum counter method. In this method, raw excitation data is divided by the excitation spectrum of a "perfect" emitter, or quantum counter. For the data reported in this thesis, Rhodamine B was used as the quantum counter.

2.6 Time-Resolved Luminescence

Lifetime measurements were performed using a NanoUV diode-pumped solid state laser manufactured by Nanolase. The laser is frequency doubled twice to give an output of .43 ns pulses at 266 nm with a repetition rate of 8.1 kHz. Each pulse outputs an average power of 4.6 mW. The detection system is comprised of a McPherson Model 2051 monochromator with a Hamamatsu R1463 photomultiplier and a Princeton Applied Research model 115 wide band preamplifier. The data were collected using a LeCroy 9310 400 MHz digital oscilloscope. The decays were averaged over 500 sweeps on the oscilloscope and a minimum of ten decays were recorded for each data point.

Time-integrated spectra were collected through an interface with a personal computer. The oscilloscope was set to obtain the area under the decay curve for the desired time frame and this number was transmitted to the computer and plotted as a function of wavelength.

2.7 Data Analysis Methods

All data were analyzed using Matlab 5.0.[61] For some of the steady-state luminescence data and the Raman data for the $K_2Na[Ag(CN)_2]_3$ sample, fits of the spectra were made to two or more Gaussian functions of the form:

$$y = C + \sum_i A_i exp(\frac{(x - \overline{x}_i)^2}{2\sigma_i^2}) \tag{2.7.1}$$

where i runs from 1 to the total number of Gaussians involved in the fit. The fits were performed using a non-linear least squares fitting program designed to run under Matlab.[62] This method requires an initial estimate for all unknown parameters and will iterate until a specified degree of "goodness" is achieved. All runs return a covariance matrix of the parameters so that the error (standard deviation) could be determined. Propagation of error was performed in the usual manner. As an example, in section 5.2.2, an emission band was fit to a sum of three Gaussians. Figure 2.2 shows the raw data and the corresponding fit. The wavelengths corresponding to the band maxima were determined through the non-linear least squares method. These wavelengths were converted to energies in cm^{-1} by inversion and simple unit

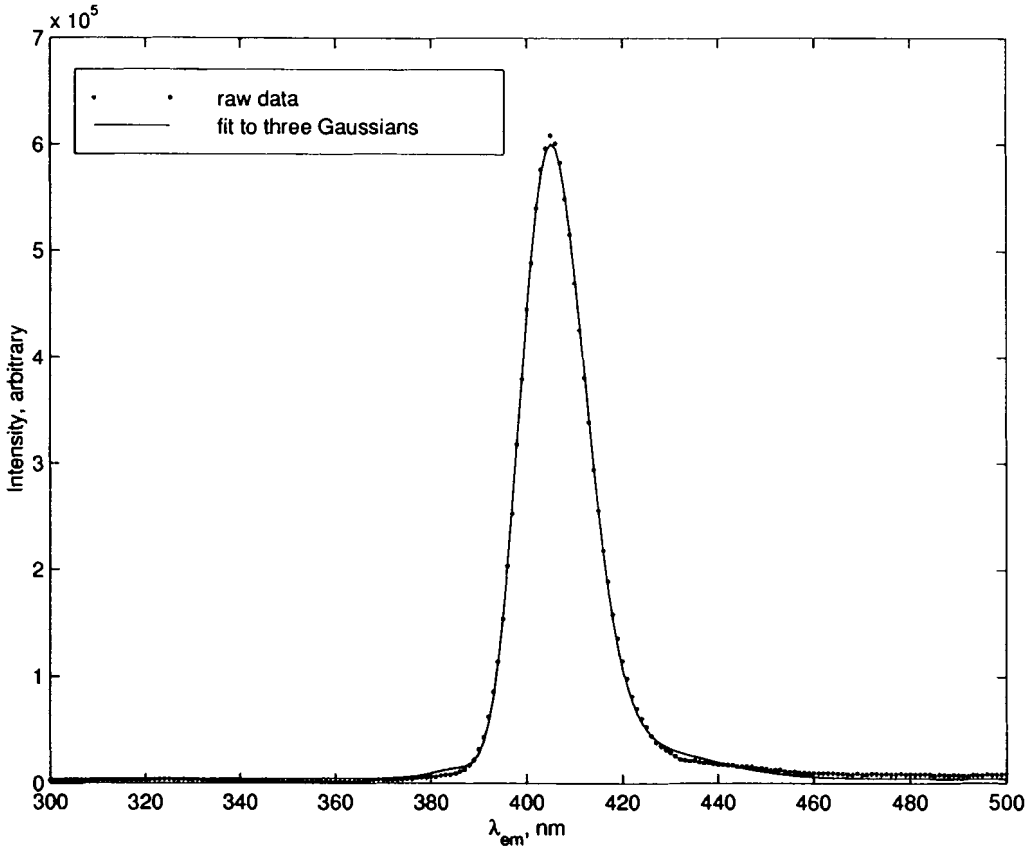

Figure 2.2: A luminescence emission band (raw data) and a fit of this data to a sum of three Gaussian functions.

conversion. The error was propagated by taking the percent error in the wavelength values and then using the same percent error to get the deviation for the wavenumber values.

To determine lifetime values, two methods were employed. The lifetime value(s) of an excited state can be obtained from the following equation for intensity as a function of time:

$$I = \sum_i I_{0i} e^{-t/\tau_i} \tag{2.7.2}$$

where the sum runs from 1 to the total number of components. When $i = 1$, the decay is a single exponential. Simply taking the natural logarithm of both sides returns the equation of a line:

$$ln(I) = ln(I_0) - \frac{t}{\tau} \tag{2.7.3}$$

and a plot of t vs. $ln(I)$ will have a slope of $-\frac{1}{\tau}$.

When $i > 1$, however, this method clearly fails. This is evidenced in the data as a nonlinear t vs. $ln(I)$ curve. In these instances, the non- linear least squares fitting method is again employed. As a general rule, no more than two components are expected. In cases where energy transfer plays a role, the decay does not follow equation 2.7.2, but rather a more complex function. This subject will be discussed in detail in Chapter 4.

3 OPTICAL STUDIES OF $K_2Na[Ag(CN)_2]_3$: EVIDENCE FOR A NOVEL TYPE OF PHASE TRANSITION

3.1 Introduction

Single crystals of $K_2Na[Ag(CN)_2]_3$ have been observed to display luminescence thermochromism, an optical phenomenon in which different emission bands occur at different temperature values.[10,63] The photoluminescence spectra of $K_2Na[Ag(CN)_2]_3$ show two emission bands: a lower energy (LE) blue emission with a maximum around 410 nm and a higher energy (HE) ultraviolet emission with a maximum near 315 nm.[13] As shown in Figure 3.1, luminescence thermochromism is observed upon increasing the temperature from 10 K to room temperature. The HE band dominates at 10 K, but upon increasing temperature, the LE band increases in intensity to become the dominant emission at 80 K. As the temperature is further increased, the HE band again becomes the dominant emission while the LE band becomes again less prominent. One possible explanation for this behavior is that the system undergoes a structural change near 80 K, which leads to a change in the distribution of the clusters responsible for the luminescence bands. For this reason, structural studies were undertaken and the results will be presented in this chapter. The results did not indicate changes near 80 K, rather at a higher temperature, at about 210 K, where the luminescence disappears.

Further study, including lifetime measurements, has led to a different explanation for the luminescence thermochromism in this crystal. A kinetic model for energy

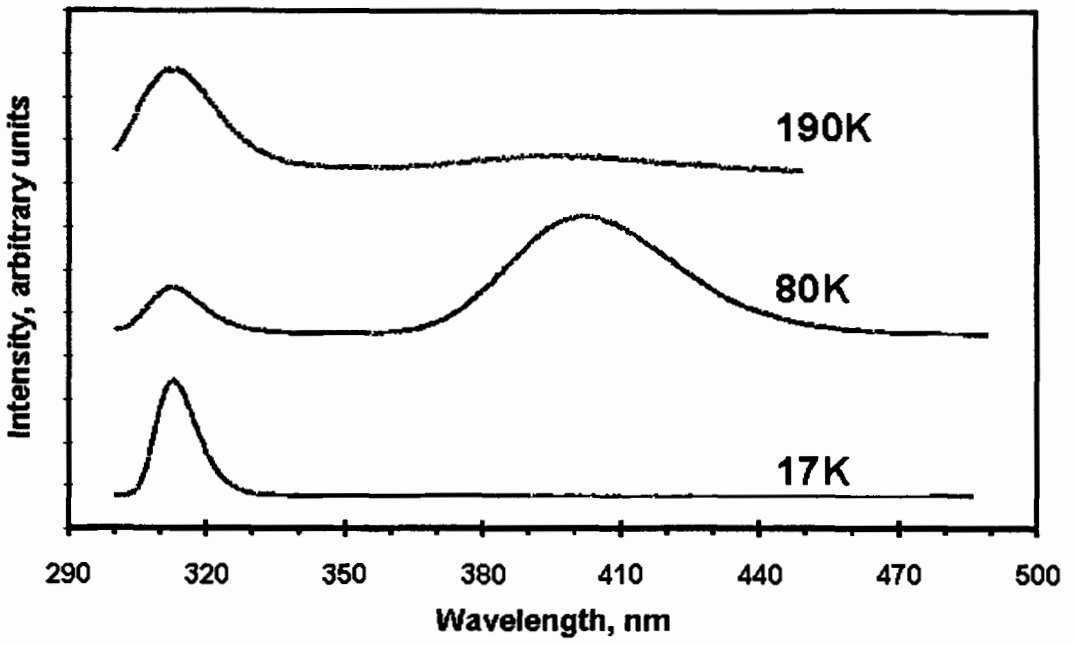

Figure 3.1: Emission spectra for $K_2Na[Ag(CN)_2]_3$ showing changes in the two luminescence bands.

transfer between the two luminescence bands will be presented with strong supporting evidence from the luminescence decay results.

The structure of $K_2Na[Ag(CN)_2]_3$ has previously been determined at room temperature by means of single crystal X-ray diffraction, corresponding to space group $P\bar{3}1m$.[64] However, since the initial luminescence data suggest structural variations, variable temperature Raman scattering, specific heat, synchrotron X-ray and neutron powder diffraction studies have been conducted to further investigate the chemical structure of this compound in the temperature range from 1.5 K to 300 K. Results from these investigations will be presented in this chapter.

Phase transitions in other dicyanoargentates (I) have previously been investigated through pressure dependent Raman scattering studies. For example, the vibrational

spectra of $KAg(CN)_2$ are well-documented in the literature,[15,18,19] as are pressure dependent spectra.[17,20] However, this is the first reported temperature dependent Raman scattering study of structural changes in a dicyanoargentate.[23]

3.2 Raman Scattering Studies

Representative Raman spectra at selected temperature values are shown in Figures 3.2 and 3.3. The $Ag(CN)_2^-$ ions are virtually linear in the crystal, with the C–Ag–C angle reported as 180° and the N–C–Ag angle as 176.65°.[64] Approximating this as a linear ion, we assign it to the space group $D_{\infty h}$. The vibrational modes of a linear A–B–C–B–A type molecule have been worked out previously[15] and the notation used in that reference will be followed here. Frequency assignments are given in Table 3.1.

ν(RT, cm^{-1})	ν(80K, cm^{-1})	Assignment	Representation	Mode
75 96 114	75 101 114	phonons		
146	154	ν_{7a}	Π_u	Ag-C bend
147	171	ν_{7b}	Π_u	Ag-C bend
255	258	ν_{5a}	Π_g	C-N bend
265	268	ν_{5b}	Π_g	C-N bend
365	365	ν_2	Σ_g^+	Ag-C stretch
2144	2148	ν_1	Σ_g^+	C-N stretch

Table 3.1: Assignments for the vibrational frequencies in the Raman spectrum of $K_2Na[Ag(CN)_2]_3$.

Examining the low frequency region of the spectrum, the splitting of the C–N bending mode (ν_5, ~265 cm^{-1}) at low temperature values is noted. To further investigate this splitting, a nonlinear least squares fitting routine was applied to fit

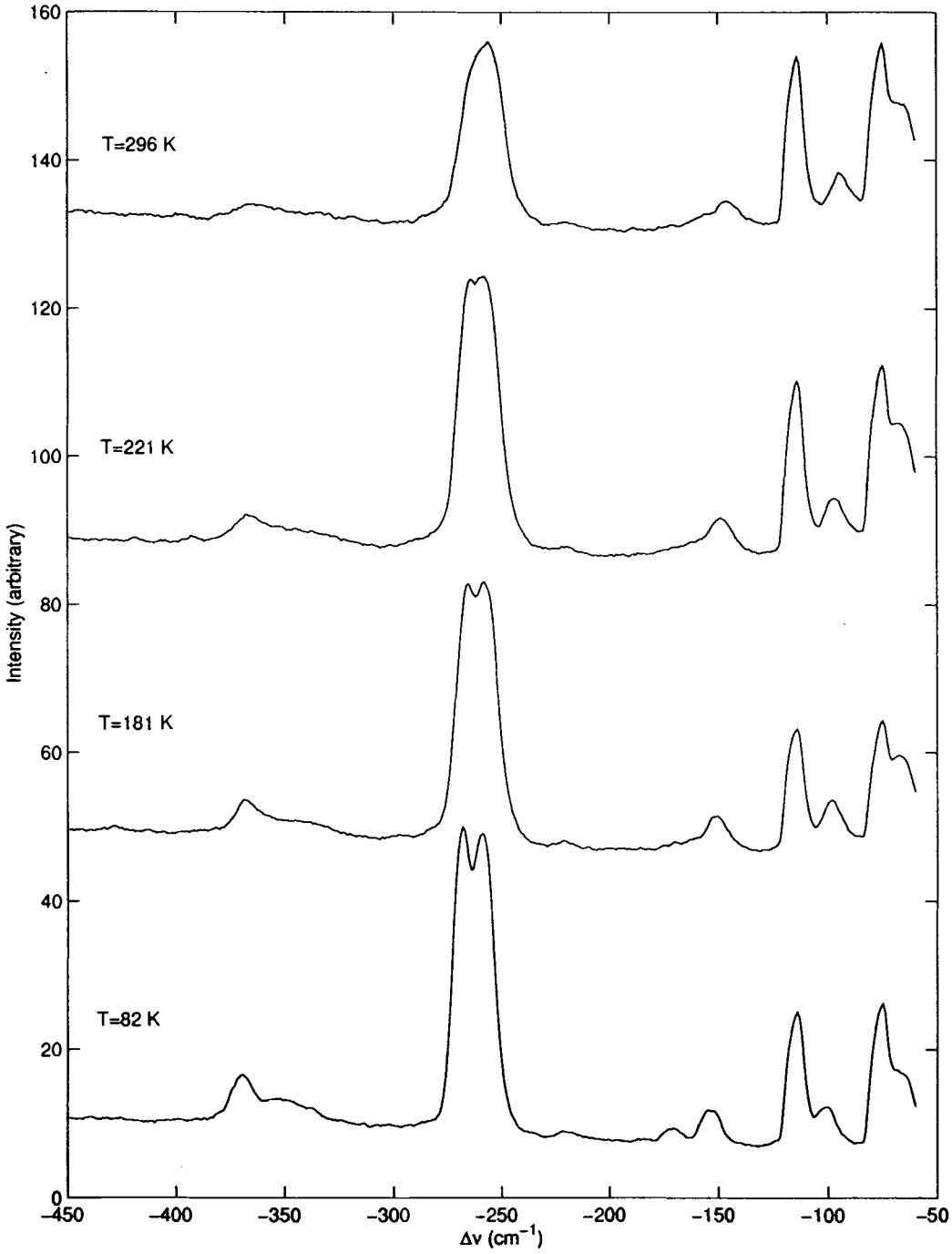

Figure 3.2: Raman shift vs. intensity for T=82 K, 181 K, 221 K, 296 K. The plots are offset by 40 units each for clarity.

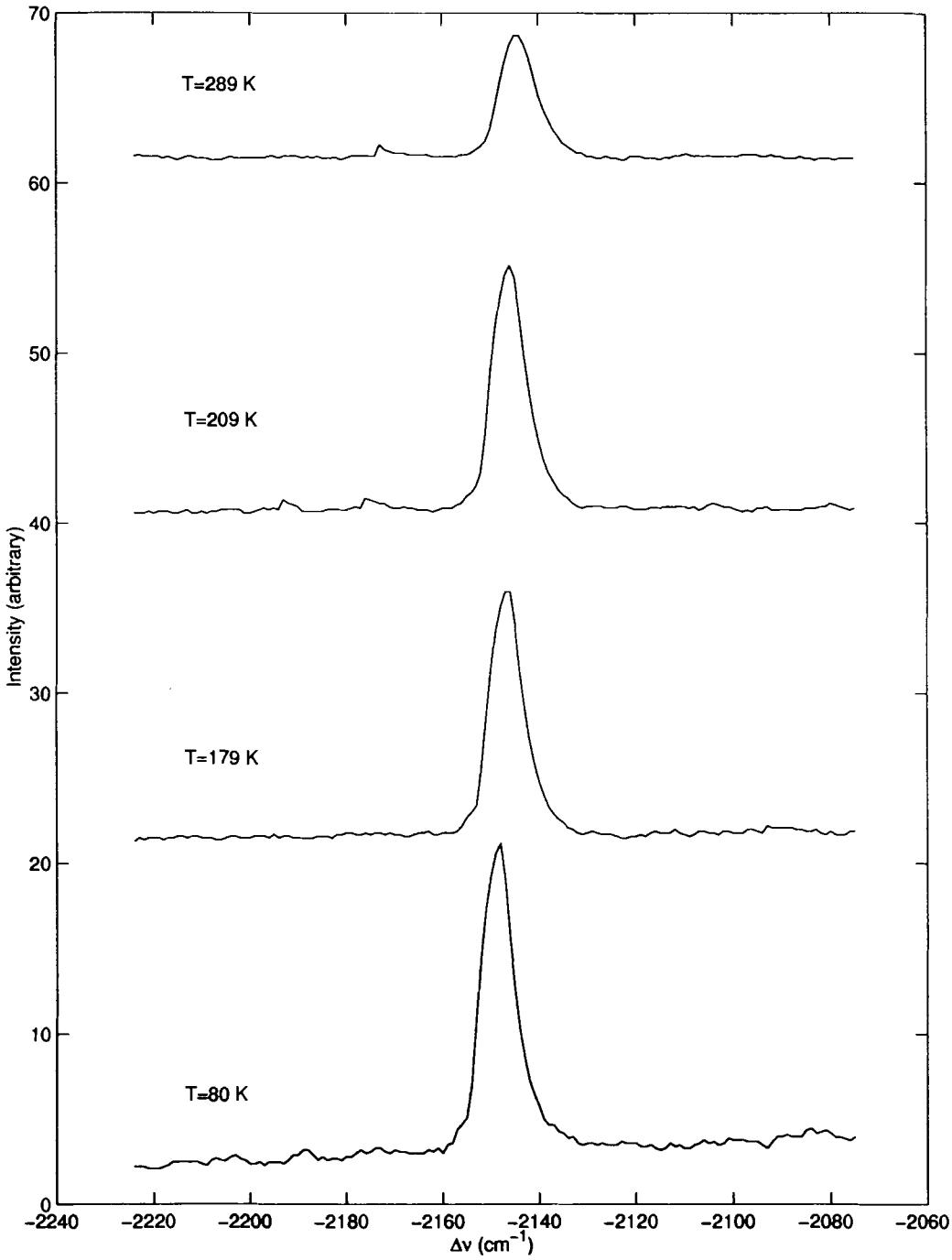

Figure 3.3: Raman shift vs. intensity for T=80 K, 179 K, 209 K, 289 K. Plots are offset by 20 units each for clarity.

the data to a sum of two Gaussian functions on a quadratic background, yielding frequencies for each of the two peaks. Figure 3.4 shows a plot of the relative frequency,

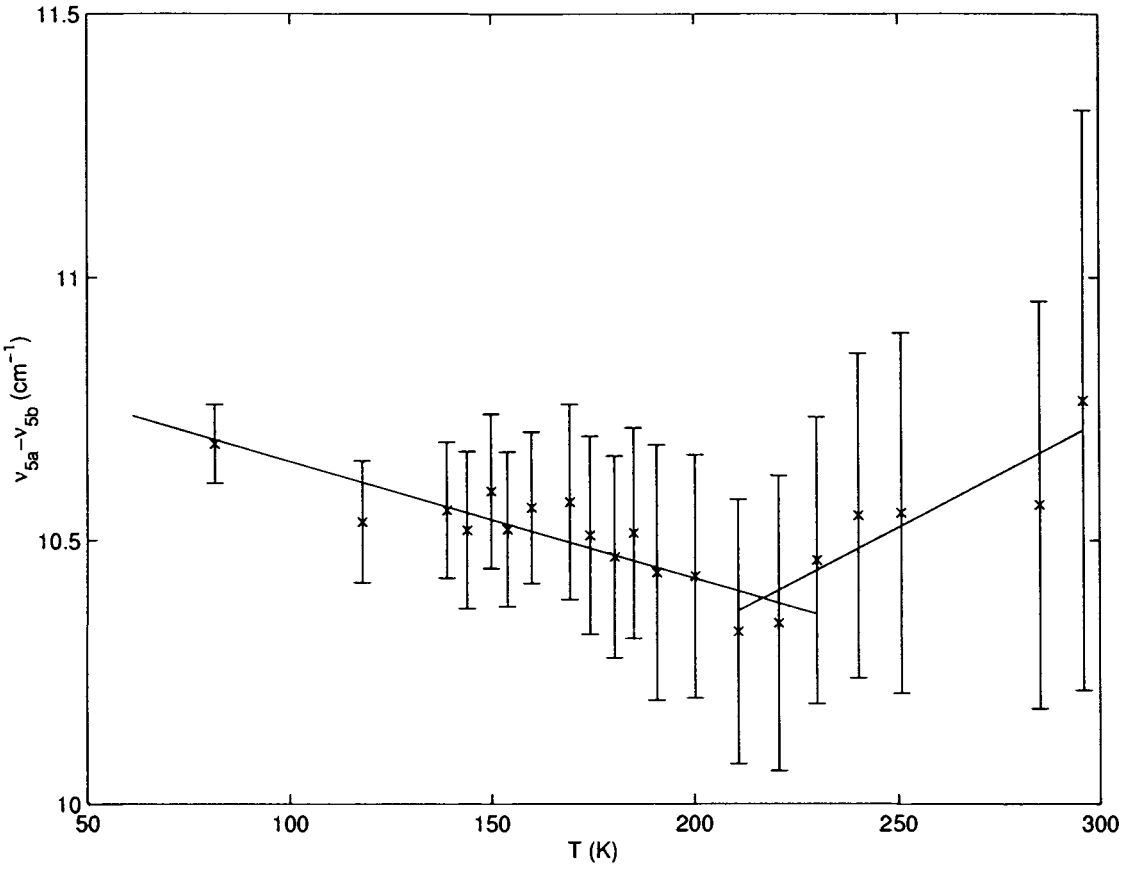

Figure 3.4: Relative energy of the split peaks in the C–N bending mode as a function of temperature.

$\nu_{5a} - \nu_{5b}$, as a function of temperature. It is noted that the peaks grow closer together until approximately 210 K at which point they begin to grow steadily further apart. The error associated with each point increases significantly at higher temperature values due to the overlapping of the peaks. Since the change is so slight and the error

is so great, we expect there to be a fair amount of uncertainty in the point of interest, 210 K, which is where structural changes are expected.

Figure 3.5 shows the position as a function of temperature of the five lowest energy

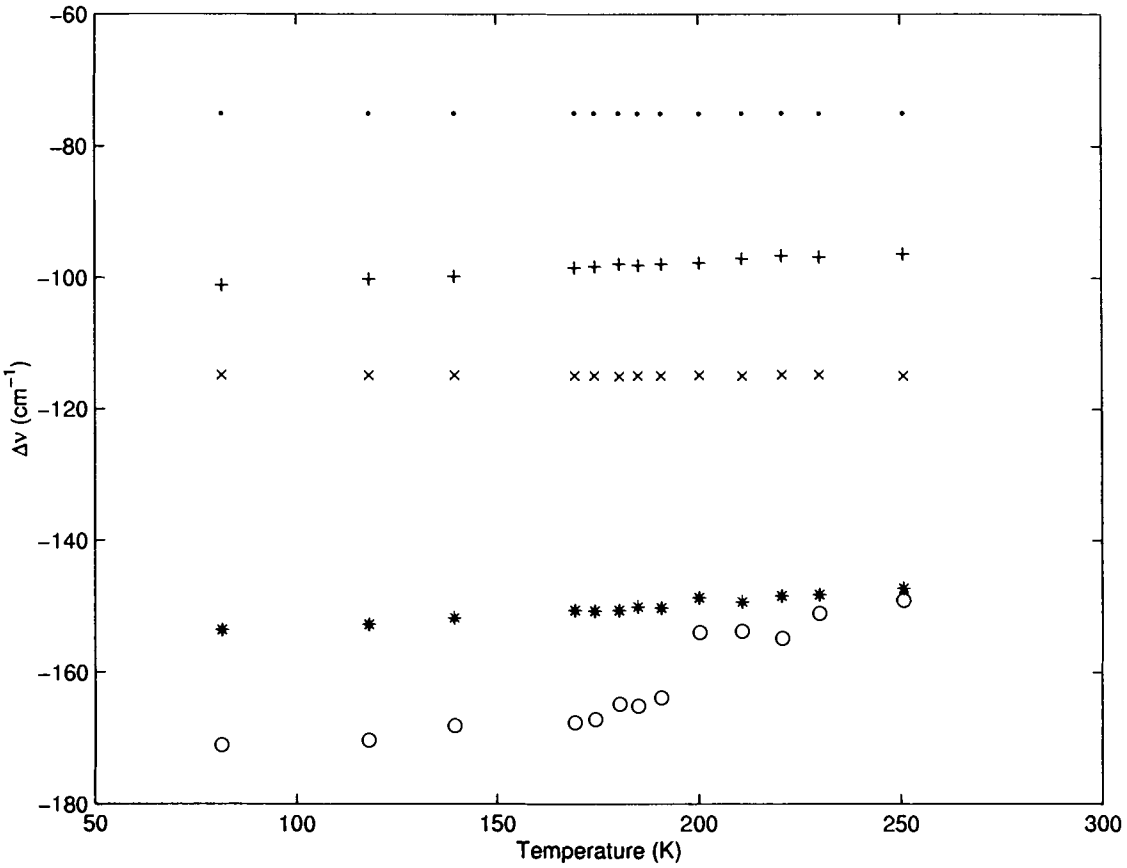

Figure 3.5: Frequencies of five low energy bands as a function of temperature.

bands resolved, three of which we have assigned as phonon bands. One of these three phonon bands experiences a small, continuous increase in energy with decreasing temperature values. However, the highest energy band in this group (open circles in the figure) exhibits a discontinuous jump of 10 cm^{-1} at $\sim$200 K, with a total shift of $\sim$24 cm^{-1} in going from 80 K to room temperature. This behavior has led us

to assign this highest energy pair to the typically Raman-inactive C–Ag–C bending mode (ν_7, Π_u). This assignment is in agreement with that of Loehr[19] and Bottger[18] from their studies of the similar compound $KAg(CN)_2$.

The C–N stretching mode (ν_1, $\sim$2150 cm^{-1}), however, does not exhibit any splitting over the entire temperature range studied. It does undergo a small, apparently continuous increase in energy as the temperature decreases, with a total shift of $\sim$5 cm^{-1}.

The very weak Ag–C stretching mode (ν_2, $\sim$360 cm^{-1}) appears to split at low temperature values. Analysis of this splitting reveals three closely spaced peaks. Preliminary examination of the frequency shifts of these three peaks reveals that the highest energy peak ($\sim$365 cm^{-1}) exhibits behavior similar to that of the C–N stretching mode, shifting a total of approximately 5 cm^{-1} between 80 K and 296 K. However, the other two peaks, which are vanishingly weak at higher temperature values, behave in a manner similar to that of the bending modes, with a discontinuity in the region of 200-220 K. This suggests that this is not one mode split into three peaks, but perhaps two separate modes. Following the findings of Loehr,[19] we tentatively assign the two lower energy peaks in this group to the typically Raman-inactive asymmetric bending mode, ν_6, Π_u and the highest energy peak to the previously mentioned stretching mode ν_2, Σ_g^+.

The discontinuous behavior in the bending modes in the region of 200-220 K indicates structural variations in this temperature range. It is suspected that the

different patterns of behavior in the stretching and bending modes (continuous as opposed to discontinuous variations) is related to the changes in the lattice parameters as a function of temperature.

3.3 X-Ray and Neutron Scattering Results

Characteristic results of the neutron and X-ray diffraction experiments are illustrated in Figure 3.6. Because of rather large preferred orientation effects in the D1A measurements with stationary sample profile matching, fits were first performed both for neutrons and X-rays with program FullProf[65] to obtain the temperature dependencies of the lattice parameters. Although the crystallinity of the powder sample of $K_2Na[Ag(CN)_2]_3$ proved to be very good in the synchrotron X-ray measurements, the small deviations from trigonal symmetry are only reflected in slightly larger peak widths of trigonal Bragg reflections such as (hk0) compared to (001), as space group $P\bar{3}1m$ does not impose extinction rules. This is presumably the reason why automatic peak indexing of the first 20 lines by programs such as DICVOL91 of e.g. the 40 K X-ray data was less conclusive, also suggesting the trigonal lattice as a possible solution. Anisotropic peak broadening was therefore also considered a possibility. However, in view of the optical results showing evidence for a structural phase transition in the region of 200-220 K, this idea was abandoned and it is believed that the true symmetry of $K_2Na[Ag(CN)_2]_3$ is monoclinic at least at temperature values below 210 K, but the synchrotron X- ray data point to at least orthorhombic symmetry at room temperature.

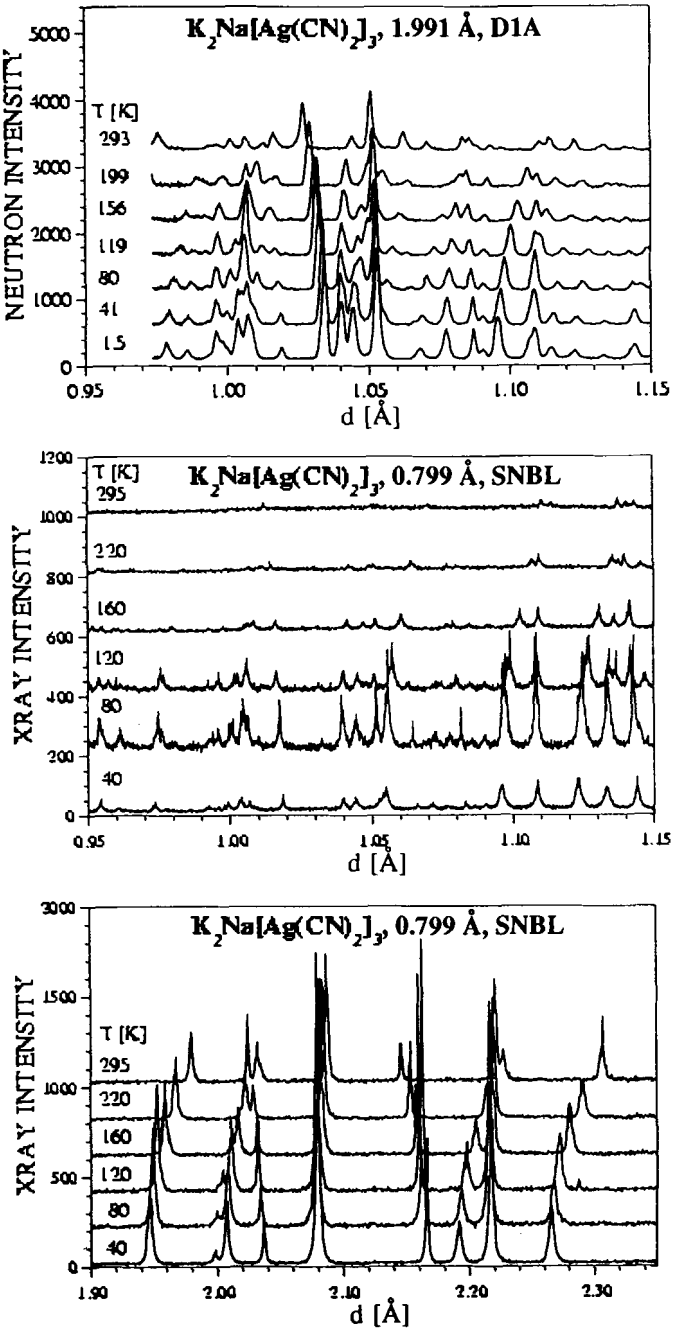

Figure 3.6: Comparison of temperature dependent neutron and SNBL X-ray diffraction data for $K_2Na[Ag(CN)_2]_3$.

The high-resolution neutron diffraction and synchrotron X-ray powder data measured at sample temperature values from 1.5 K to 300 K were analyzed using the profile constrained structural refinement computer program ZOMBIE based on the Rietveld refinement method,[66].[67] The $Ag(CN)_2^-$ ions were constrained to be linear with interatomic distances Ag–C and C–N kept constant at essentially those distances found in the previously reported single crystal X-ray diffraction study at room temperature.[64] It was found that although the previously reported structure with space group $P\bar{3}1m$[64] gave good agreement with the observed profile data, small but significantly better agreement could be obtained for a monoclinic structure with space group C2/m. The relationship between the $P\bar{3}1m$ structure and the now proposed C2/m structure is shown in Figure 3.7. The pseudo-hexagonal unit cell (Z=1) for the $P\bar{3}1m$ structure and the monoclinic unit cell (Z=2) for the C2/m structure are closely related. The resulting layered structure is illustrated in Figure 3.8.

3.3.1 Monoclinic (C2/m)

The interatomic distances between the neighbouring Ag-atoms, and unit cell dimensions, are shown in Tables 3.2 & 3.3, respectively, for sample temperature values between 40 K and 295 K. Coordinates of equivalent (silver) positions are:

$(0,0,0;\frac{1}{2},\frac{1}{2},0)+$

Ag(1): $(0,\frac{1}{2},0)$; site symmetry (2/m) $\rightarrow$ 2 atoms per (monoclinic) unit cell

Ag(2): $(\frac{1}{4},\frac{1}{4},0);(\frac{1}{4},\frac{3}{4},0)$; site symmetry $(\bar{1})$ $\rightarrow$ 4 atoms per (monoclinic) unit cell.

Monoclinic (C2/m)

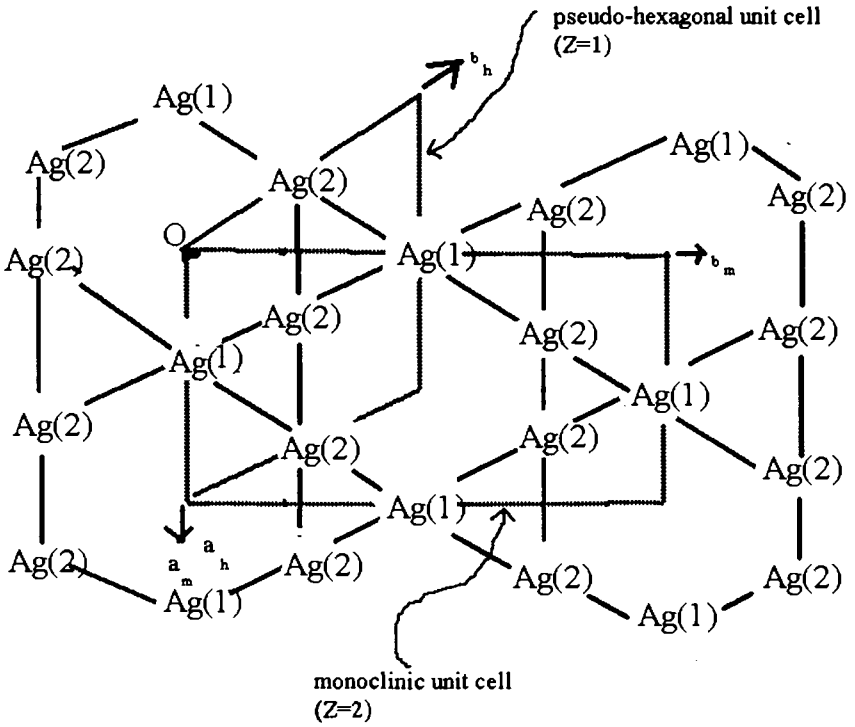

Figure 3.7: Relationship between the monoclinic unit cell for the C2/m structure and the pseudo-hexagonal unit cell for the P$\bar{3}$1m atomic structure (for clarity, only the Ag atoms are shown).

3.3.2 Pseudo-hexagonal (trigonal) P$\bar{3}$1m

The relationship between the monoclinic unit cell (C2/m) and the pseudo-hexagonal unit cell is given by:

$$a_h = a_m; b_h = \frac{1}{2}\sqrt{(a_m^2 + b_m^2)}, c_h = c_m,$$

$$\alpha_h = 90°, \beta_h \approx 90°, \gamma_h = 90° + tan^{-1}\left(\frac{a_m}{b_m}\right)$$

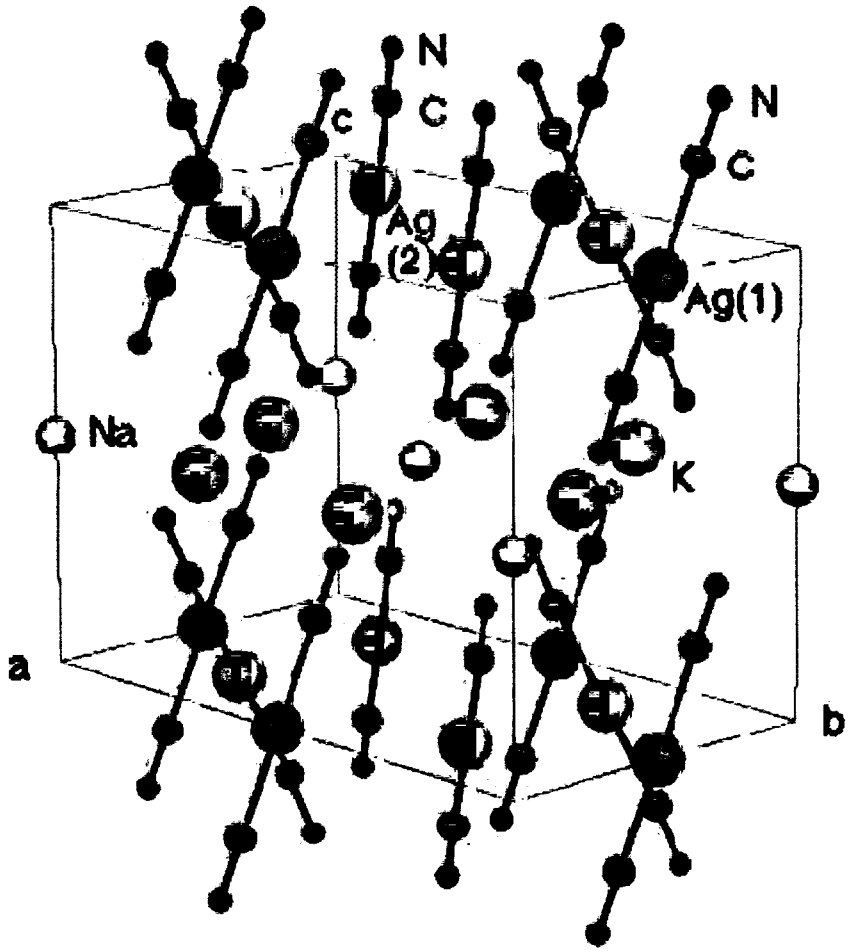

Figure 3.8: 30 K structural model of $K_2Na[Ag(CN)_2]_3$.

It is noted that the pseudo-hexagonal (trigonal) structure would become actual hexagonal (trigonal) with space group $P\bar{3}1m$, if the following relationships are satisfied:

$$a_h = a_m = b_h = \left(\frac{1}{\sqrt{3}}\right) b_m, c_h = c_m,$$

$$\alpha_h = \alpha_m = 90°, \beta_h = \beta_m = 90°, \gamma_h = 90° + tan^{-1}\left(\frac{a_m}{b_m}\right) = 120°$$

T (K)	Ag(1)...Ag(2) (Å)	Ag(2)...Ag(2′) (Å)	
40	3.46192(3)	3.45805(3)	Ag(1)...Ag(2)>Ag(2)...Ag(2′)
80	3.46641(3)	3.46222(4)	"
120	3.47247(4)	3.46870(5)	"
160	3.48502(3)	3.48146(4)	"
220	3.49818(3)	3.50208(3)	Ag(1)...Ag(2)<Ag(2)...Ag(2′)
295	3.52232(4)	3.52535(5)	"

Table 3.2: Interatomic Ag...Ag distances as a function of temperature for the C2/m structural model for $K_2Na[Ag(CN)_2]_3$.

T (K)	a_m (Å)	b_m (Å)	c_m (Å)	β(°)
40	6.91610(6)	11.99690(11)	8.66420(6)	90.026(2)
80	6.92445(9)	12.01281(15)	8.65184(8)	90.039(2)
120	6.93740(9)	12.03333(16)	8.63869(8)	90.036(2)
160	6.96292(8)	12.07656(14)	8.63117(8)	89.978(2)
220	7.00415(6)	12.11355(11)	8.61212(7)	89.969(2)
295	7.05070(10)	12.19818(18)	8.58368(9)	90.035(2)

Table 3.3: Unit cell dimensions as a function of temperature for the C2/m structural model, as determined from synchrotron X-ray data for $K_2Na[Ag(CN)_2]_3$.

The two site symmetries for C2/m would both become (2/m) and

$$\text{Ag(1)...Ag(2)} = \text{Ag(2)...Ag(2')} = \frac{1}{2}a_h = \frac{1}{2}b_h.$$

From Tables 3.2 and 3.3, this closely occurs when T=200 K and the Ag-atom environments become essentially identical (Figure 3.7).

Coordinates of equivalent Ag-atom positions are:

Ag(1)≡Ag(2); $\frac{1}{2}, 0, 0; 0, \frac{1}{2}, 0; (2/m) \rightarrow$ 3 atoms per (hexagonal) unit cell.

Both Figure 3.6 and the corresponding lattice parameters, which are shown in Table 3.3 and Figure 3.9, indicate essential, continuous changes of the chemical struc-

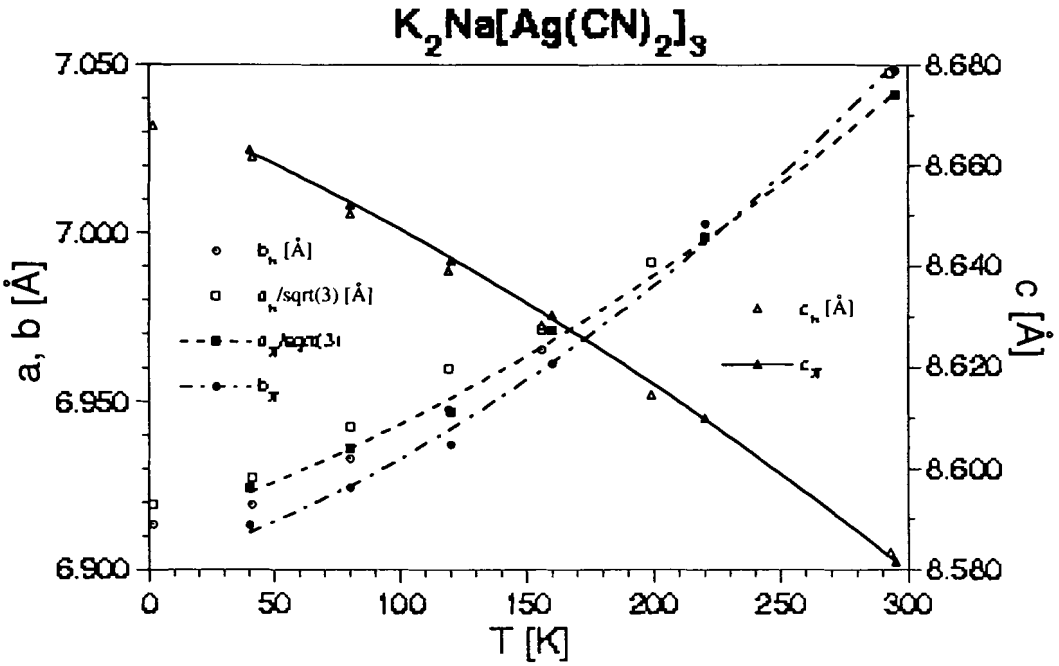

Figure 3.9: Temperature dependence of pseudo-hexagonal lattice parameters of $K_2Na[Ag(CN)_2]_3$, as determined by profile matching.

ture as a function of temperature in the range from 1.5 K to 300 K. However, the c-lattice parameter increases anomalously with decreasing temperature.

Apart from a possible slight change in slope around 150 K, the specific heat data of $K_2Na[Ag(CN)_2]_3$ do not indicate a traditional structural phase transition.

3.4 Group Theory Analysis

The synchrotron X-ray and neutron diffraction studies indicate that the crystal belongs to space group $C2/m$ at all temperature values except the transition temperature (approximately 220K) at which point it belongs to space group $P\bar{3}1m$. In the $C2/m$ unit cell, there are six $[Ag(CN_2)]^-$ ions, two of which are located at sites of symmetry C_{2h} and four of which are located at sites of symmetry C_i. In the $P\bar{3}1m$

unit cell, there are three $[Ag(CN_2)]^-$ ions, all of which are located at sites of symmetry C_{2h}.

Close inspection of the correlation diagrams (Tables 3.4 & 3.5) for the previously mentioned site symmetries under space group $C2/m$ reveals several relevant pieces of information. There is no indication that any of the modes which are not Raman active under $D_{\infty h}$ would become Raman active in the lower symmetry of the unit cell (C_{2h}). This clearly counterindicates the presence of the C-Ag-C bending mode, ν_7. Also, it is clear that the doubly degenerate C-N bending mode (ν_5, Π_g) is no longer degenerate under either of the site symmetries. The splitting seen in the Raman spectra of this mode may therefore be attributed to the lifting of this degeneracy. The splitting of the C-Ag-C bending mode could also be explained in a similar manner.

However, comparing the two Raman-active stretching modes, ν_1 and ν_2, we see what is apparently anomalous behavior. It is clear from the Raman scattering data that the C-N stretching mode (ν_1) does not exhibit any splitting, while the Ag-C stretching mode (ν_2) appears to have three components. Examining the correlation diagrams for these modes, we see that there is no splitting indicated due to site

Modes	Ion ($D_{\infty h}$)	Site (C_{2h})
ν_1, ν_2	$\underline{\Sigma_g^+} \longrightarrow$	$\underline{A_g}$
ν_5, R_x, R_y	$\underline{\Pi_g} \Longrightarrow$	$\underline{B_g}$
ν_3, ν_4, T_z	$\Sigma_u^+ \longrightarrow$	A_u
ν_6, ν_7, T_x, T_y	$\Pi_u \Longrightarrow$	B_u

Table 3.4: Correlation diagram for $[Ag(CN)_2]^-$ under site symmetry C_{2h}. Raman active modes are underlined. Further correlation to the unit cell is unnecessary as the unit cell is also of symmetry C_{2h}.

Modes	Ion ($D_{\infty h}$)		Site (C_i)		Unit Cell (C_{2h})
ν_1, ν_2	$\underline{\Sigma_g^+}$				$\underline{A_g}$
ν_5, R_x, R_y	$\underline{\Pi_g}$	$\searrow \Longrightarrow \nearrow$	$\underline{A_g}$	$\nearrow \longrightarrow \searrow$	$\underline{B_g}$
ν_6, ν_7, T_x, T_y	Π_u	$\Longrightarrow$	$\underline{A_u}$	$\longrightarrow$	A_u
ν_3, ν_4, T_z	Σ_u^+				B_u

Table 3.5: Correlation diagram for $[Ag(CN)_2]^-$ under site symmetry C_i. Raman active modes are underlined.

symmetry in either case, while the sites with C_i symmetry do show potential splitting due to molecular interactions within the unit cell. While this might account for the degree of multiplicity within the ν_2 stretching mode, it does not explain the lack of splitting in the ν_1 mode.

As this ion is not *perfectly* linear, it is prudent to consider the symmetry reduction for the C_{2v} group, corresponding to a bent A-B- C-B-A type molecule. In this case, the *sites* have a higher symmetry than the ion. Under C_{2v}, the C-N and Ag-C bending modes are no longer degenerate as there exists in plane and out of plane bending modes. Only the in plane bending modes are expected to be Raman active, while the out of plane bending modes would be IR active.

3.5 Lifetime Results

Lifetimes for both the HE and LE bands were obtained as a function of temperature between 4.4 K and 190 K and are tabulated in Table 3.6. The luminescence was too weak to obtain reliable results at temperature values higher than 150 K.

T, K	313 nm band lifetime, μs	T, K	403 nm band lifetime, μs
4.4	1.10 (.02)		
8.0	1.00 (0.05)		
11.0	0.87 (0.02)	11.5	57.6 (1.3)
15	0.76 (0.02)	15	55.2 (0.7)
18	0.84 (0.01)	20	60.9 (1.3)
42	0.56 (0.02), 2.3 (0.2)	42	44.3 (1.8)
62	2.2 (0.2)	62	33.1 (4.4)
86	5.3 (0.1)	86	20.8 (0.1)
148	4.6 (0.1)	148	6.4 (0.1)

Table 3.6: Lifetimes as a function of temperature for the two luminescence bands present in $K_2Na[Ag(CN)_2]_3$.

The LE (402 nm) band has a purely single exponential decay at all temperature values. In contrast, however, the HE (313 nm) band exhibited a dual exponential decay at 40 K, but a single exponential at all other temperature values. All lifetime values were on the order of microseconds, indicating that both of the bands are the result of decay from triplet states to the singlet ground state.

It is proposed that the changes in the luminescence spectra are due to energy transfer from the HE band to the LE band between 4 K and 60 K, followed by back energy transfer from the LE band to the HE band between 60 K and 190 K. This is supported by the lifetime data as the lifetime of the higher energy band first decreases (when energy transfer grows in) and then increases (when back transfer begins to play a role). Figure 3.10 shows the proposed kinetic model. Part (a) shows the major pathway at 4 K where only the higher energy band is present, excitation of the higher energy band followed by emission from a triplet state. The presence of only one band at this temperature is due to the fact that energy transfer processes

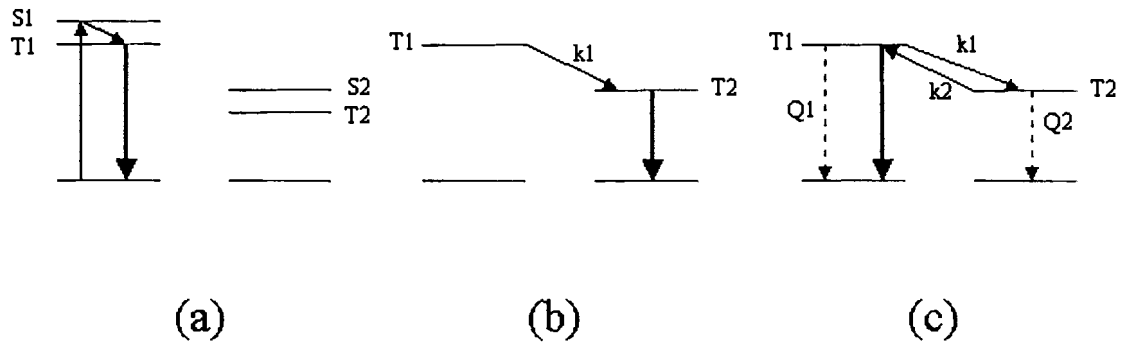

Figure 3.10: Kinetic model for luminescence in $K_2Na[Ag(CN)_2]_3$. The parts of the figure are explained in detail in the text.

are non-radiative in nature and therefore are strongly dependent on temperature. At lower temperature values, the energy transfer is effectively turned off. Part (b) shows the additional pathways present between 4 K and 60 K where forward energy transfer from the higher energy band to the lower energy band dominates. The symbol "k1" represents the rate of energy transfer from the higher energy band to the lower energy band. Part (c) shows the additional pathways between 60 K and 150 K (and possibly above), where back energy transfer (also a non-radiative process) plays a role. The symbol "k2" represents the rate of back-energy transfer from the lower energy band to the higher energy band. At temperature values above 200 K, non-radiative decay processes dominate and the emission is completely quenched. The rate of quenching is represented by the symbols "Q1" and "Q2" and is depicted in the Figure as dashed lines. The heavier lines indicate radiative emission.

In the case of the back-transfer, one must consider whether the energy barrier to the transfer is on the order of kT so that there is no thermal barrier to the transfer.

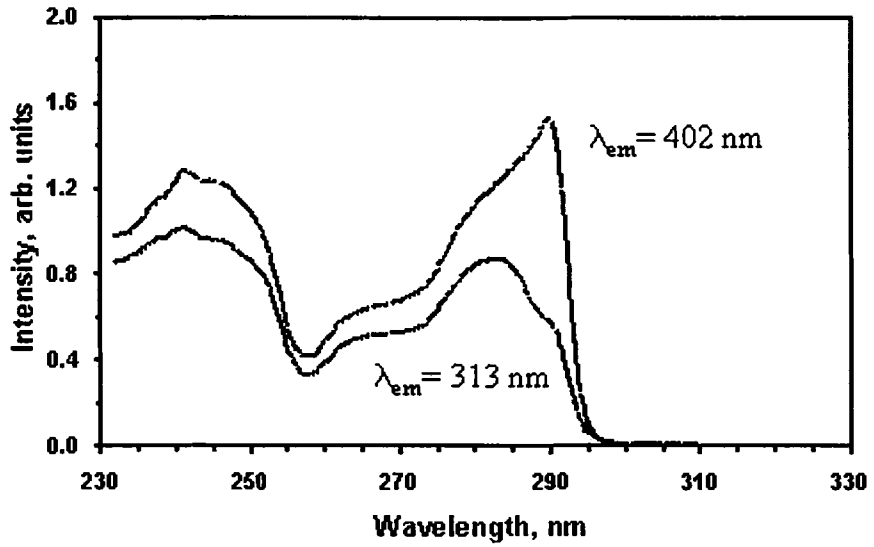

Figure 3.11: Corrected excitation spectra for the two emission bands present in $K_2Na[Ag(CN)_2]_3$.

Since the transfer occurs between the excited singlet states rather than between the emissive triplet states, the excitation energies must be used to calculate ΔE. Figure 3.11 shows the excitation spectra for the two emission bands. These spectra overlap significantly and it can therefore be inferred that the energy difference between the two excited states is inconsequential compared to kT.

3.6 Discussion and Conclusions

Raman, synchrotron X-ray and neutron diffraction as well as lifetime data have been presented which provide evidence for essential, gradual structural changes as a function of temperature in the layered compound $K_2Na[Ag(CN)_2]_3$ in the temperature range from 1.5 K to 300 K, indicating monoclinic symmetry.

The results in this study do not indicate the presence of any phase transitions in the vicinity of 80 K, the temperature at which we see a reversal in the trend of the intensity ratio of the two luminescence bands. It is therefore concluded that the changes in the luminescence behavior above and below 80 K are not due to phase transitions near that temperature.

Instead, it is proposed that the luminesence thermochromism is due to energy transfer from the HE band to the LE band at temperature values below 80 K and back energy transfer at temperature values above 80 K. This conclusion is supported by the lifetime data which showed a decrease in the lifetime of the higher energy band between 4 K and 60 K (where energy transfer from this band to the lower energy band dominates) and an increase in lifetime above 60 K (where back transfer to this band dominates).

The presence of structural changes in the region of 200-220 K certainly might indicate changes in the luminescence spectrum in this region, just as the changes in the luminescence seen around 80 K led to a suspicion of a phase transition. Unfortunately, this sample's luminescence is vanishingly weak at temperature values above 200 K, so this aspect of the structural changes could not be explored.

From the neutron and X-ray powder diffraction data analysis, we conclude that the structural changes detected differ significantly from what may be described as a "conventional" phase transition. In such transitions major changes normally occur in the atomic structure when the transition takes place, usually accompanied by rela-

tively large energy changes in the crystalline system (e.g. the specific heat measured as a function of temperature shows a sharp peak at the transition temperature). For the structural changes observed here, no such peak in the specific heat curve occurs, the atomic structural change with temperature change seems to be one of gradual and continuous change with relationships that cause the positions to coincide with what would be the hexagonal (trigonal) $P\bar{3}1m$ structure from the monoclinic C2/m atomic structure at the sample temperature of approximately 200 K. In this regard, the present investigation may be considered to show the possibility of a novel type of phase change with temperature.

4 ENERGY TRANSFER IN R[M(CN)$_2$]$_3$ (R=La, Tb; M=Ag, Au)

4.1 Introduction

It has been established in dicyanoaurates(I) and dicyanoargentates(I) doped with Tb^{3+} and Eu^{3+} that exclusive excitation of the $M(CN)_2^-$ donor ions leads to sensitized luminescence of the Tb^{3+} and Eu^{3+} acceptor ions.[3,40,41] It has also been shown that the emission energies of the donors can be *tuned* by varying certain physical parameters, such as temperature,[3] pressure,[40] excitation wavelength[31] and donor concentration.[32]

In this chapter, the goal is to characterize the electronic properties of the donor ions and model the *tunable*, radiationless energy transfer in a series of compounds co-doped with both La^{3+} and Tb^{3+}.

4.2 Characterization of the Donor Ions

It is known that the lanthanide ion La^{3+} has no optically active energy levels. Additionally, in density functional theory calculations carried out by collaborators at Universidad de Zaragoza for La[Ag(CN)$_2$]$_3$ during this study, it was found that the La^{3+} orbitals contribute less than 1% to any of the occupied molecular orbitals. It can therefore be concluded that the La^{3+} ion has no effect on the energy levels or the luminescence decay dynamics of La[Ag(CN)$_2$]$_3$ and La[Au(CN)$_2$]$_3$. For this reason,

λ_{max}^{em}, nm	Assignment	
285-300	$*[Ag(CN)_2^-]_2$	excimers
320-360	cis-$*[Ag(CN)_2^-]_3$	localized exciplexes
390-430	trans-$*[Ag(CN)_2^-]_3$	localized exciplexes
490-530	$*[Ag(CN)_2^-]_n$	delocalized exciplexes

Table 4.1: Band assignments for dicyanoargentate emissions arising from exciplex formation within the crystal.

these two compounds have been chosen to represent and characterize the donor ions $Ag(CN)_2^-$ and $Au(CN)_2^-$.

4.2.1 $La[Ag(CN)_2]_3$

The formation of exciplexes has been demonstrated in compounds containing $Ag(CN)_2^-$ ions,[30,31] leading to a phenomenon referred to as site-selective excitation. Site-selective excitation refers to the presence of different emission bands when different excitation wavelengths are used, a result of absorption by and emission from $[Ag(CN)_2]_n$ oligomers of different n. A number of different emission bands have been identified and assigned to exciplex emission in dicyanoargentates.[13,32] These bands are listed in Table 4.1.

Site-selective excitation is observed in $La[Ag(CN)_2]_3$, as shown in Figure 4.1. Two of the bands listed in Table 4.1 are found in $La[Ag(CN)_2]_3$. The fact that the higher energy band has two components is attributed to the presence of $[Ag(CN)_2^-]_n$ oligomers of different n. This theory is supported by the fact that the two individual bands are selectable by excitation wavelength. This phenomenon provides a method of *tuning* the emission by selection of excitation wavelength.

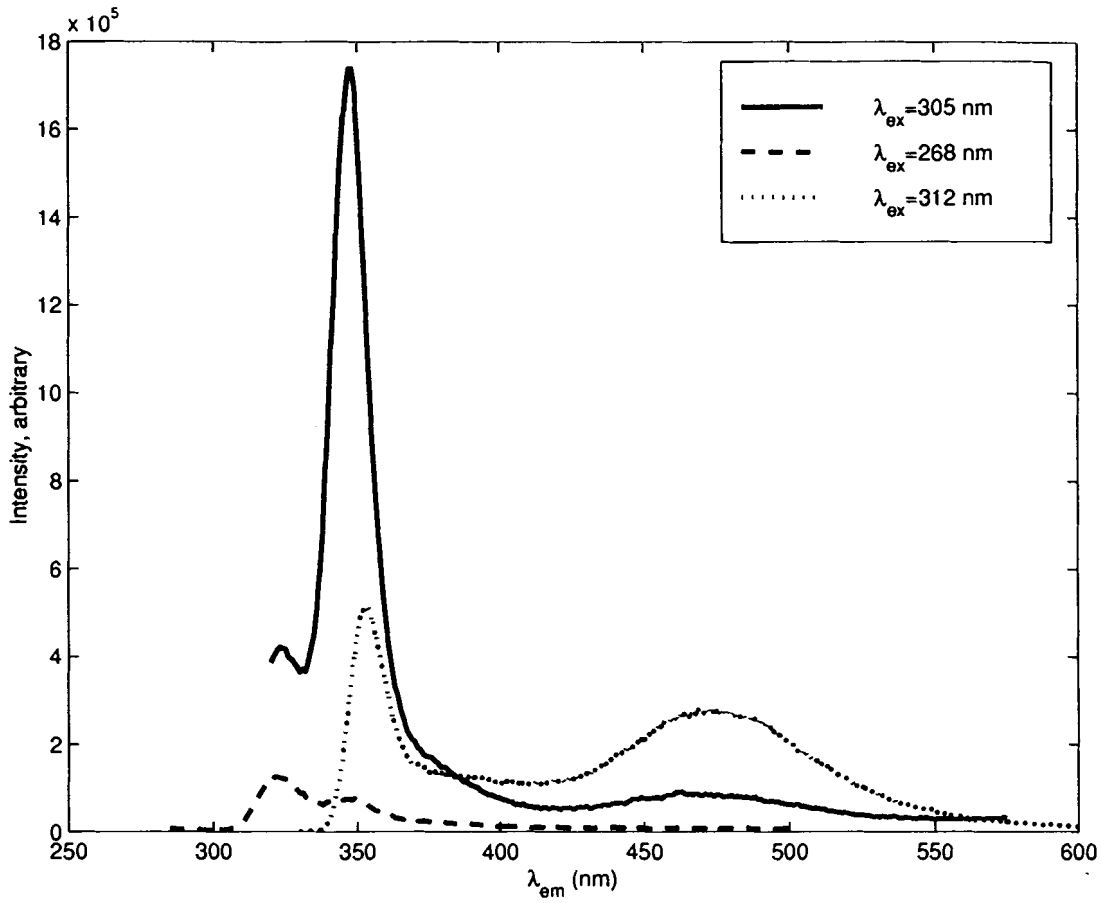

Figure 4.1: Emission spectra for $La[Ag(CN)_2]_3$ at 80 K for a variety of excitation wavelengths.

The luminescence decay dynamics were studied using an excitation wavelength of 266 nm, so the steady-state emission properties will be explored with this wavelength as well. There exists a significant spectral overlap between the 320 nm emission and the 350 nm absorption at room temperature values when the sample is excited with a wavelength of 266 nm (see Figure 4.2). This spectral overlap decreases as the temperature is lowered to 80 K. Comparison with the excitation spectrum for the 320 nm band (see Figure 4.3) shows a very similar profile with the exception of a

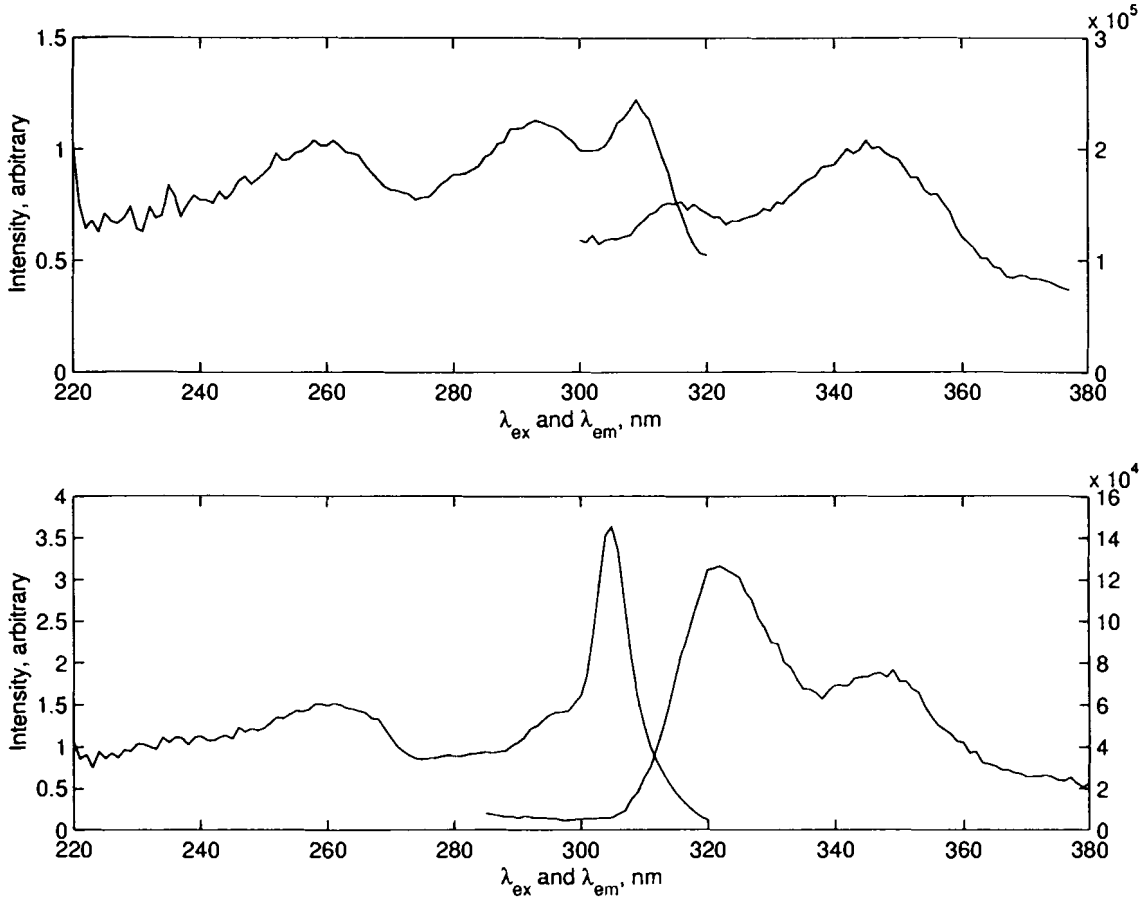

Figure 4.2: Emission (λ_{ex}=266 nm) and excitation (λ_{em}=348 nm) spectra at room temperature (top) and 80 K (bottom) for $La[Ag(CN)_2]_3$.

strong band at 305 nm. This indicates that the presence of the 350 nm band is a result of energy transfer from the higher energy 320 nm band and that the 350 nm band does not otherwise absorb at 266 nm. This theory is further supported by the fact that the relative intensity of the 350 nm band (under 266 nm excitation) decreases as the temperature is decreased, gradually disappearing as the temperature drops below 80 K.

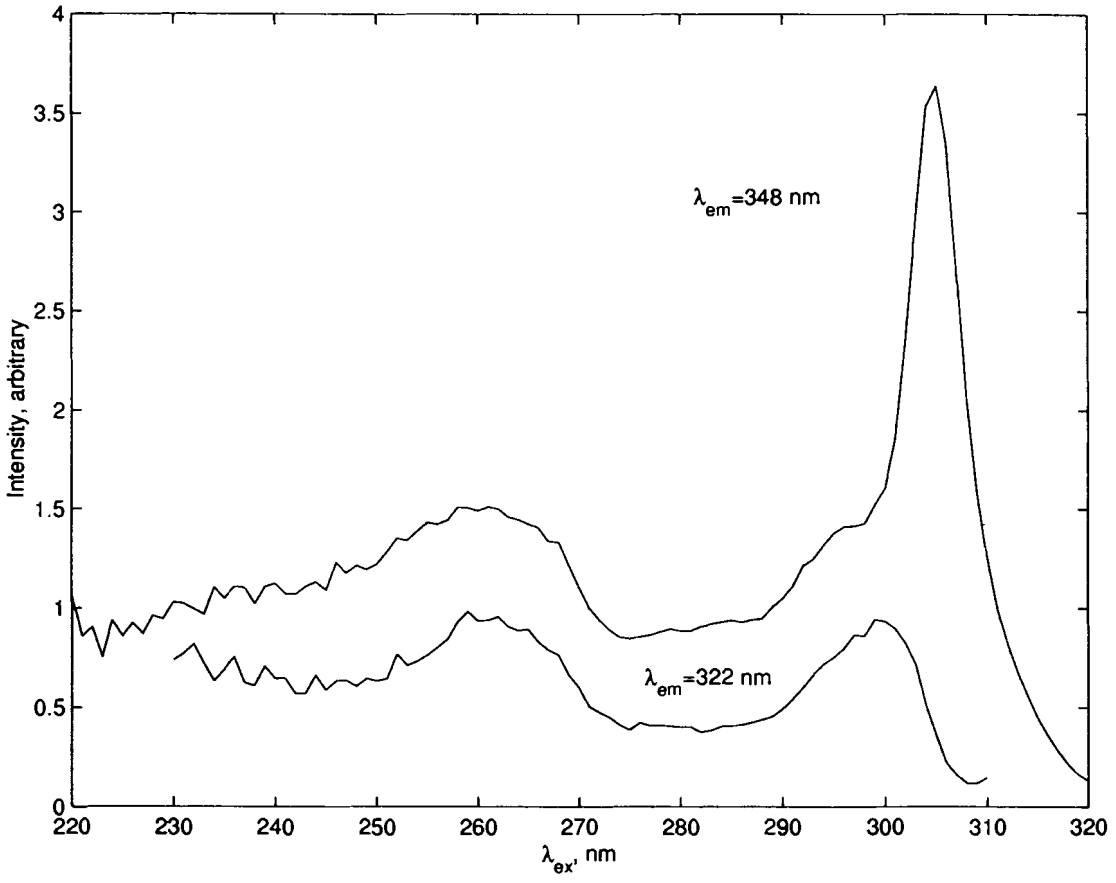

Figure 4.3: Comparison of the excitation spectra for the 320 nm band and the 350 nm band.

Luminescence decay data have been obtained for the 320 nm band at all temperature values and the 350 nm at temperature values greater than 80 K. The lower energy 470 nm band is not present under an excitation of 266 nm, so lifetime data could not be obtained for that band. As discussed above, the 350 nm band is not observed under this excitation wavelength below 80 K, so lifetime data in that range could not be obtained.

The lifetime of the 320 nm band was determined to have a single exponential character for temperature values below 80 K. This lifetime is quite short, increasing from 325 (15) ns at 60 K to 355 (15) ns at 10 K. This would indicate that this is a singlet-singlet transition (fluorescence). Above 80 K, the decay was non-exponential, further indicating the presence of energy transfer to the 350 nm emission band. At 80 K, the 350 nm band has a relatively long lifetime of 2.3 (0.4) μs, indicating that this is a triplet-singlet transition. The luminescence intensity drops off rapidly as the temperature goes above 80 K, so lifetime values were not determined in this temperature range.

The structure of $La[Ag(CN)_2]_3$ has been determined at room temperature by means of single crystal X-ray diffraction. The structure was solved in the space group $P\bar{3}c1$. Three waters of hydration were found to be coordinated with the La^{3+} ions. The $Ag(CN)_2^-$ ions were found to be linear with a C-Ag-C angle of 180° and a N-C-Ag angle of 179.5°. The crystal structure is layered, as expected, with layers of

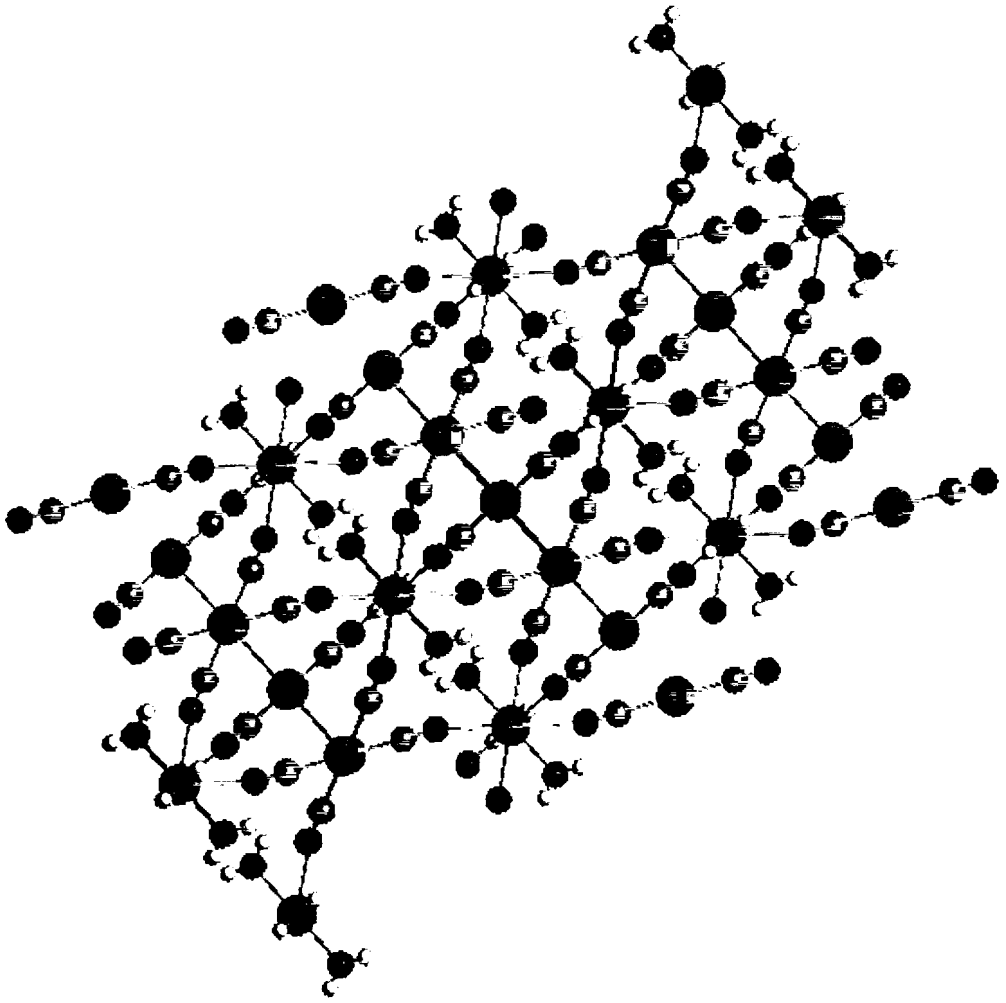

Figure 4.4: Crystal structure of $La[Ag(CN)_2]_3$.

$Ag(CN)_2^-$ ions alternating with layers of La^{3+} ions and waters of hydration. Figure 4.4 shows this layered structure.

4.2.2 $La[Au(CN)_2]_3$

While site-selective excitation is *not* observed in $La[Au(CN)_2]_3$, the emission bands do red shift with decreasing temperature. This result is in accord with previous

results for $Eu[Au(CN)_2]_3$.[41] There exist two emission bands in this compound, at low temperature values (about 80 K), one appears at approximately 430 nm and the other at approximately 490 nm. These bands are red-shifted by approximately 1550 cm^{-1} and 850 cm^{-1} respectively from their positions at room temperature. Inspection of the excitation spectra in Figure 4.5 for the 490 nm band reveals a small spectral overlap between the 430 nm emission and the 490 nm absorption which increases with increasing temperature (bottom to top in figure). The fact that the relative intensity

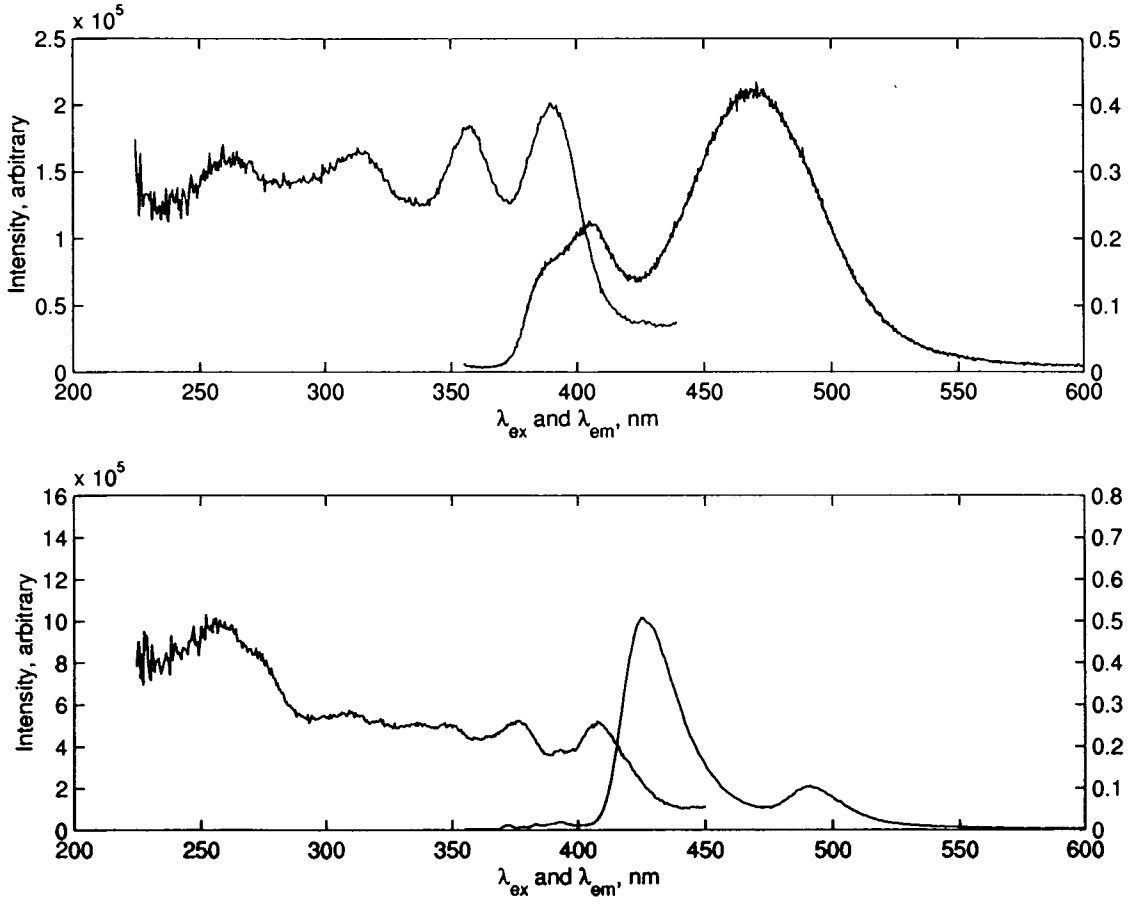

Figure 4.5: Excitation spectra (left) monitoring the emission at 490 nm and emission spectra (right) for λ_{ex}=337 nm at room temperature values (top) and 25 K (bottom).

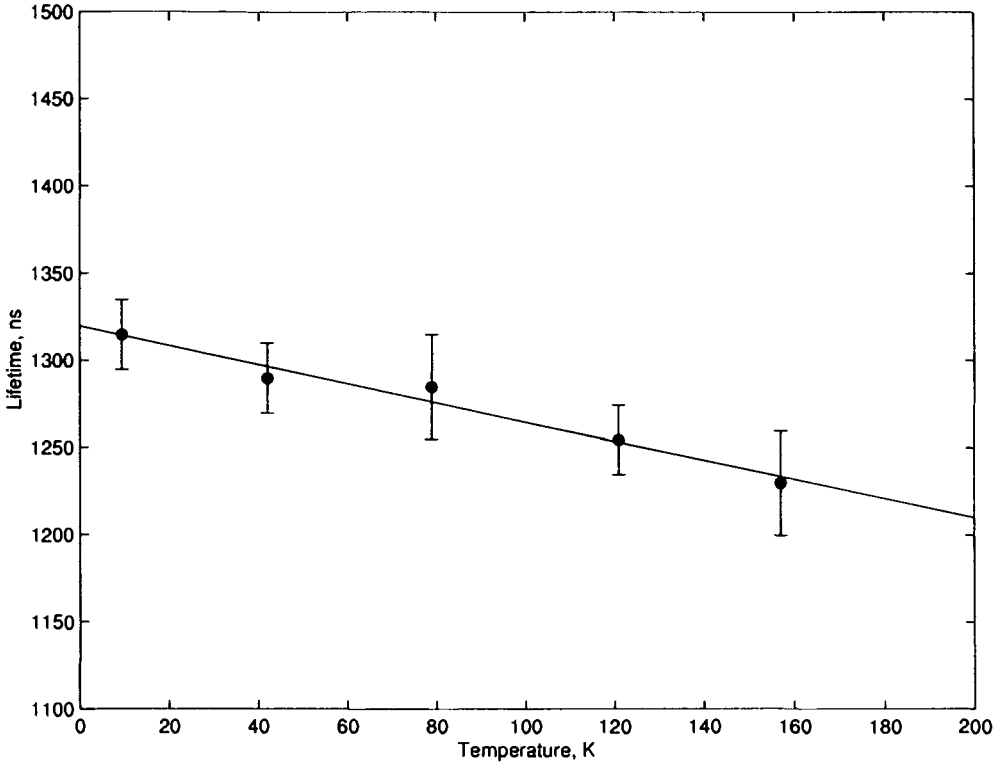

Figure 4.6: Lifetime values as a function of temperature for the 490 nm emission band of $La[Au(CN)_2]_3$.

of this band increases with increasing temperature coupled with the fact that there exists this spectral overlap indicates that its presence is at least partially a result of energy transfer from the higher energy 430 nm band. This hypothesis is supported by the fact that the 430 nm (donor) band lifetime values are non-exponential, while the 490 nm band lifetime values are single exponential.

A plot of the 490 nm band lifetime as a function of temperature is shown in Figure 4.6 along with a straight line fit to the data. Extrapolation to T=0 K gives τ_{rad}=1320 ns. The lifetime for this band decreases only slightly as the temperature is increased, indicating that the non-radiative decay rate is quite small.

The 430 nm band's luminescence decay will be discussed and analyzed in Section 4.5.

An X-ray crystallographic structural study of this compound is currently underway. Preliminary results indicate that the structure is essentially the same as that of $La[Ag(CN)_2]_3$ and the space group is P62m. As in the silver compound, there are three waters of hydration.

4.3 Variation of the Donor Ion: Energy Transfer in $Tb[M(CN)_2]_3$

An energy level diagram for Tb^{3+} is shown in Figure 4.7. Also included are the emission energies for the $Ag(CN)_2^-$ and $Au(CN)_2^-$ donor states. Arrows indicate the spectral overlap between the donor and acceptor.

Following the transfer of energy from the $Ag(CN)_2^-$ donor, the Tb^{3+} ions will be excited into the upper levels and will rapidly decay (non-radiatively) to the $^5D_3$ level. At this point, decay will proceed to the ^7F_J levels either by direct decay or via the $^5D_4$ level, which is reached by either non-radiative decay or cross-relaxation with other Tb^{3+} ions. In the dicyanoargentate(I), the highest energy phonon is approximately 2150 cm^{-1}. Since the difference in energy between the $^5D_3$ and $^5D_4$ levels is approximately 6000 cm^{-1}, the non-radiative process is quite favorable and it is unlikely that transitions from the $^5D_3$ level will be observed.

In the case of the $Au(CN)_2^-$ donor, the energy transfer occurs directly to the $^5D_4$ level, as can be seen from the spectral overlap in Figure 4.7.

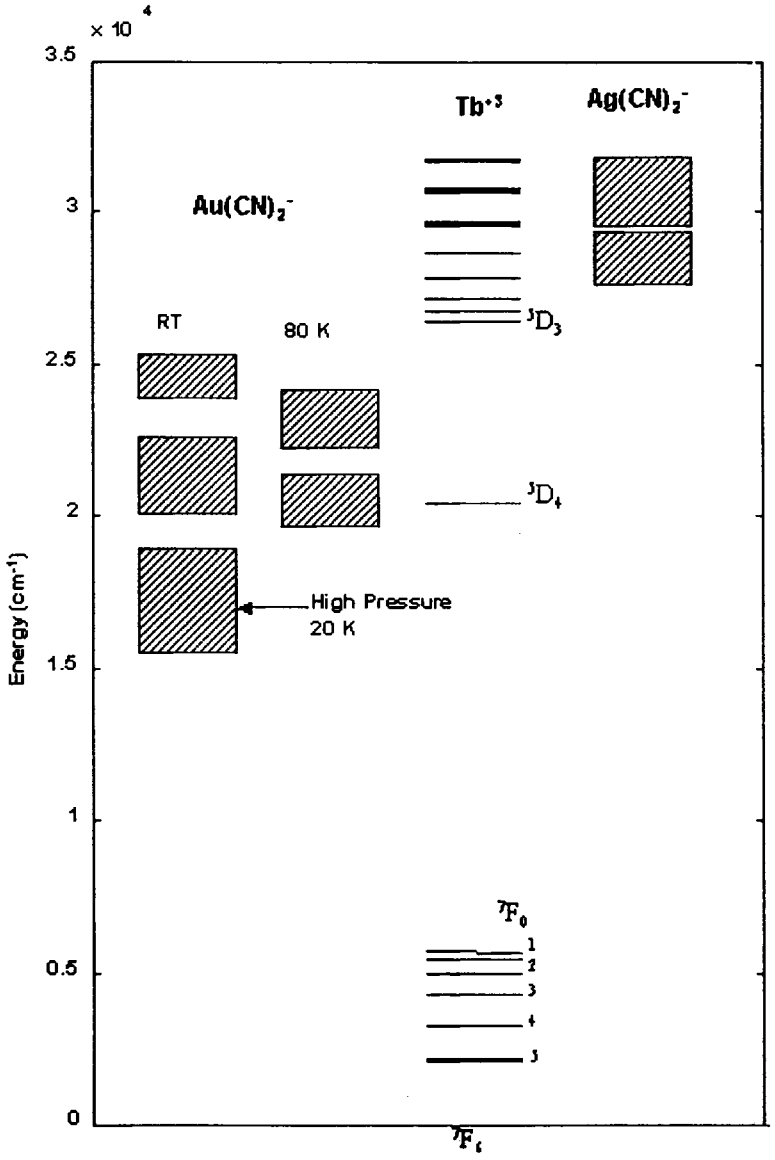

Figure 4.7: Tb^{3+} energy levels. Also shown are energy levels for the $Ag(CN)_2^-$ and $Au(CN)_2^-$ donor ions to demonstrate the spectral overlap between donor and acceptor.

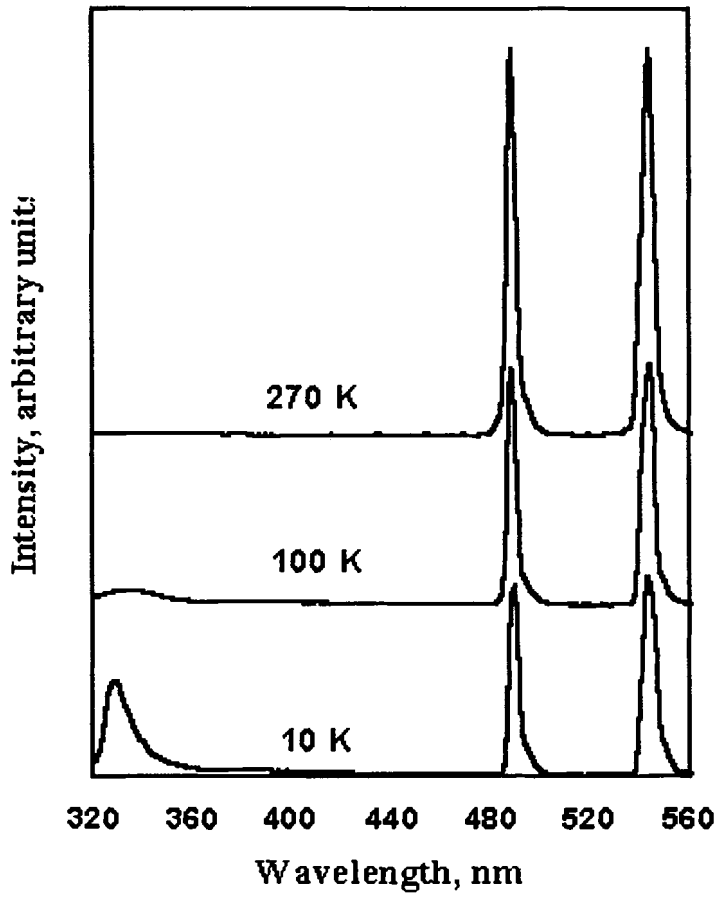

Figure 4.8: Emission spectra as a function of temperature for $Tb[Ag(CN)_2]_3$. Reproduced with permission.[3]

4.3.1 $Tb[Ag(CN)_2]_3$

There exists a significant spectral overlap between the $Ag(CN)_2^-$ donor and Tb^{3+} acceptor, as seen in Figure 4.7. It is significant enough that the energy transfer is so efficient that the donor emissions (325 nm and 350 nm) are almost completely quenched at all temperature values studied, as shown in Figure 4.8. Also noted is the decrease in the relative intensity of the Tb^{3+} emissions (491 nm and 545 nm) with decreasing temperature.

	Temperature (K)	Lifetime (μs)
$Tb[Ag(CN)_2]_3$	85	320 (20)
	230	350 (10)
	100	380 (10)
$Tb[Au(CN)_2]_3$	85	500 (40)
	170	370 (20)

Table 4.2: Lifetime values for the Tb(III) emission at 491 nm as a function of temperature for $Tb[Ag(CN)_2]_3$ and $Tb[Au(CN)_2]_3$.

Lifetime values have been obtained for the Tb^{3+} emission at 491 nm at several temperature values and are shown in Table 4.2. The acceptor lifetime increases from 320 (20) μs to 380 (10) μs upon heating the sample from 80 K to 200 K. This result is in agreement with the steady-state luminescence data, which show an increase in the relative intensity of the Tb^{3+} emissions with increasing temperature. As the donor emission was almost completely quenched at temperature values $\geq$ 80 K, it was not detectable for the purposes of lifetime measurements. Unfortunately, this prevents a conclusive determination of the mechanism of energy transfer. This issue will be further addressed in Section 4.4.

4.3.2 $Tb[Au(CN)_2]_3$

As can be seen in Figure 4.7, in this compound, the spectral overlap between the donor and acceptor is much less significant than in the corresponding silver compound. In fact, only the lower energy 490 nm level will act as a donor state. It has already been shown that the 490 nm band exists at least partially as a result of energy transfer from the higher energy 430 nm band. In order to characterize the energy transfer between the $Au(CN)_2^-$ and the Tb^{3+} ions, the decay of the donor state must be

analyzed. Unfortunately, as can be seen in Figure 4.9, this donor state is completely quenched (although the 430 nm band is present) at all temperature values. This figure also shows that the relative intensity of the Tb^{3+} emsission decreases with increasing temperature.

The Tb^{3+} acceptor decay is single exponential, with a lifetime of 500 (40) μs at 80 K. This lifetime decreases upon heating to 370 (20) μs at 170 K (see Table 4.2). The luminescence was not detectable at temperature values above 170 K. This decrease in the Tb^{3+} lifetime with an increase in temperature is in agreement with the steady-state luminescence data (Figure 4.9), which show a decreased relative intensity for the Tb^{3+} emissions with increasing temperature.

4.4 Further Study: Energy Transfer in $Tb_xLa_{1-x}[Ag(CN)_2]_3$

It is clear that energy transfer is more efficient in $Tb[Ag(CN)_2]_3$ due to the greater spectral overlap between the donor and acceptor species. However, in order to more definitively model the energy transfer, the dynamics of the donor decay must be obtained. As shown in Sections 4.3.1 and 4.3.2, the donor emission is completely quenched and undetectable for the purposes of obtaining lifetime values. To overcome this problem, a series of dicyanoargentates co-doped with both La^{3+} and Tb^{3+} have been investigated. As stated previously, La^{3+} has no optically active energy levels and will therefore not participate in the dynamics of the energy transfer.

While definitive structural data exists for $La[Ag(CN)_2]_3$ (see Section 4.2.1), the structures of the co-doped compounds have yet to be determined. In order to show

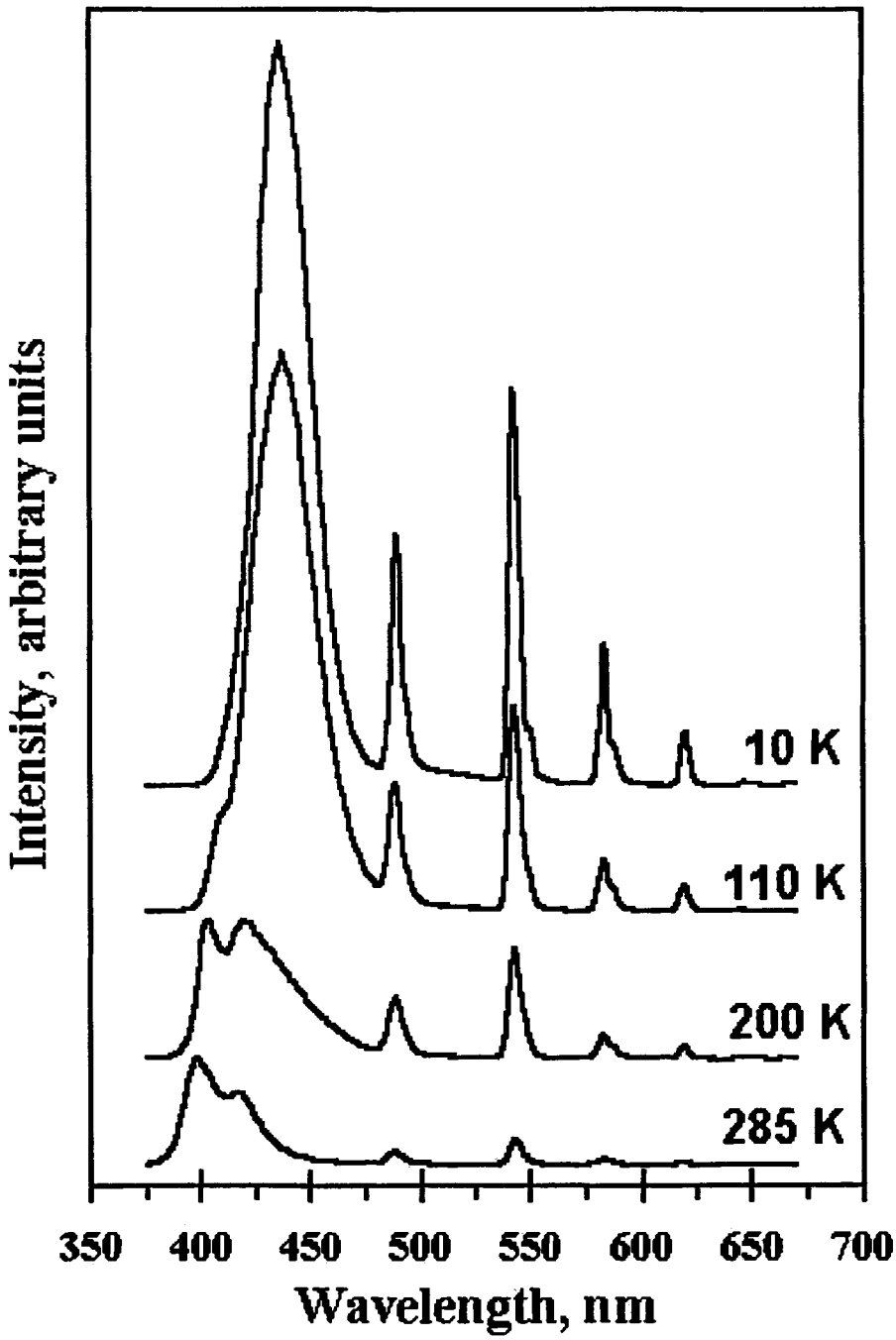

Figure 4.9: Steady-state emission spectra for $Tb[Au(CN)_2]_3$ as a function of temperature. Reproduced with permission.[3]

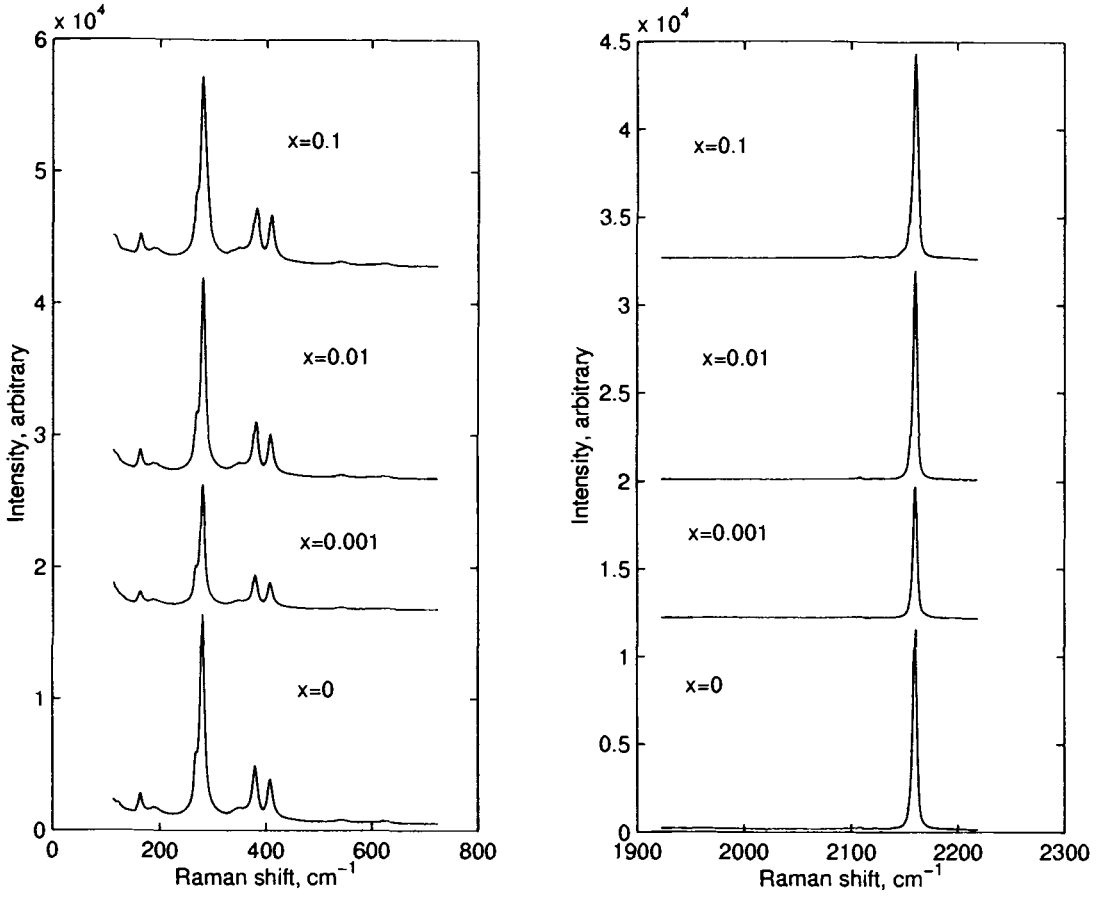

Figure 4.10: Raman data for $Tb_xLa_{1-x}[Ag(CN)_2]_3$, with x=0, 0.001, 0.01, 0.1.

that substituting Tb^{3+} for La^{3+} does not significantly change the structure (and the electronic properties), Raman scattering data was obtained. Fig 4.10 shows this Raman data for $Tb_xLa_{1-x}[Ag(CN)_2]_3$ for x=0, 0.001, 0.01, 0.1. No significant differences (shifts in energy or splitting of the bands) are noted in any of the vibrational modes, indicating that the $Ag(CN)_2^-$ ion environments have not changed.

Steady-state luminescence results at 80 K for the donor in $Tb_xLa_{1-x}[Ag(CN)_2]_3$ are shown in Figure 4.4. It is noted that the intensity of the 325 nm band relative to that of the 350 nm band decreases with increasing x. That is, increasing the amount

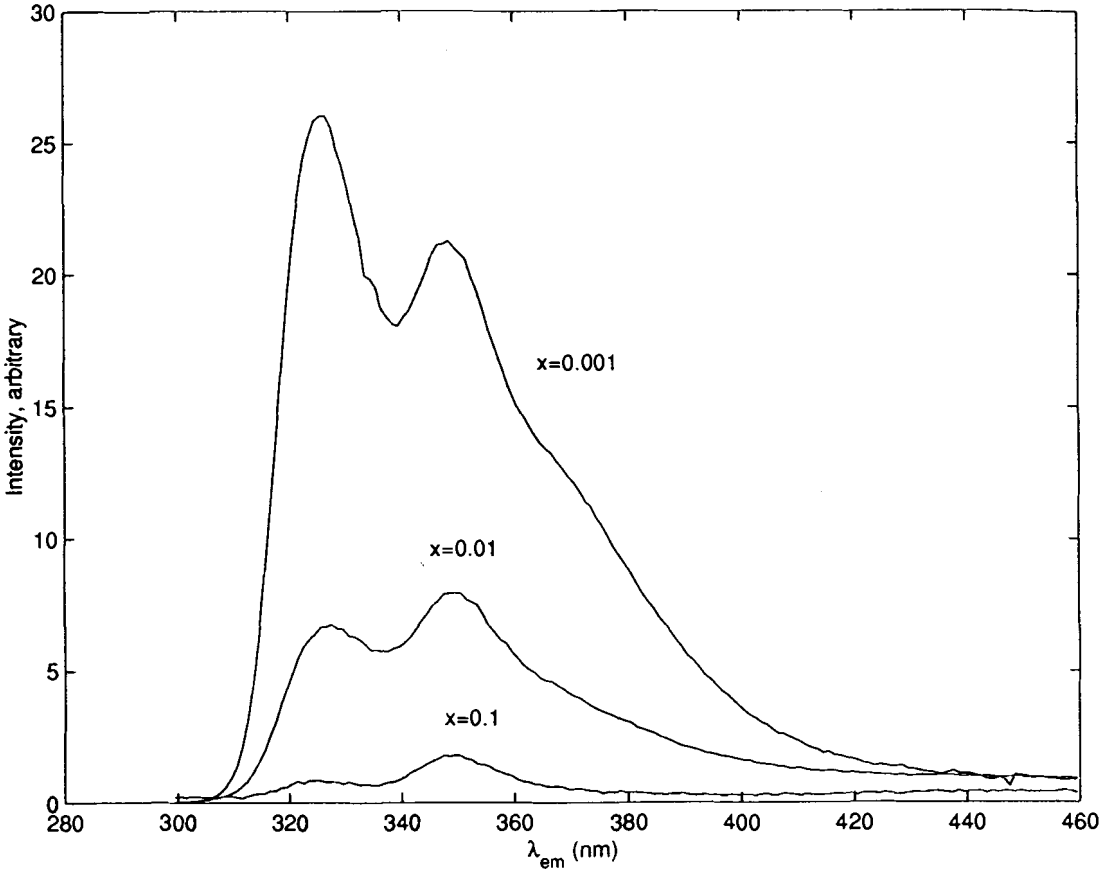

Figure 4.11: Steady-state luminescence for x=0.1, 0.01. 0.001 (bottom to top) in $Tb_xLa_{1-x}[Ag(CN)_2]_3$.

of Tb^{3+} doped in the sample decreases the relative intensity of the higher energy 325 nm band. This would indicate that the 325 nm band plays a role in the transfer of energy to the acceptor ions.

As mentioned in Section 4.2.1, the lifetime of the 350 nm emission in $La[Ag(CN)_2]_3$ is single exponential at 80 K, with a value on the order of 2.3 μs. Figures 4.12 and 4.13 show semilog plots of this 350 nm emission decay as a function of x. It is clear that the decay is not a simple exponential in the co-doped samples, but does approach

the same lifetime as the pure sample at long times. At short times, the increased rate of decay (increased slope) and non-exponential character clearly indicate the presence of energy transfer, as expected. It is also observed that in the sample with greatest x, the rate of decay at short times is the greatest (greatest slope at short times).

The presence of energy transfer between the 320 nm band and the 350 nm band was already discussed for $La[Ag(CN)_2]_3$. Comparing the decay of the 320 nm band for this case with that of the co-doped, x=0.1 case (Figure 4.14) shows that the decays are similar at long times. At short times, however, the co-doped sample follows a less rapid decay indicating the presence of an additional pathway for the transfer of energy from this energy level.

4.5 Mechanism of Energy Transfer

A scheme for the transfer of energy in $Tb_xLa_{1-x}[Ag(CN)_2]_3$ is shown in Figure 4.15. As shown previously, UV excitation results in emission from two closely spaced bands (320 nm and 350 nm). It has also been shown that the lower energy (350 nm) band exists at least partially as a result of energy transfer from the higher energy (320 nm) band. Due to the great spectral overlap between these emissions and the Tb^{3+} absorption, energy transfer is also present between both of these bands and the acceptor ion, followed by fast non-radiative decay to the $^5D_4$ Tb^{3+} level and emission is observed from this energy level.

A rough idea of the rate of energy transfer can be obtained from the decay of the 350 nm donor state. It was noted in the previous section that the decay of

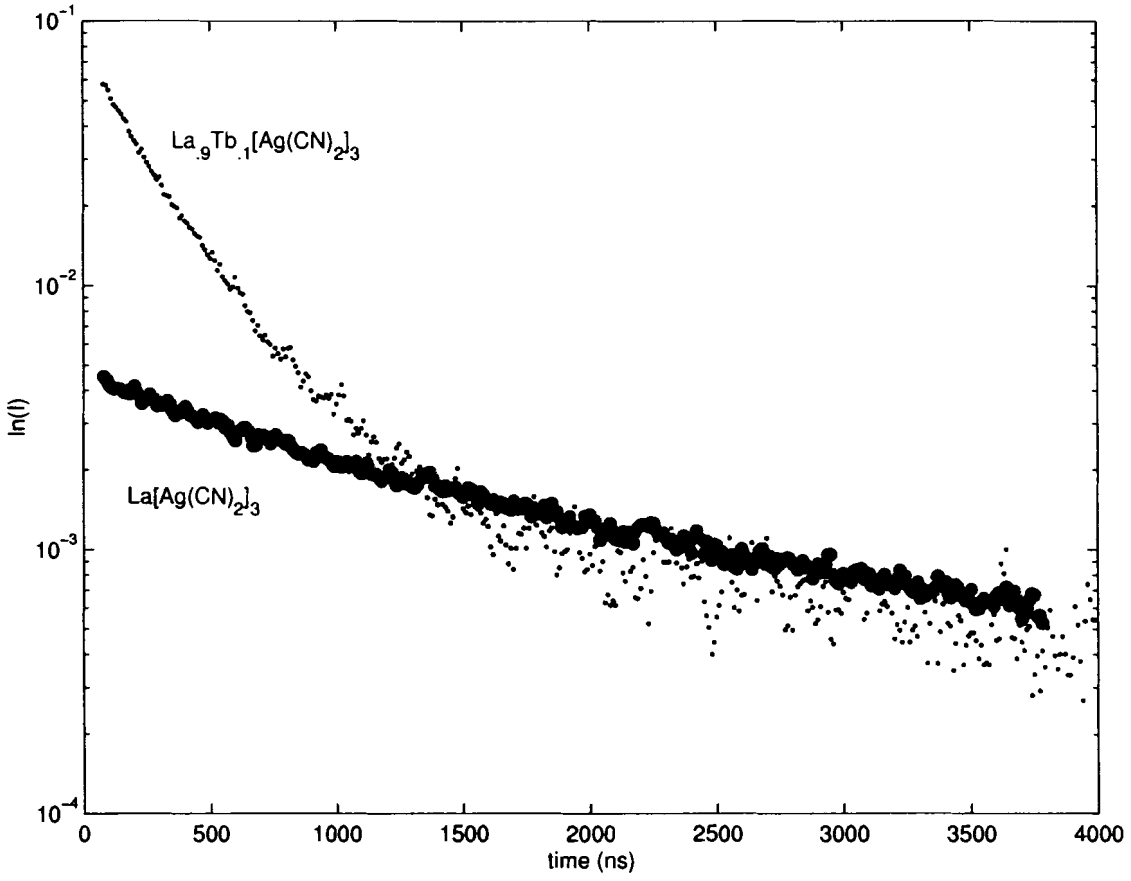

Figure 4.12: Semilog plot of the luminescence decay of the 350 nm band in both $La[Ag(CN)_2]_3$ and the co-doped case with x=0.1.

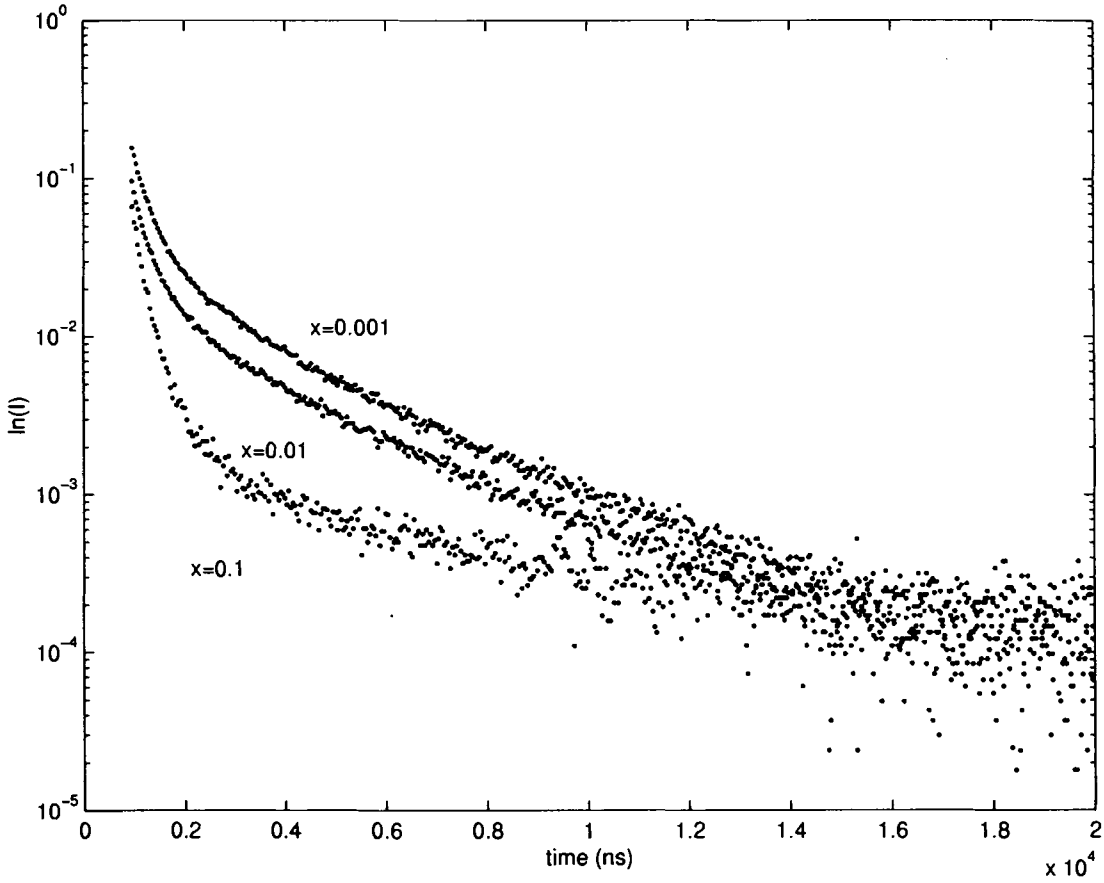

Figure 4.13: Semilog plot of the luminescence decay of the 350 nm band in the co-doped samples with x=0.1, 0.01 and 0.001 as marked.

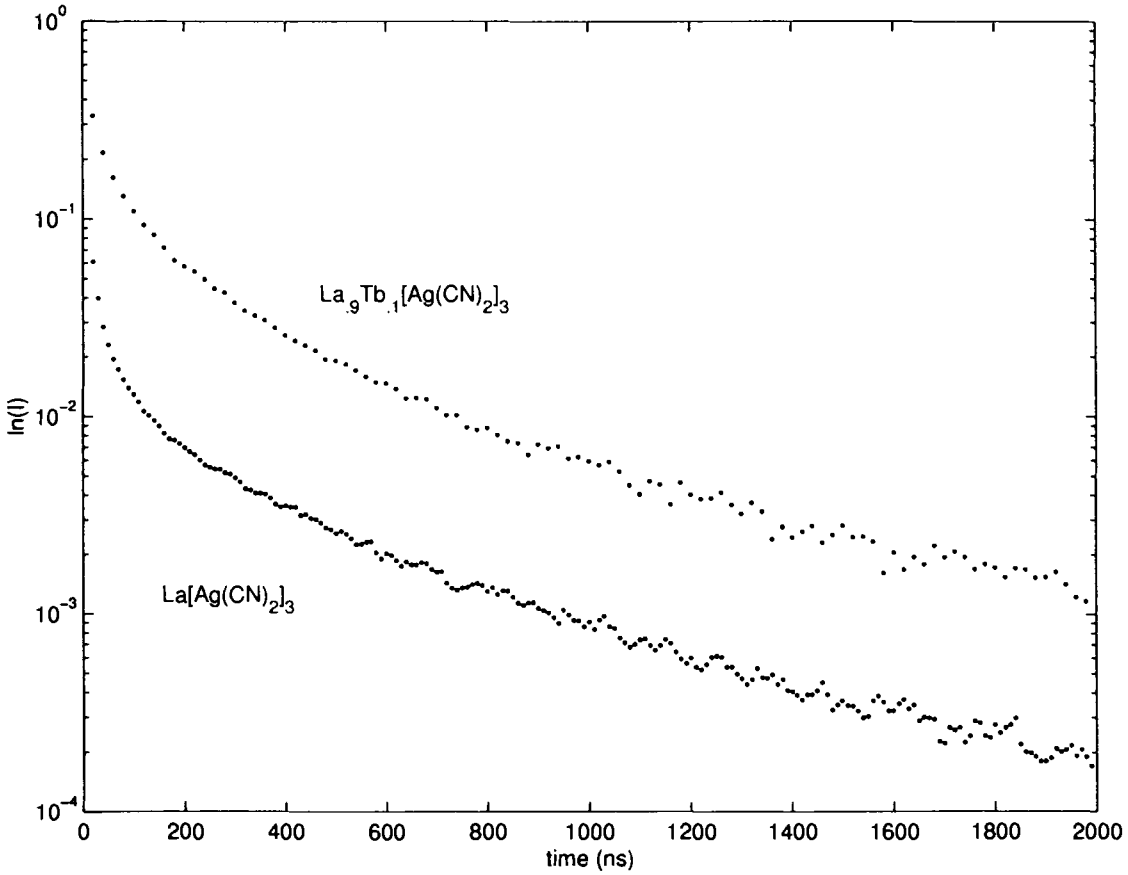

Figure 4.14: Semilog plot of the luminescence decay of the 320 nm band in both $La[Ag(CN)_2]_3$ and the co-doped case with x=0.1.

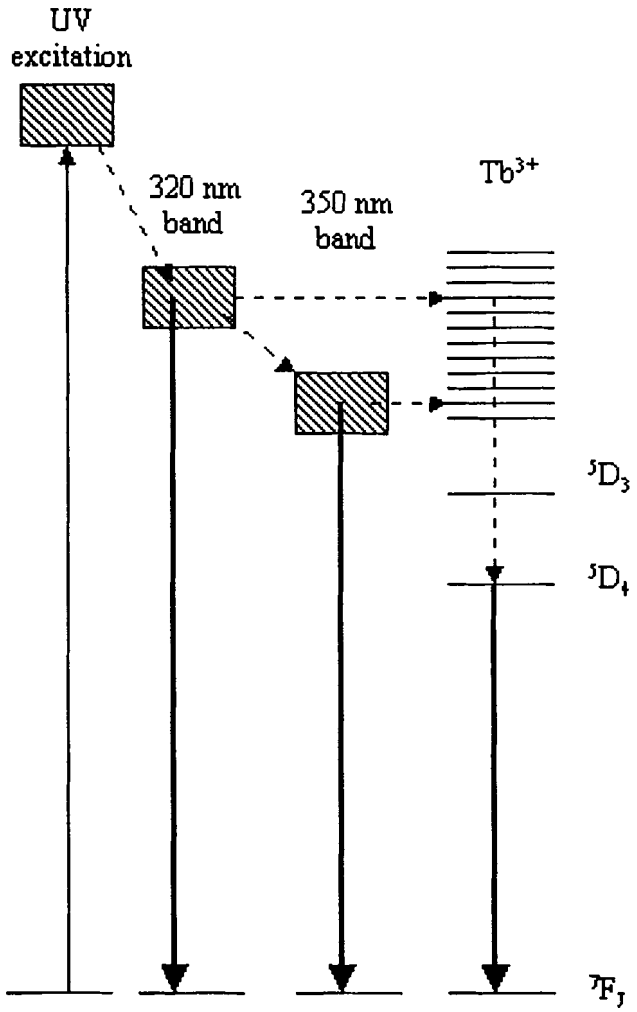

Figure 4.15: Scheme for the transfer of energy in $Tb_xLa_{1-x}[Ag(CN)_2]_3$.

the doped system is the same as that of the pure system at long times, but is non-exponential at short times. This indicates that there is another pathway with a fast rate constant. This rate constant can be estimated by subtracting off the long component and analyzing the short component. This process was completed for each of the three co-doped systems. The lifetime for the short decay increased from 285 (25) ns for the x=0.1 sample to 485 (40) ns for the x=0.01 sample and 525 (50) ns for the x=0.001 sample. This increase in lifetime translates to a decrease in rate of energy transfer, as is expected when the percentage of dopant decreases. These values are plotted in Figure 4.16, along with a least squares fit to a straight line. Although three values of x are not enough to conclusively determine a relationship between percentage of dopant and rate of energy transfer, the preliminary results do indicate a linear trend.

In cases such as this one where the donor's luminescence decay is nonexponential and it is known that the intrinsic donor decay in the absence of any acceptors is single exponential, two possible mechanisms should be suspected. The multipolar (dipole-dipole, dipole-quadrupole, or quadrupole-quadrupole) interaction mechanism and the Dexter exchange mechanism are both indicated when the donor decay is non-exponential (these mechanisms are described in the Introduction, Section 1.2.5). Other possible mechanisms, including simple kinetic rate equation models, such as the one proposed by Kambli and Güdel[68] are only indicated in such cases where the donor's luminescence follows an exponential decay.

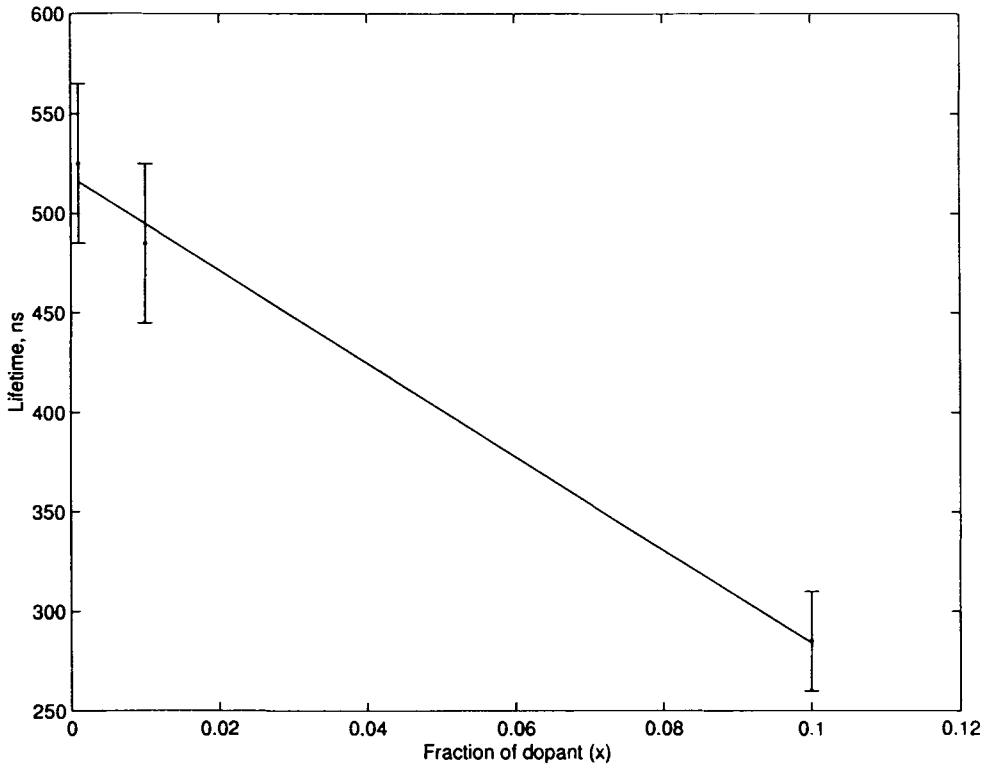

Figure 4.16: Plot of the short lifetime component for each of the three co- doped samples $Tb_xLa_{1-x}[Ag(CN)_2]_3$, with x=0.1, 0.01 and 0.001.

Time-resolved measurements can be used to rule out several mechanisms of energy transfer that occur via multipolar interaction. Energy transfer via multipolar interaction can be described by the following equation:

$$I(t) = I(0)exp\Big[-\frac{t}{\tau_0} - \Gamma\Big(1-\frac{3}{s}\Big)\frac{c}{c_0}\Big(\frac{t}{\tau_0}\Big)^{\frac{3}{s}}\Big] \qquad (4.5.1)$$

where τ_0 is the intrinsic lifetime of the donor, c is the acceptor concentration, c_0 is a parameter called the critical transfer concentration, and s=6, 8 or 10 for dipole-dipole, dipole-quadrupole or quadrupole-quadrupole interactions respectively. After some manipulation,[37] a graph of ln[I(t)] $+t/\tau_0$ vs. $(t/\tau_0)^{3/s}$ should be a straight line if the transfer mechanism occurs via a multipolar interaction.

Such graphs have been constructed for the three co-doped samples (Figure 4.17). None of these graphs with s=6, 8, and 10 has resulted in a straight line for the 350 nm emisson (donor decay) in any of the three samples, suggesting a mechanism other than multipolar interaction (in agreement with the conclusion above that the mechanism is the Dexter exchange mechanism).

Graphs have also been made for the 430 nm decay (Figure 4.18) for $La[Au(CN)_2]_3$. In Section 4.2.2 it was proposed that this decay is non- exponential due to the presence of energy transfer to the lower energy state. It is clear from the figure that energy transfer must occur by a mechanism other than a multipolar interaction.

On the other hand, the Dexter exchange mechanism is suspected in systems that have a short donor-acceptor separation because it assumes the occurrence of a bi-

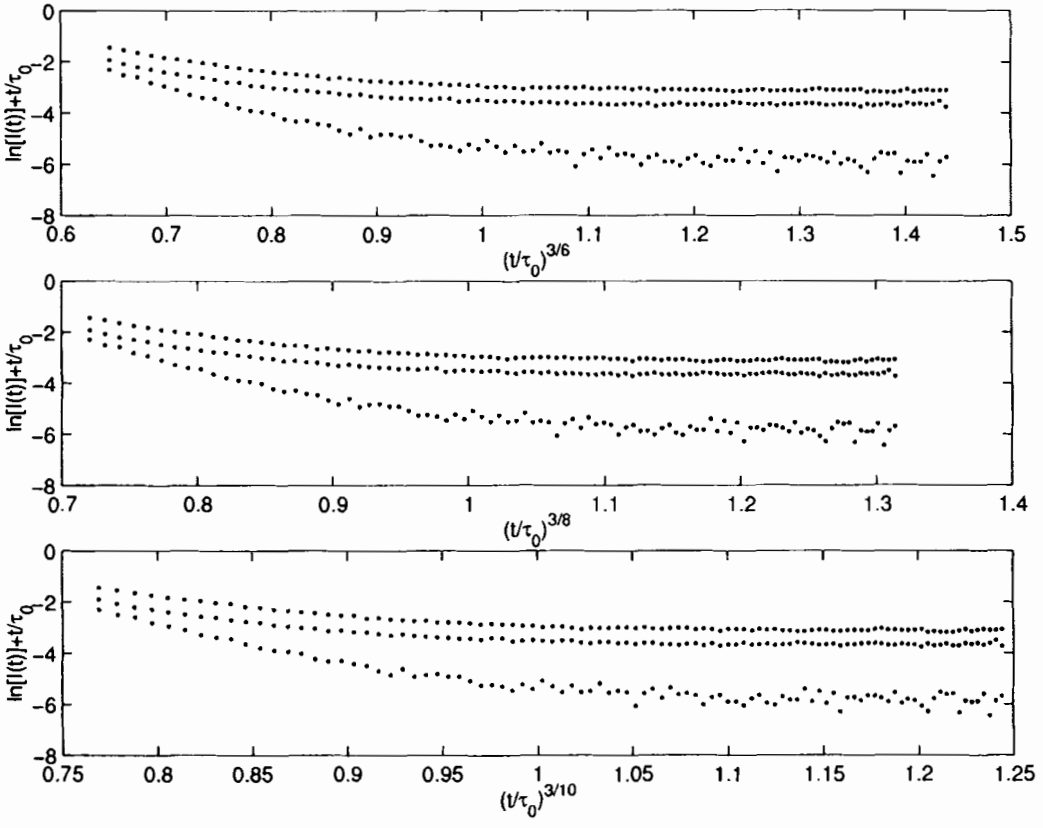

Figure 4.17: Plots of ln[I(t)] $+t/t_0$ vs. $(t/t_0)^{3/s}$ for the three co-doped samples, $Tb_xLa_{1-x}[Ag(CN)_2]_3$ with x=0.1 (bottom line in each graph), 0.01 (middle line), 0.001(top line). The parameter s=6, 8, 10 from top to bottom in the figure.

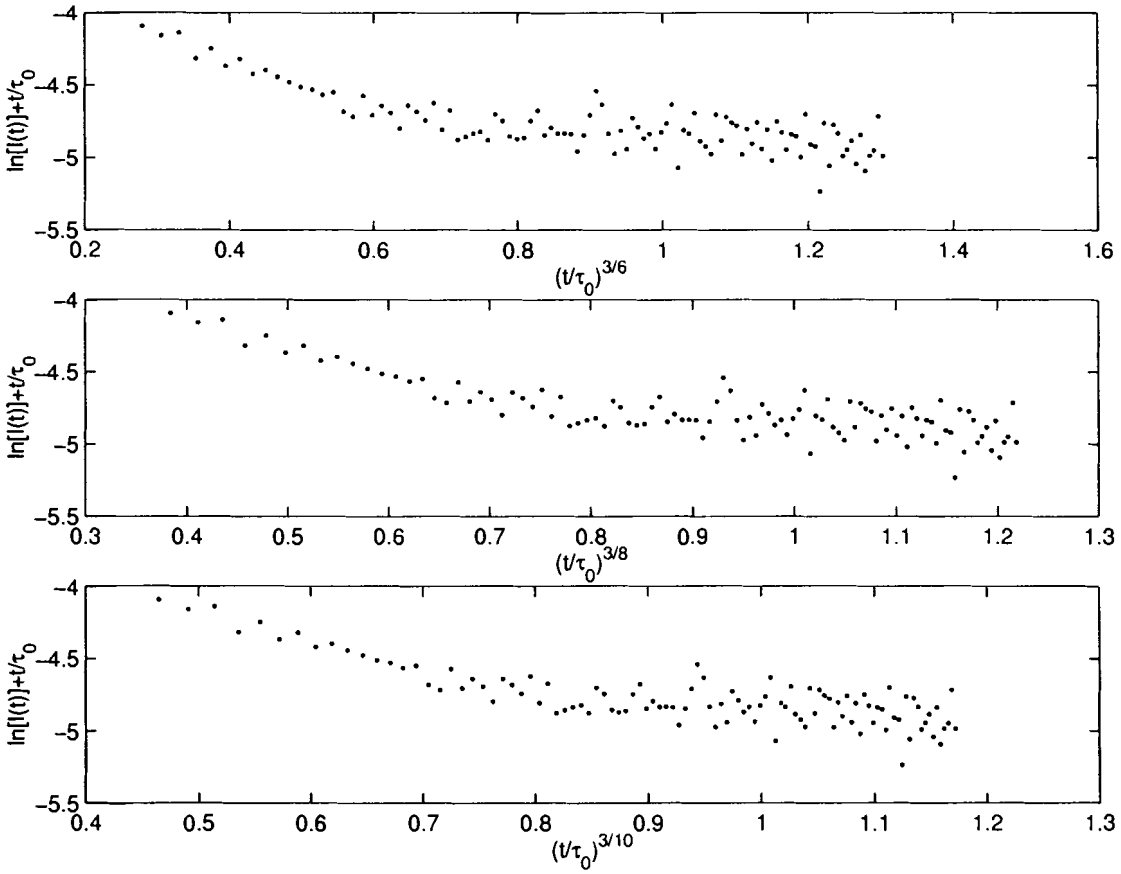

Figure 4.18: Plots of ln[I(t)] $+t/t_0$ vs. $(t/t_0)^{3/s}$ for the 430 nm decay in $La[Au(CN)_2]_3$. The parameter s=6, 8, 10 from top to bottom in the figure.

molecular encounter (collision) between the donor and the acceptor.[42] Also, theoretical calculations of the energy transfer rate between organic ligands and lanthanide ions under the exchange mechanism show that this rate can be very high.[69]

It is proposed that the mechanism of energy transfer in all cases studied is the Dexter exchange mechanism. This hypothesis is supported by several experimental facts. First, the crystal structures of various $Ln[M(CN)_2]_3$ (M=Au, Ag) have been determined and show that Ln^{3+} ions such as Tb^{3+} are directly bonded to the cyanide ligands of $[M(CN)_2^-]$ with short Ln-N distances.[21,41] For example, a Tb-N distance of 2.45 Å is present in $Tb[Au(CN)_2]_3$.[21] The crystal structure of $Tb[Ag(CN)_2]_3$ has not been determined yet but the electronic factors that govern the Tb-N interactions are similar to those in the analogous gold compound. This short donor-acceptor distance is consistent with the Dexter exchange mechanism. Also, no risetimes were observed in the acceptor decays, while in systems where multipolar interaction mechanisms are suspected, long risetimes are often seen in the decays of the acceptors.[37] This lack of risetimes indicates a very fast rate of energy transfer, also characteristic of the exchange mechanism. For the sake of comparison, it has also recently been suggested that energy transfer in the similar compound $Eu[Au(CN)_2]_3$ follows the Dexter exchange mechanism.[40]

4.6 Summary and Conclusions

This study has identified interesting trends for energy transfer processes in crystals of dicyanoaurates(I) and dicyanoargentates(I) doped with Tb^{3+} as well as dicyanoar-

gentates co-doped with both Tb^{3+} and La^{3+}. The efficiency of energy transfer in these systems is strongly dependent on the extent of the spectral overlap between the donor emission and the acceptor absorption, and also on temperature. It was also found that there exists energy transfer within the dicyanoargentate(I) and dicyanoaurate(I) energy levels.

While energy transfer is present in both $Tb[Ag(CN)_2]_3$ and $Tb[Au(CN)_2]_3$, resulting in Tb^{3+} sensitized luminescence in both compounds, the energy transfer is more efficient in $Tb[Ag(CN)_2]_3$ than in $Tb[Au(CN)_2]_3$. This is a result of the much greater spectral overlap between the donor and the acceptor in this case. Since this spectral overlap exists at all temperature values, increasing the temperature leads to a more efficient energy transfer. The reason is that energy transfer in the systems studied is a radiationless process that occurs by the Dexter exchange mechanism. Consequently, the efficiency of this nonradiative (thermal) process is enhanced by a temperature increase. In the case of the $Tb[Au(CN)_2]_3$, however, the donor emission that overlaps with the acceptor absorption shifts to higher energies upon a temperature increase, causing a decrease in the spectral overlap with the acceptor absorption. Consequently, the energy transfer is switched off by increasing the temperature.

The luminescence decay of the donor, which was completely quenched in the purely Tb^{3+} doped compounds was obtained by studying compounds co- doped with both La^{3+} and Tb^{3+}. The data supports the conclusion that the energy transfer occurs via the Dexter exchange mechanism, through a process of deduction and elimination

of other possibilities. While it has not been possible to directly model the Dexter exchange mechanism, circumstantial evidence is strong that this is the correct energy transfer mechanism.

5 ELECTRONIC PROPERTIES OF SILVER-GOLD MIXED-METAL COMPOUNDS AND THEIR SUITABILITY AS DONORS FOR ENERGY TRANSFER

5.1 Introduction

The motivation behind studying compounds of the type $La[Ag_xAu_{1-x}(CN)_2]_3$ is to investigate their potential as donors for energy transfer as discussed in Chapter 4. Four compounds of this type were synthesized and studied: x=0, 0.5, 0.9, 1.0. Content analysis of the x=0.5 and x=0.9 samples will be carried out in the future to confirm the Ag/Au ratios. For the purpose of this thesis, the x reported will correspond to the (stoichiometric) ratio present in the mother solution. A detailed description of the crystal growing process is given in Section 2.1.

Qualitative observation reveals strong luminescence at room temperature for the mixed-metal (x=0.5 and x=0.9) samples, a property which is not observed in the pure metal (x=0,1.0) samples. This gives these compounds great potential for success in practical applications where room temperature luminescence is desirable. It is also noted that the mixed-metal samples each display properties characteristic of each of the pure samples. These properties lead to the *tunability* of the emission, a desirable property for energy transfer donor species.

This study has a two-fold goal. First is to determine the underlying mechanism for the unusually strong luminescence of the mixed-metal samples at room temperature. Secondly, a detailed analysis of their suitability as donors for energy transfer will be presented with specific recommendations for compounds to synthesize and study.

5.2 Steady-State Luminescence Results

5.2.1 The Pure Metal Compounds

The luminescence properties of these compounds were discussed in detail in Section 4.2. Relevant points and additional information will be summarized in this section.

Emission spectra for $La[Ag(CN)_2]_3$ and $La[Au(CN)_2]_3$ are shown in Figure 5.1 at both room temperature and 80 K. Comparison of these spectra clearly reveals a significant decrease in luminescence intensity with increasing temperature for these pure metal samples. In fact, in the case of the silver sample, the luminescence is barely detectable at room temperature.

As discussed in Chapter 4, the silver sample displays site- selective excitation, or *tunability* of emission with changes in excitation wavelength. While the gold sample does not exhibit site- selectivity, its emission energy does red-shift with decreasing temperature values, providing *tunability* of its emission with changes in temperature.

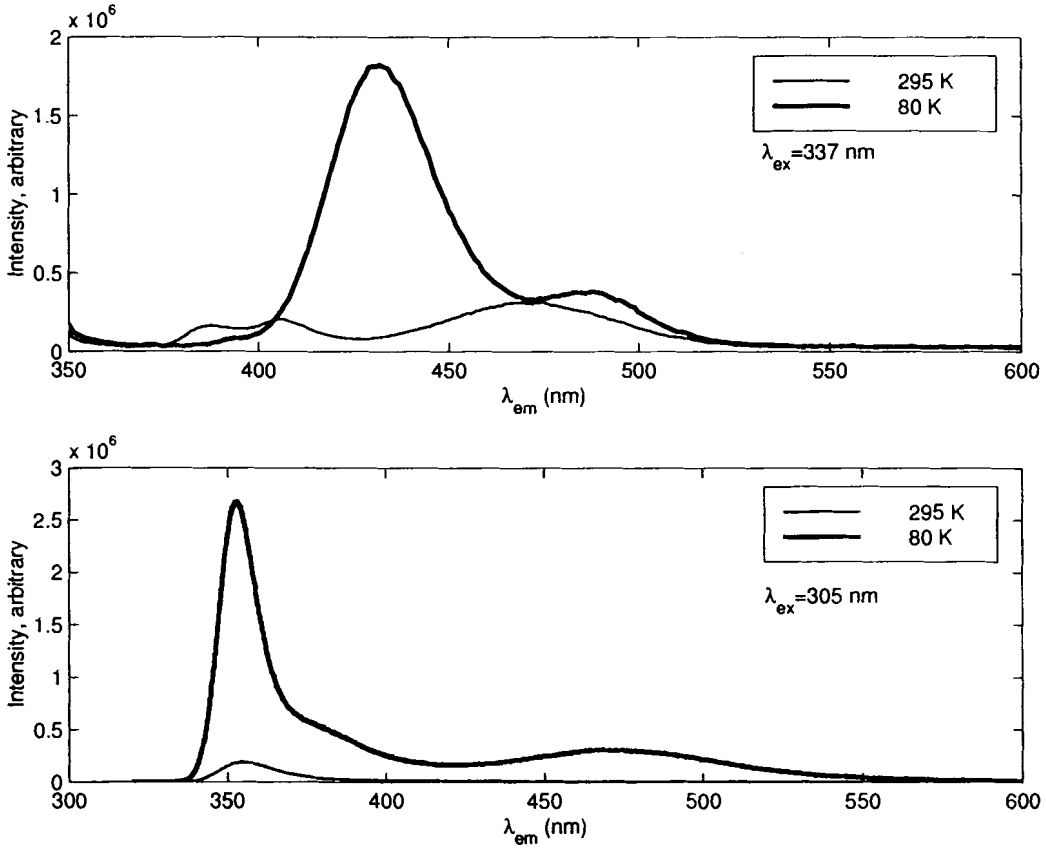

Figure 5.1: Emission spectra at room temperature and 80 K for $La[Au(CN)_2]_3$ (top) and $La[Ag(CN)_2]_3$ (bottom). Intensities are comparable for individual samples, but not between different samples.

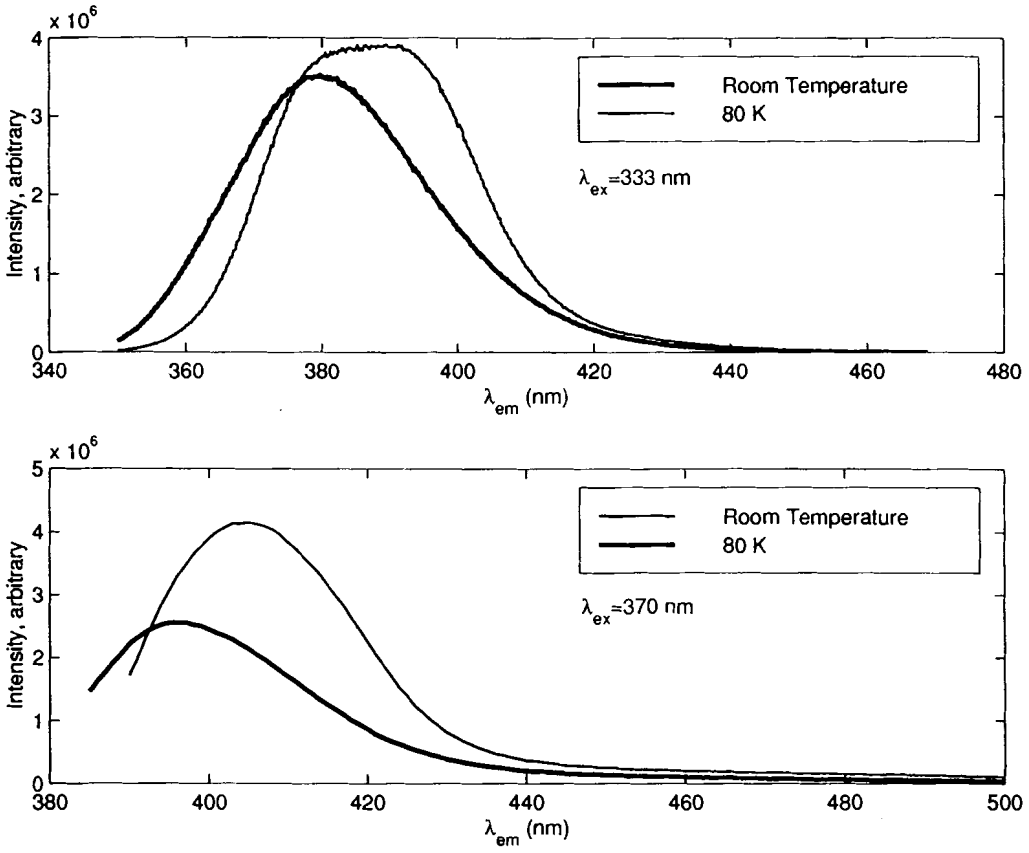

Figure 5.2: Emission spectra at room temperature and 80 K for the mixed-metal samples $La[Ag_{0.9}Au_{0.1}(CN)_2]_3$ (top) and $La[Ag_{0.5}Au_{0.5}(CN)_2]_3$ (bottom). Intensities are comparable for individual samples, but not between different samples.

5.2.2 The Mixed-Metal Compounds

Figure 5.2 shows emission spectra for both of the mixed-metal compounds. It is noted that the luminescence intensity at ambient temperature values is comparable to that at low temperature values for both compounds, in stark contrast to the behavior of the pure systems.

In the $La[Ag_{0.9}Au_{0.1}(CN)_2]_3$ crystals, there are two closely spaced emission bands (380 nm and 400 nm) which lie in energy between the emission energies of the silver

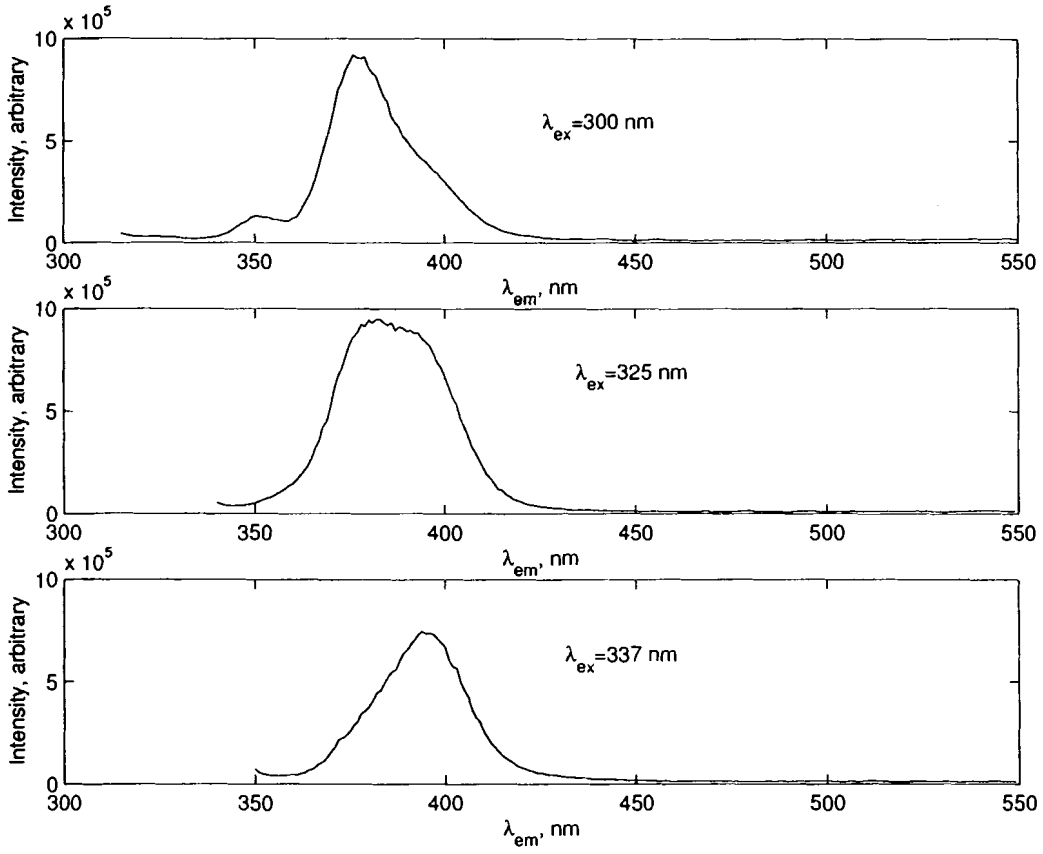

Figure 5.3: Emission spectra as a function of excitation wavelength, showing the site-selectivity of $La[Ag_{0.9}Au_{0.1}(CN)_2]_3$. Spectra taken at 80 K.

and gold pure compounds and can be selected by excitation wavelength, as shown in Figure 5.3. Since this particular compound has significantly more silver than gold, it is not surprising that a property characteristic of the pure silver compound is observed.

As the temperature is increased from 40 K to 290 K, an excitation wavelength of 337 nm produces first only the 400 nm band, then as the temperature rises both bands are present, then finally at room temperature, the 380 nm band is predominant (see Figure 5.4). One possible explanation for this is that at higher temperature values back-energy transfer (a radiationless process that is strongly temperature dependent)

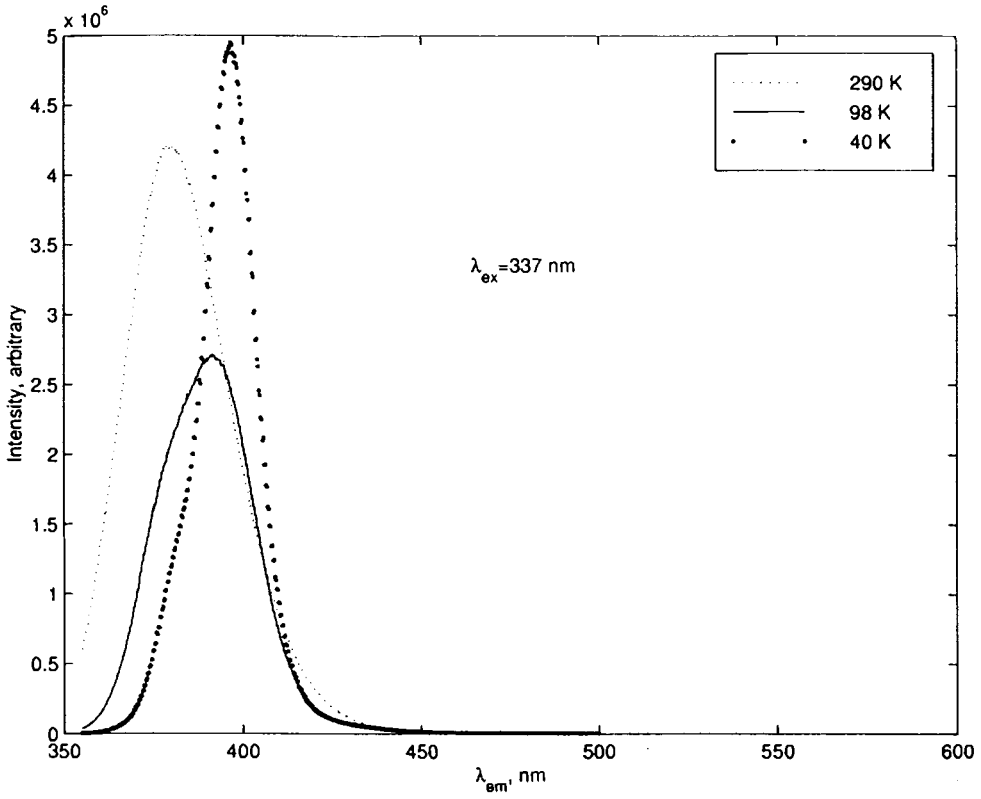

Figure 5.4: Emission spectra as a function of temperature for $La[Ag_{0.9}Au_{0.1}(CN)_2]_3$ using an excitation wavelength of 337 nm. Intensities are not comparable between spectra.

from the lower energy band to the higher energy band dominates, while at lower temperature values either direct excitation into the 400 nm band or forward energy transfer from the 380 nm band dominate. This hypothesis unfortunately can not be explored without obtaining lifetime values as a function of temperature for an excitation wavelength of 337 nm.

In $La[Ag_{0.5}Au_{0.5}(CN)_2]_3$, there exists both site-selectivity *and* a red-shift of the emission wavelength. At room temperature, the site- selectivity is not apparent and only one band at about 400 nm is observed, however at low temperature values, there

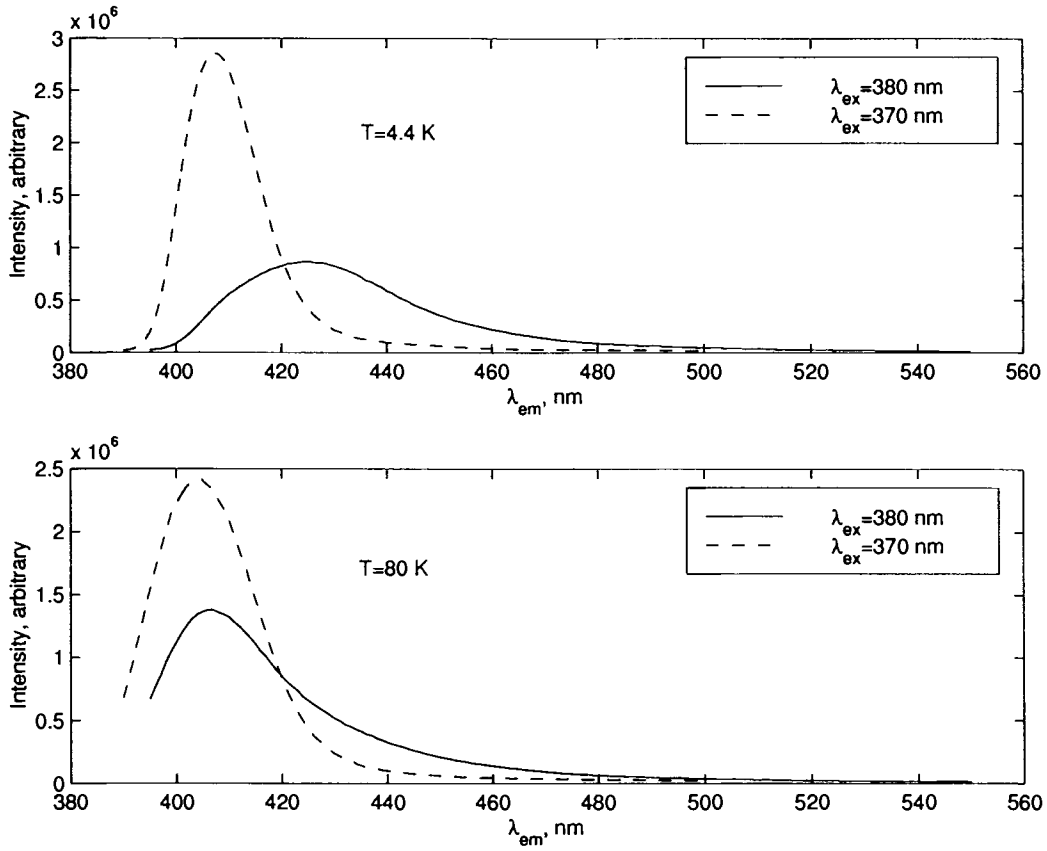

Figure 5.5: Emission spectra as a function of excitation wavelength, showing the site-selectivity of $La[Ag_{0.5}Au_{0.5}(CN)_2]_3$.

exists a low energy band (430 nm) with a completely different excitation profile. This band blue-shifts with increasing temperature until it is indistinguishable from the higher energy band, as can be seen in Figure 5.5. The red-shift is shown in Figure 5.6.

The higher energy (400 nm) band has been decomposed into three Gaussian functions. The relative positions of these bands (labelled a, b and c) are detailed in Table 5.2.2 and plotted in Figure 5.7. It is noted that ΔE_{ab} is on the order of 400-500

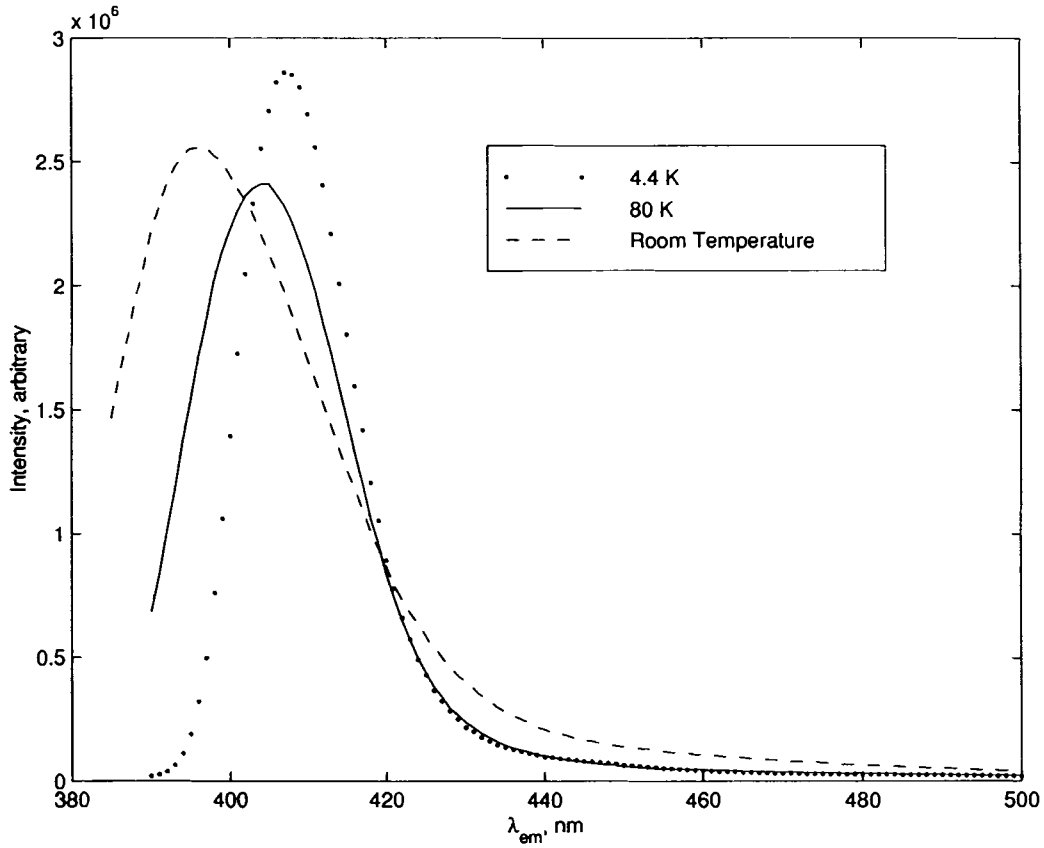

Figure 5.6: Emission spectra as a function of temperature showing the red- shift of emission in $La[Ag_{0.5}Au_{0.5}(CN)_2]_3$. Intensities are not comparable between spectra.

T, K	λ_a, nm	E_a, cm^{-1}	λ_b, nm	E_b, cm^{-1}	λ_c, nm	E_c, cm^{-1}
4.4	403.8 (0.1)	24764 (6)	410.3 (0.1)	24372 (6)	431.4 (1.7)	23180 (90)
19	403.9 (0.1)	24759 (6)	410.3 (0.1)	24372 (6)	433.0 (2.0)	23095 (106)
40	403.6 (0.1)	24777 (6)	411.0 (0.1)	24331 (6)	439.2 (2.4)	22769 (125)
59	402.5 (0.2)	24845 (12)	410.7 (0.1)	24349 (6)	442.0 (3.0)	22624 (154)
77	401.4 (0.4)	24913 (25)	410.4 (0.3)	24366 (18)	443.8 (4.4)	22533 (223)
295	395.4 (0.1)	25291 (6)	403.0 (0.1)	24814 (6)	435.5 (3.8)	22962 (200)

Table 5.1: Variation with temperature of the three closely spaced emission bands in $La[Ag_{0.5}Au_{0.5}(CN)_2]_3$.

cm^{-1} at all temperature values while ΔE_{bc} decreases from over 2000 cm^{-1} at room temperature to about 1200 cm^{-1} at 4 K.

5.3 Luminescence Lifetime Results

5.3.1 $La[Ag_{0.5}Au_{0.5}(CN)_2]_3$

As mentioned in Chapter 2, all lifetime values were obtained using an excitation wavelength of 266 nm. At this excitation wavelenth, this sample displays only one emission band, at approximately 400 nm and the lower energy band observed at 430 nm at low temperature values is not present and it's lifetime could therefore not be studied.

The lifetime for this sample is single exponential and on the order of 100 ns or less from room temperature down to 80 K. Below 80 K, the lifetime begins to increase significantly and is no longer single exponential. In the last section, this band was decomposed into three closely spaced, overlapping components. This change in the lifetime would indicate that the two higher energy bands now have distinctly different lifetime values instead of very similar values. It is assumed that the third, lower energy

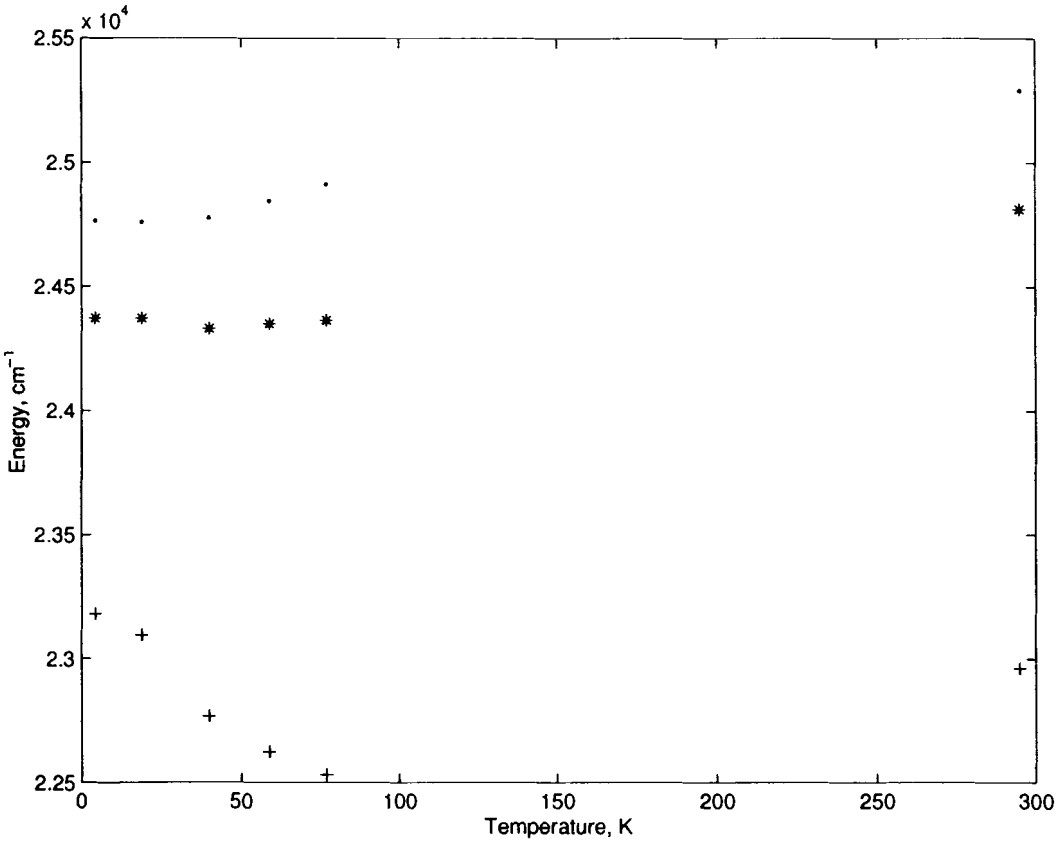

Figure 5.7: Variation with temperature of the three closely spaced emission bands in $La[Ag_{0.5}Au_{0.5}(CN)_2]_3$

T, K	τ, ns
4.4	684 (24), 2358 (54)
9	203(5), 1004 (8)
22	126 (4), 343 (4)
40	95 (5), 220 (10)
62	95 (10), 200 (12)
80	95 (15)
170	80 (10)
230	70 (10)
290	65 (15)

Table 5.2: Lifetime values as a function of temperature for $La[Ag_{0.5}Au_{0.5}(CN)_2]_3$. Lifetime values were obtained at an emission wavelength of 400 nm.

band does not contribute in the lifetime analysis, as all lifetime values were obtained at 400 nm and there is only a very insignificant overlap of this component at 400 nm. The decay can be decomposed into two components at 62 K and below (see Table 5.3.1), one with a significantly longer lifetime.

5.3.2 $La[Ag_{0.9}Au_{0.1}(CN)_2]_3$

The 90/10 sample's luminescence decay follows a single exponential at all temperature values increasing from 225 ns to 1390 ns as the temperature is lowered from room to liquid helium temperature values. The lifetime values are tabulated in Table 5.3.2.

5.4 Discussion of Theoretical Model for Results

The question of why these samples exhibit such strong luminescence at room temperature is expected to be answered through a detailed analysis of the structure. X-ray diffraction studies are currently underway to investigate whether structural

T, K	τ, ns
8	1390 (90)
18	570 (10)
40	350 (10)
60	310 (10)
86	285 (10)
126	250 (15)
200	245 (15)
285	225 (20)

Table 5.3: Lifetime values as a function of temperature for $La[Ag_{0.9}Au_{0.1}(CN)_2]_3$. Lifetime values were obtained at an emission wavelength of 397 nm.

differences between the pure samples and the mixed-metals could account for this. Preliminary results indicate that the 50-50 sample belongs to the same space group as $La[Au(CN)_2]_3$ (P62m), but there is only one water of hydration in this sample, while the pure samples have three waters of hydration coordinated with the La^{3+} ions. It is suspected that this could be responsible for this effect as fewer waters leads to fewer non-radiative decay pathways for the system. In addition, density functional theory calculations have begun on both the pure samples and the mixed-metal systems so that the compositions of the orbitals involved in the relevant transitions may be compared to see if metal- metal interactions are important.

5.4.1 $La[Ag_{0.9}Au_{0.1}(CN)_2]_3$

The results obtained for this sample are similar to those obtained for a series of quasi-one-dimensional mixed Pt-Pd and Pt-Ni tetracyanide systems and their corresponding pure Pt and pure Pd tetracyanides by Viswanath *et al.*[53,54,70] The authors observed that one of the emission bands observed in the mixed system did not match

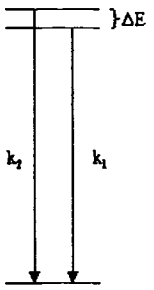

Figure 5.8: Scheme for the emission from the mixed-metal delocalized excited states

with any observed in the pure systems and concluded that this emission band was due to a delocalized excited state, that is, delocalized over the Pt and Pd sites.

A two level system is proposed, where the emission arises from two closely spaced states that arise from splitting of a single triplet state due to spin-orbit coupling. This splitting is dictated by the symmetry of the site the ion is in. It is assumed that these states are in thermal equilibrium. Since the excitation source is a pulsed laser, one might wonder whether the high power involved would force the system into a non-equilibrium state. This possibility could be tested by obtaining lifetime values as a function of excitation power. Unfortunately, the current experimental set-up does not allow for such a study. However, the layered structure of these compounds and the close metal-metal contacts within the layers allows for very rapid communication of the excitation energy along the $M(CN)_2^-$ layers. This lends support to the assumption that equilibrium is rapidly attained. This scheme is shown in Figure 5.8. In this scheme, the observed lifetime can be described as a function of temperature by the

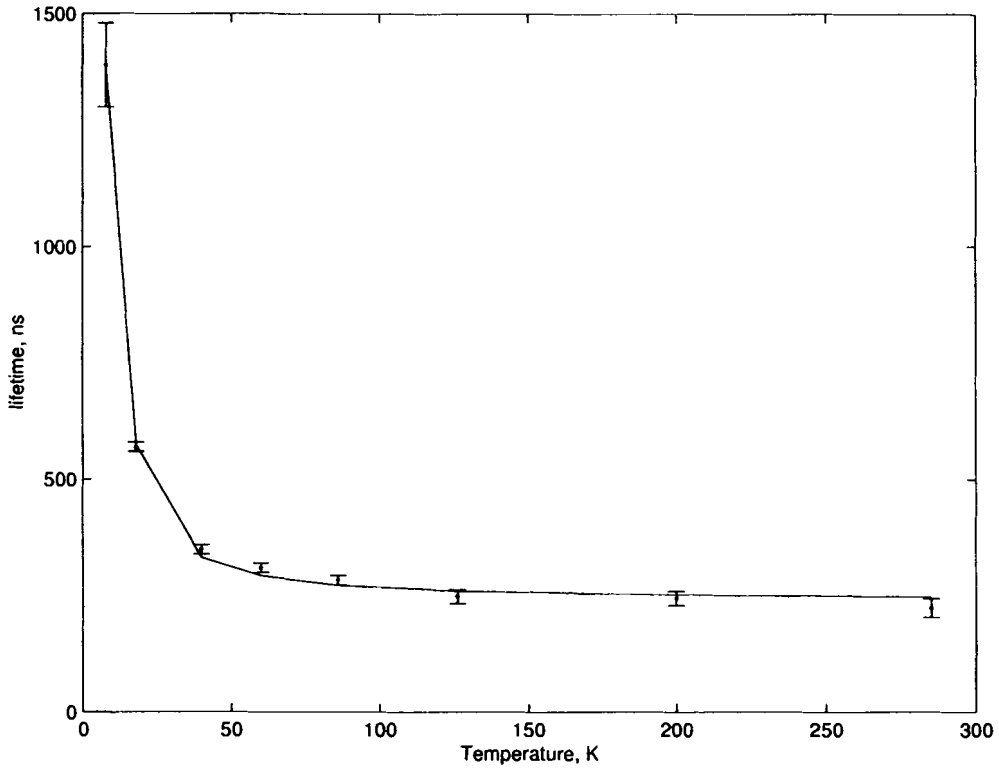

Figure 5.9: Lifetime data as a function of temperature along with a fit to equation 5.4.1.

following equation:[71,72]

$$\tau = \frac{1 + 2e^{-\Delta E/kT}}{k_1 + 2k_2 e^{-\Delta E/kT}}. \tag{5.4.1}$$

A similar model was proposed for this type of situation in bis(4- chlorothiophenol)(1,10-phananthroline)zinc(II) by Crosby *et al.*[73] and applied successfully for $Tl[Au(CN)_2]_3$[72] and $Cs[Au(CN)_2]_3$.[71] A comparison of these results with previous results will be given in the next section.

The lifetime values from Table 5.3.2 have been fit to equation 5.4.1 with results shown in Figure 5.9. The parameters obtained from the fit are given in Table 5.4.

ΔE, cm^{-1}	k_1, s^{-1}	k_2, s^{-1}
25.2 (1.5)	6.07 (0.02) $\times$ 10^5	5.97 (0.05) $\times$ 10^6

Table 5.4: Parameters obtained from a fit of the lifetime values as a function of temperature to equation 5.4.1 for $La[Ag_{0.9}Au_{0.1}(CN)_2]_3$.

	ΔE, cm^{-1}	k_1, s^{-1}	k_2, s^{-1}
long lifetime component	23.1 (1.9)	4.12 (0.02) $\times$ 10^5	1.20 (0.02) $\times$ 10^7
short lifetime component	12.0 (1.3)	7.87 (0.03) $\times$ 10^5	1.83 (0.05) $\times$ 10^7

Table 5.5: Parameters obtained from a fit of the lifetime values as a function of temperature to equation 5.4.1 for $La[Ag_{0.5}Au_{0.5}(CN)_2]_3$.

5.4.2 $La[Ag_{0.5}Au_{0.5}(CN)_2]_3$

Examining the excitation and emission spectra as a function of temperature, it is clear that the two closely spaced energy levels are coupled at high temperature values, but not at lower temperature values (below 60 K). This is evident in the lifetime data in that a single lifetime component is found at higher temperature values, while at lower temperature values two components are resolved.

Both components of the decays have been individually fit to the same model applied for the 90/10 sample in the previous section with results given in Table 5.5. This fit now assumes that each of the two bands has two energy levels split by different energies ΔE.

The values obtained for ΔE can be compared with values obtained for similar compounds. For $Tl[Au(CN)_2]$, a ΔE of 36.0 (0.4) cm^{-1} was obtained,[72] and for $Cs[Au(CN)_2]$, a value of 45.22 (0.03) cm^{-1} was obtained.[71] The smaller values obtained for the mixed-metals in this study can be understood using the fact that the

spin-orbit coupling energy is proportional to Z^2. Since $Z_{Au} > Z_{Ag}$, it is reasonable to expect that ΔE will be smaller in compounds containing Ag.

5.5 Analysis of the Suitability of Mixed Silver-Gold Compounds as Donors for Energy Transfer

These samples have a room temperature luminescence intensity that is comparable to the low temperature intensity, a fact that makes them promising for photoluminescence applications. Furthermore, these samples have *tunable* emission energies, which could lead to a variety of choices for acceptors in the energy transfer study, due to changes in the spectral overlap. It was found that the energies are tunable by site-selective excitation and in one of the samples that site- selectivity was turned on by decreasing the temperature. Clearly the emission is also selectable by changing the Ag/Au ratio present in the sample. All of these characteristics make these samples good candidates for donors in energy transfer studies.

The short lifetime values are not a concern in the context of energy transfer efficiency, as it was shown in Chapter 4 that energy transfer from dicyanoaurates and dicyanoargentates occurs very rapidly.

Figure 5.10 shows an energy level diagram for three of the lanthanide ions. Also shown are the full-width half-maximum emission bands for the mixed-metal systems that have been studied. These lanthanide ions have been selected for the degree of spectral overlap between their absorptions and the donor's emissions.

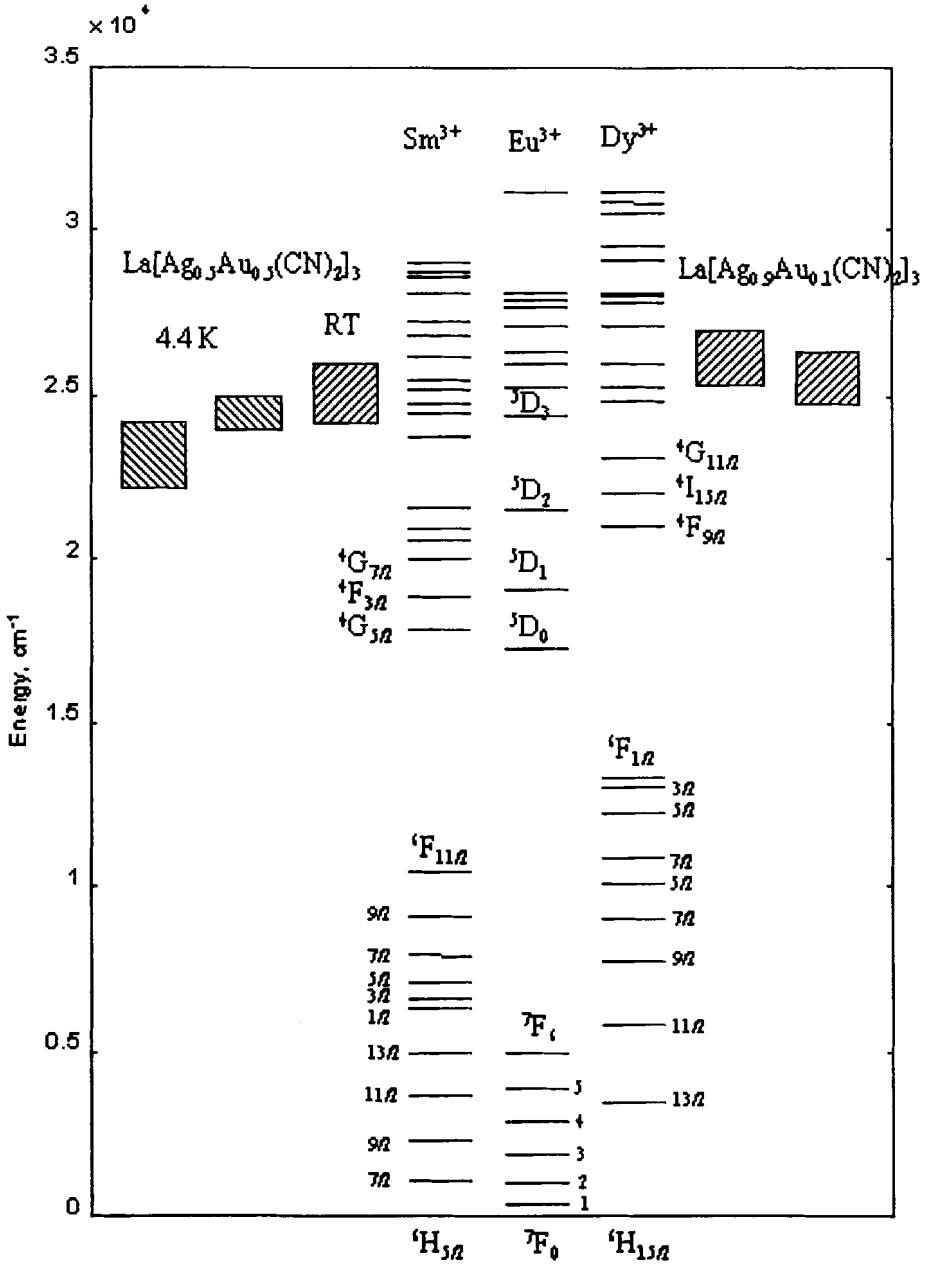

Figure 5.10: Energy levels for the two mixed-metal samples as well as three lanthanide ions chosen for the degree of spectral overlap between their absorptions and the mixed-metal samples' emissions.

5.6 Summary and Conclusions

It has been shown that these mixed-metal samples display luminescence properties characteristic of each of the pure metal compounds, notably site-selective excitation and a red-shift of emission wavelength with decreasing temperature. In addition, they exhibit ambient luminescence that is comparable with the low-temperature luminescence, a property not observed in the pure samples that is very desirable. This strong luminescence at room temperature has been attributed to the fact that there are fewer waters of hydration in the mixed samples, leading to less potential for non-radiative decay.

6 SUMMARY, CONCLUSIONS AND FUTURE DIRECTIONS

The purpose of this chapter is to provide a summary of the important conclusions made in this thesis in regard to each of the three project areas. In addition, suggestions for future follow-up work will be made.

6.1 Luminescence Thermochromism and $K_2Na[Ag(CN)_2]_3$

The interesting photoluminescence properties of this compound have been probed extensively in an attempt to explain the presence of a phenomenon known as luminescence thermochromism. There exist two luminescence bands, a high energy band (HE) and low energy band (LE) that show an interesting trend as a function of temperature. The HE band dominates at very low temperature values (4 K) and very high temperature values (200 K), while at intermediate temperature values (60 K) the LE band dominates.

A structural study was undertaken with the premise that a phase transition at an intermediate temperature might explain the changes in the luminescence. However, X-ray diffraction results, which have been corroborated with Raman scattering data, show a structural change at a much higher temperature than expected (210 K).

Further study, including luminescence lifetime data, lends support to a new hypothesis. At 4 K, non-radiative processes are highly unlikely, so emission is seen only from the HE band. Between 4 K and 60 K, energy transfer from the HE band to the

LE band grows in and begins to be the dominant process. However, as the temperature is further increased, back-energy transfer begins to play a role and LE band begins to grow out.

Further work on this system will likely involve mathematical modeling of the behavior of the lifetime results as a function of temperature in order to more completely understand the role of energy transfer and back-energy transfer on its luminescence.

6.2 Energy Transfer in Dicyanoargentates and Dicyanoaurates

It has been shown that in dicyanoargentates and dicyanoaurates doped with Tb^{3+}, exclusive excitation of the dicyanoargentate or dicyanoaurate donor ion leads to sensitized luminescence from the Tb^{3+} acceptor ion. It was also observed that the energy transfer efficiency is so high that the donor luminescence is effectively quenched in the singly doped samples $Tb[Au(CN)_2]_3$ and $Tb[Ag(CN)_2]_3$, to the extent that the dynamics of the decay process could not be studied. To circumvent this problem, a series of samples co-doped with both Tb^{3+} and La^{3+} (which has no optical activity) was studied. It was noted that increasing the percentage of Tb^{3+} dopant increased the rate of energy transfer. The Dexter exchange mechanism has been proposed as the mechanism of energy transfer and other mechanisms have been ruled out through mathematical modeling.

One area in this field that has yet to be explored is that of dicyanoargentates(I) and dicyanoaurates(I) doped with multiple acceptors, such as $Tb_{0.5}Eu_{0.5}[Ag(CN)_2]_3$. The *tunability* of the donors that was explored in detail in this thesis could give rise to

the possibility of *tuning off* the emission of one acceptor while *tuning on* the emission of a second acceptor.

6.3 Novel Mixed-Metal Compounds as Donors for Energy Transfer

The results for mixed-metals is novel and exciting in that they display the desirable *tunability* of the pure metal compounds studied, but in contrast to the pure compounds, their luminescence at room temperature is strong. It is hypothesized that their room temperature luminescence intensity is comparable to the low temperature luminescence intensity is related to the fact that the structure shows fewer waters of hydration and therefore fewer radiationless decay pathways. A complete temperature dependent structural study is proposed to further understand this observation and support or refute this hypothesis.

Future study will include a conclusive determination of the Ag/Au ratio in each of the studied samples. A full determination of the structure as a function of temperature as well as completion of the density functional theory calculations (to be compared with similar studies on the pure metal samples) will help to explain the strong ambient luminescence.

A logical extension of this study would be the synthesis of mixed- metal compounds doped with optically active lanthanide ion acceptors. The luminescence of these mixed-metals is well understood and a number of lanthanides with good spectral overlap have been suggested for use as acceptors.

References

[1] Howard H. Patterson, Sofian M. Kanan, and Mohammad A. Omary. Luminescent homoatomic exciplexes in dicyanoargenate(I) ions doped in alkali halide crystals. 'Exciplex tuning' by site-selective excitation and variation of the dopant concentration. *Coordination Chemistry Reviews*, 208:227, 2000.

[2] E. L. Wehry, editor. *Modern Fluorescence Spectroscopy.* Plenum Press, 223 Spring Street, New York, NY 10013, 1981.

[3] Manal A. Raweshdeh-Omary, C. L. Larochelle, and Howard H. Patterson. Tunable energy transfer from dicyanoaurate(I) and dicyanoargentate(I) donor ions to terbium(III) acceptor ions in pure crystals. *Inorganic Chemistry*, 39:4527, 2000.

[4] Sofian M. Kanan, Mohammad A. Omary, and Howard H. Patterson. Characterization of the excited states responsible for the action of Silver(I)-doped ZSM zeolites as photocatalysts for nitric oxide decomposition. *Journal of Physical Chemistry B*, 104:3507, 2000.

[5] Weiping Su, Maochun Hong, Jiabao Weng, Rong Cao, and Shaofang Lu. A semiconducting lamella polymer $[(Ag(C_5H_4NS))_n]$ with a graphite-like array of silver(I) ions and its analogue with a layered structure. *Angewandte Chemie*, 39:2911, 2000.

[6] Kenji Nomiya, Ryusuke Noguchi, and Munehiro Oda. Synthesis and crystal structure of coinage metal(I) complexes with tetrazole (Htetz) and triphenylphosphine ligands, and their antimicrobial activities. a helical polymer of silver(I) complex $[Ag(tetz)(PPh_3)_2]_n$ and a monomeric gold(I) complex $[Au(tetz)(PPh_3)]$. *Inorganica Chimica Acta*, 298:24, 2000.

[7] Kenji Nomiya, Satoshi Takahashi, and Ryusuke Noguchi. Water-soluble silver(I) complexes of (R)-(+)- and (S)-(-)-2-pyrrolidone-5-carboxylic acid and their antimicrobial activities. chiral helical polymer and polymer sheet structures in the solid-state formed by self-assembly of dimeric $[Ag(Hpyrrld)]_2$ cores. *Journal of the Chemical Society, Dalton Transactions*, 23:4369, 2000.

[8] M. Adnan Mansour, William B. Connick, Rene J. Lachicotte, Henry J. Gysling, and Richard Eisenberg. Linear chain Au(1) dimer compounds as environmental sensors: A luminescent switch for the detection of volatile organic compounds. *Journal of the American Chemical Society*, 120:1329, 1998.

[9] H.D. Hardt and A. Pierre. Fluorescence thermochromism and symmetry of copper(i) complexes. *Inorganica Chimica Acta*, 25:L59–L60, 1977.

[10] H. D. Hardt. Lumineszenzthermochromie, ein vergessenes phanomen. *Naturwissenschaften*, 61:107, 1974.

[11] Peter C. Ford. Photochemical and photophysical studies of tetranuclear copper(I) halide clusters: An overview. *Coordination Chemistry Review*, 132:129, 1994.

[12] Manal A. Raweshdeh-Omary, Mohammad A. Omary, George E. Shankle, and Howard H. Patterson. Luminescence thermochromism in dicyanoargentate(I) ions doped in alkali halide crystals. *Journal of Physical Chemistry B*, 104:6143, 2000.

[13] Mohammad A. Omary. *Photoluminescence, Molecular Structure, and Electronic Structure of Dicyano Silver(I) Complexes: A New Class of Luminescent Metal-Metal-Bonded Exciplexes.* PhD thesis, University of Maine, 1997.

[14] Abraham Rosenzweig and Don T. Cromer. The crystal structure of $KAu(CN)_2$. *Acta Crystallographica*, 12:709, 1959.

[15] Llewellyn H. Jones. Vibrational spectrum and structure of metal-cyanide complexes in the solid state. I. $KAg(CN)_2$. *Journal of Chemical Physics*, 26:1578, 1957.

[16] Llewellyn H. Jones. Vibrational spectrum and structure of metal-cyanide complexes in the solid state. II. $KAu(CN)_2$. *Journal of Chemical Physics*, 27:468, 1957.

[17] David M. Adams and Patrick A. Fletcher. Vibrational spectroscopy at high pressures–52. A study of the phase behaviour of $K[M(CN)_2]$, M=Ag, Au, at high pressure by Raman scattering. *Spectrochimica Acta*, 44A:437–443, 1988.

[18] G. L. Bottger. The vibrational spectrum of crystalline $KAg(CN)_2$. *Spectrochimica Acta*, 24A:1821, 1968.

[19] Thomas M. Loehr and Thomas Veach Long. Laser-Raman spectrum (10-4500 cm^{-1}) of potassium dicyanoargentate (I). *Journal of Chemical Physics*, 53:4182, 1970.

[20] P. T. T. Wong. Pressure-induced phase transitions and pressure dependence of zone-center phonons of the $K[Ag(CN)_2]$ crystal investigated by Raman scattering. *Journal of Chemical Physics*, 70:456, 1979.

[21] Angeline M. Stier. *Darstellung und Kristallstruktur Von Dicyanometallaten.* PhD thesis, Universität Regensburg, 1996.

[22] Mohammad A. Omary, Thomas R. Webb, Zerihun Assefa, George E. Shankle, and Howard H. Patterson. Crystal structure, electronic structure, and temperature-dependent Raman spectra of $Tl[Ag(CN)_2]$: Evidence for ligand-unsupported argentophilic interactions. *Inorganic Chemistry*, 37:1380, 1998.

[23] C. L. Larochelle, M. A. Omary, H. H. Patterson, P. Fischer, F. Fauth, P. Allenspach, B. Lucas, and P. Pattison. Optical, synchrotron x-ray and neutron diffraction investigations of structural changes in the layered compound $K_2Na[Ag(CN)_2]_3$. *Solid State Communications*, 114:155, 2000.

[24] The Faraday Society, editor. *Transfer Mechanisms of Electronic Excitation*, volume 27, 6 Upper Kirkgate, Aberdeen Scotland, 1959. The Aberdeen University Press Ltd.

[25] A. Horváth and K. L. Stevenson. Transition metal complex exciplexes. *Coordination Chemistry Reviews*, 153:57, 1996.

[26] J. K. Nagle and B. A. Brennan. Luminescent exciplex formation involving tetrakis(μ-diphosphito)diplatinate(II) and -thallium(I) in aqueous solution. *Journal of the American Chemical Society*, 110:5931, 1988.

[27] Cheryl N. Pettijohn, Evan B. Jochnowitz, Bao Chuong, Jeffrey K. Nagle, and Arnd Vogler. Luminescent excimers and exciplexes of PtII compounds. *Coordination Chemistry Reviews*, 171:85, 1998.

[28] Kyeong-Sook Kim Shin, James D. Barrie, Bruce Dunn, and Jeffrey I. Zink. Optical spectroscopy of Cu^+/Ag^+ doped β"-alumina. *Journal of the American Chemical Society*, 112:5701, 1990.

[29] J. D. Barrie, B. Dunn, Gary Hollingsworth, and Jeffrey I. Zink. Optical spectroscopy of copper(I)-doped Na^+–β"-alumina. *The Journal of Physical Chemistry*, 93:3958, 1989.

[30] Mohammad A. Omary and Howard H. Patterson. Temperature-dependent photoluminescence properties of $Tl[Ag(CN)_2]$: Formation of luminescent metal-metal-bonded inorganic exciplexes in the solid state. *Inorganic Chemistry*, 37:1060, 1998.

[31] Mohammad A. Omary and Howard H. Patterson. Luminescent homoatomic exciplexes in Dicyanoargentate(I) ions doped in alkali halide crystals. 1. Exciplex tuning by site-selective excitation. *Journal of the American Chemical Society*, 120:7696, 1998.

[32] Mohammad A. Omary, Derek R. Hall, George E. Shankle, Aleksander Siemiarczuk, and Howard H. Patterson. Luminescent homoatomic exciplexes in dicyanoargentate(I) ions in alkali halide crystals. 2. "Exciplex tuning" by varying the dopant concentration. *Journal of Physical Chemistry B*, 103:3845, 1999.

[33] A. Edwards, C. Claude, I. Sokolik, T. Y. Chu, Y. Okamoto, and R. Dorsinville. Photoluminescence and electroluminescence of new lanthanide-(methyoxybenzoyl)benzoate complexes. *Journal of Applied Physics*, 82:1841–1846, 1997.

[34] N. C. Chang. Fluorescence and stimulated emission from trivalent europium in yttrium oxide. *Journal of Applied Physics*, 34:3500–3504, 1963.

[35] Xingren Liu, Xiaojun Wang, and Zhongkai Wang. Selectively excited emission and $Tb^{3+} \rightarrow Ce^{3+}$ energy transfer in yttrium aluminum garnet. *Physical Review B*, 39:10633, 1989.

[36] Ishenkumba A. Kahwa, Charmaine C. Parkes, and Gary L. McPherson. Energy transport in photoexcited crystals of $K_3[Tb(C_2O_4)_3(H_2O)].2H_2O$: Transfer from Tb^{3+} to Nd^{3+} and Eu^{3+}. *Physical Review B*, 52:11777–11783, 1995.

[37] Toshihiro Yamase and Haruo Naruke. Luminescence and energy transfer phenomena in Tb3+/Eu3+-mixed polyoxometallolanthanoates $K_{15}H_3[Tb_{1.4}Eu_{1.6}(H_2O)_3(SbW_9O_33)]_{.25}.5H_2O$ and $Na_7H_{19}[Tb_{4.3}Eu_{1.7}O_2(OH)_6(H_2O)6Al_2(Nb_6O_{19})_5].47H_2O$. *Journal of Physical Chemistry B*, 103:8850–8857, 1999.

[38] I. R. Martin, A. C. Yanes, J. Méndez-Ramos, M. E. Torres, and V. D. Rodríguez. Cooperative energy transfer in Yb^{3+}–Tb^{3+} codoped silica sol-gel glasses. *Journal of Applied Physics*, 89:2520, 2001.

[39] Markus Wermuth, Toni Riedener, and Hans U. Güdel. Spectroscopy and upconversion mechanisms of $CsCsBr_3:Dy^{3+}$. *Physical Review B*, 57:4369–4376, 1998.

[40] Hartmut Yersin, Dietrich Trümbach, Johann Strasser, Howard H. Patterson, and Zerihun Assefa. Tunable radiationless energy transfer in $Eu[Au(CN)_2]_3 \cdot 3H_2O$ by high pressure. *Inorganic Chemistry*, 37:3209–3216, 1998.

[41] Zerihun Assefa, George Shankle, Howard H. Patterson, and Ross Reynolds. Photoluminescence studies of lanthanide ion complexes of gold and silver dicyanides: A new low-dimensional solid-state class for nonradiative excited-state energy transfer. *Inorganic Chemistry*, 33:2187, 1994.

[42] D. L. Dexter. A theory of sensitized luminescence in solids. *Journal of Chemical Physics*, 21:836–850, 1953.

[43] Mitio Inokuti and Fumio Hirayama. Influence of energy transfer by the exchange mechanism on donor luminescence. *Journal of Chemical Physics*, 43:1978–1989, 1965.

[44] Mario Yokota and Osamu Tanimoto. Effects of diffusion on energy transfer by resonance. *Journal of the Physical Society of Japan*, 22:779–784, 1967.

[45] I. R. Martin, V. D. Rodriguez, U. R. Rodriguez-Mendoza, V. Lavin, E. Montoya, and D. Jaque. Energy transfer with migration: Generalization of the Yokota-Tanimoto model for any kind of multipole interaction. *Journal of Chemical Physics*, 111:1191–1194, 1999.

[46] S. H. Lin, W. Z. Xiao, and W. Dietz. Generalized Forster-Dexter theory of photoinduced intramolecular energy transfer. *Physical Review E*, 47:3698–3706, 1993.

[47] Marianne E. Von Arx, Emanuele Burattini, Andreas Hauser, Liesbeth Van Pieterson, Rene Pellaux, and Silvio Decurtins. Luminescence and energy transfer of $[Ru(bpy)_3]^{2+}$, $[Cr(ox)_3]^{3-}$, and $[Os(bpy)_3]^{2+}$ in three-dimensional oxalato-networks. *Journal of Physical Chemistry A*, 104:883–893, 2000.

[48] Alexander Blumen. On the direct energy transfer via exchange to randomly distributed acceptors. *Journal of Chemical Physics*, 72:2632, 1998.

[49] Atsuko Hara and Yasuhiko Gondo. Energy-donor phosphorescence and energy transfer by exchange interaction in a rigid matrix. *Journal of Chemical Physics*, 85:1894, 1986.

[50] Shoji Taen. Molecular size and luminescence decay influenced by energy transfer by the exchange mechanism. *Journal of Chemical Physics*, 108:6857, 1998.

[51] C. Z. Hadad and S. O. Vásquez. Energy-transfer processes induced by exchange interactions. *Physical Review B*, 60:8586, 1999.

[52] Peter Fischer, Joël Mesot, Brian Lucas, Andreas Ludi, Howard Patterson, and Alan Hewat. Pressure dependence investigation of the low-temperature structure of $TlAu(CN)_2$ by high-resolution neutron powder diffraction and optical studies. *Inorganic Chemistry*, 36:2791, 1997.

[53] A. Kasi Viswanath, Jeanette Vetuskey, Rosemary Leighton, Mary-Beth Krogh-Jespersen, and Howard H. Patterson. Luminescence and absorption study of delocalized and localized electronic states in quasi-one-dimensional mixed metal Ba(Pt, Pd)$(CN)_4$ and Ba(Pt, Ni)$(CN)_4$ systems. *Molecular Physics*, 48:567–579, 1983.

[54] A. Kasi Viswanath and Howard H. Patterson. Energy transfer from a platinum-nickel excited state to platinum clusters in quasi-one-dimensional Ba(Pt, Ni)$(CN)_4 \cdot H_2O$ crystals. *Chemical Physics Letters*, 82:25–28, 1981.

[55] SMART V 5.050 (NT). *Software for the CCD Detector System.* Bruker Analytical X-ray Systems, Madison, WI, 1998.

[56] SAINT V 5.01 (NT). *Software for the CCD Detector System.* Bruker Analytical X-ray Systems, Madison, WI, 1998.

[57] R. H. Blessing. Program for absorption corrections using Siemens CCD based on the method of Robert Blessing. *Acta Crystallographica*, A51:33–38, 1995.

[58] G. M. Sheldrick. *SHELXS-90, Program for the Solution of Crystal Structure.* University of Göttingen, Germany, 1990.

[59] G. M. Sheldrick. *SHELXL-97, Program for the Refinement of Crystal Structure.* University of Göttingen, Germany, 1997.

[60] SHELXTL 5.10 (PC-Version). *Program Library for Structure Solution and Molecular Graphics.* Bruker Analytical X-ray Systems, Madison, WI, 1998.

[61] *MATLAB 5.0 (Student Edition).* Prentice Hall, Upper Saddle River, NJ 07458, 1997.

[62] Ray Muzic. nlleasqr.m, a matlab m-file for performing non-linear least squares analysis, 1994 (last modification).

[63] P.C. Ford and A. Vogler. Photochemical and photophysical properties of tetranuclear and hexanuclear clusters of metals with d^{10} and s^2 electronic configurations. *Acc. Chem. Res.*, 26:220, 1993.

[64] Manfred Zabel, Sabine Kühnel, and Klaus-Jürgen Range. Dipotassium sodium tris[dicyanoargentate(I)]. *Acta Crystallographica*, C45:1619, 1989.

[65] J. Rodriguez-Cravajal. Recent advances in magnetic structure determination by neutron powder diffraction. *Physica B*, 192:55, 1993.

[66] P. G. Byrom, S. E. Hoffmann, and B. W. Lucas. MORGUE, a neutron powder diffraction profile refinement program with control-file facility to include structural and rigid-body thermal-motion constraints. *Journal of Applied Crystallography*, 22:629, 1989.

[67] P. G. Byrom and B. W. Lucas. Crystal structure determination by neutron powder diffraction using structural and packing constraints. *Journal of Applied Crystallography*, 24:1005, 1991.

[68] Ursula Kambli and Hans U. Güdel. Transfer of electronic excitation energy in the antiferromagnets $RbMnCl_3$, $CsMnCl_3$, $CsMnBr_3$, and Rb_2MnCl_4. *Inorganic Chemistry*, 23:3479–3486, 1984.

[69] Fabiana R. G. de Silva and Oscar L. Malta. Calculation of the ligand-lanthanide ion energy transfer rate in coordination compounds: Contributions of exchange interactions. *Journal of Alloys and Compounds*, 250:427, 1997.

[70] William D. Ellenson, A. Kasi Viswanath, and Howard H. Patterson. Laser-excited luminescence study of the chain compound $BaPd(CN)_4 \cdot 4H_2O$. *Inorganic Chemistry*, 20:780–783, 1981.

[71] J. T. Markert, N. Blom, G. Roper, A. D. Perregaux, N. Nagasundaram, M. R. Corson, A. Ludi, J. K. Nagle, and H. H. Patterson. Luminescence of cesium dicyanoaurate(I). evidence for extended Au(I)-Au(I) interactions in two dimensions. *Chemical Physics Letters*, 118:258, 1985.

[72] Zerihun Assefa, Frank DeStafano, Mohammad A. Garepapaghi, Joseph H. LaCasce, Jr., Steve Ouellete, Michael R. Corson, Jeffrey K. Nagle, and Howard H. Patterson. Photoluminescence and electronic structure of $Tl[Au(CN)_2]$: Evidence for relativistic effects in thallium-gold and gold-gold interactions. *Inorganic Chemistry*, 30:2868, 1991.

[73] R. G. Highland and G. A. Crosby. Determination of the activation barrier to energy transfer from $^3\pi\pi*$ to charge transfer levels via steady-state and transient luminescence measurements on bis(4-chlorothiophenol)(1,10-phenanthroline)zinc(II). *Chemical Physics Letters*, 119:454, 1985.

BIOGRAPHY OF THE AUTHOR

Christie L. Larochelle was born in Norway, Maine on March 23, 1973. Her family eventually settled in Waterville, Maine where she attended high school. She left Maine to attend Johns Hopkins University in Baltimore, Maryland in 1991 and received her B.S. in Biomedical Engineering there in May 1995. She came to the University of Maine in 1996 to pursue an advanced degree in Physics.

After receiving her degree, Christie will join the faculty of Dickinson College in Carlisle, Pennsylvania as an Assistant Professor of Physics. Christie is a candidate for the Doctor of Philosophy degree in Physics from The University of Maine in August, 2001.